GYRO Technical Guide

J. Candy and E. Belli

January 26, 2011

Contents

Chapter 1

Flux-surface Geometry

1.1 Introduction

The goal of this chapter is to present a self-contained derivation and cataloguing of all geometrical quantities required for gyrokinetic or neoclassical simulation of plasmas with an arbitrary cross-sectional shape. The method represents a refinement and generalization of a class of approaches which fall under the category of local equilibrium techniques [ML74]. These have a long history of application to ballooning mode analysis [GC81, BKC$^+$84, MCG$^+$98], and are described in historical detail by Miller [MCG$^+$98]. The unified method we propose can be consistently applied to either a local or global equilibrium, and to flux-surfaces of model or general shape. A global equilibrium, in this context, refers to a preexisting numerical solution of the Grad-Shafranov equation over the entire plasma volume, whereas a local equilibrium refers to Grad-Shafranov force-balance at a single surface only, without reference to adjacent surfaces. The latter scenario has proven to be a powerful tool for understanding the effect of plasma shape [KWC07, Bel08] on transport.

The unified approach requires that the major radius $R(\Psi_t, \theta)$ and elevation $Z(\Psi_t, \theta)$ along a given flux-surface contour are tabulated as functions of the poloidal angle θ (or, more generally, any parameter that labels position on the flux surface at constant toroidal angle). In the local case, the toroidal flux, Ψ_t, need not be specified, and geometrical quantities can be evaluated up to an unknown constant (the so-called *effective field*, B_{unit}), with flux-surfaces labeled by the *midplane minor radius*, r. Both B_{unit} and r will be precisely defined later. If a global plasma equilibrium exists, such that the toroidal flux, Ψ_t, has been computed, then the functions $r = r(\Psi_t)$ and $B_{\text{unit}}(r)$ can be uniquely determined for all r (i.e., on each flux-surface). A special case, in which R and Z are approximated by up-down symmetric contours with finite ellipticity and triangularity (the so-called Miller geometry method [MCG$^+$98]), is treated by numerous codes worldwide [DJKR00, CW03, CPC$^+$03]. Unfortunately, the implementations of this method are not standardized, and documentation is typically unavailable. For example, in certain cases, the model shape is assumed but Grad-Shafranov force balance is not enforced. This gives rise to implementation differences which significantly complicate code benchmarking exercises. The challenges are further amplified for the consistent treatment of general (numerically-generated) flux-surface shape corresponding to global plasma equilibria [XMJ$^+$08]. Then, not only is there an even greater liklihood of significant implementation difference, but the connections to the local limit and to the limit of model shape are obscured. The present work is an attempt to define a standard approach which unifies the treatment of local and global equilibria, as well as model and general flux-surface shape. By using

a general Fourier-series expansion for the flux-surface shape, we show how to estimate the error in approximating a general closed contour with a model shape (often referred to as the Miller shape [MCG+98, WM99]). We also show how to consistently identify the local limit of a global equilibrium on each flux surface. The results herein modify certain conventions in the local equilibrium theory and, further, correct a variety of sign and typographical errors in an earlier paper by Waltz and Miller [WM99].

In Sec. 1.2, we give the most general definitions of coordinates and associated flux functions. In Sec. 1.3, we use the local equilibrium method to compute all geometrical quantities required for gyrokinetic or neoclassical simulation of plasmas, given (R, Z) coordinates and associated derivatives on a flux-surface. We specialize these results, in Sec. 1.4, to the specific cases of model (Miller) and general (Fourier series) flux-surface parameterizations, and provide error estimates for each method. Finally, in the appendix, we give a large-aspect-ratio expansion of the geometry coefficients, useful for purposes of code checking, and to make contact with the s-α model [CHT78].

1.2 Field-aligned coordinates and flux functions

1.2.1 Clebsch representation

In what follows we adopt the right-handed, field-aligned coordinate system (ψ, θ, α) together with the Clebsch representation [KK58] for the magnetic field

$$\mathbf{B} = \nabla\alpha \times \nabla\psi \quad \text{such that} \quad \mathbf{B}\cdot\nabla\alpha = \mathbf{B}\cdot\nabla\psi = 0\,. \tag{1.1}$$

The angle α is written in terms of the toroidal angle φ as

$$\alpha \doteq \varphi + \nu(\psi,\theta)\,. \tag{1.2}$$

In Eqs. (1.1) and (1.2), ψ (as we will show) is poloidal flux divided by 2π, and θ refers simultaneously to (a) an angle in the poloidal plane (at fixed φ), or (b) a parameterization of distance along a field line (at fixed α). In these coordinates, the Jacobian is

$$\mathcal{J}_\psi \doteq \frac{1}{\nabla\psi\times\nabla\theta\cdot\nabla\alpha} = \frac{1}{\nabla\psi\times\nabla\theta\cdot\nabla\varphi}\,. \tag{1.3}$$

Since the coordinates (ψ,θ,α) and (ψ,θ,φ) form right-handed systems, the Jacobian $\mathcal{J}_\psi$ is positive-definite. In the latter coordinates, the magnetic field becomes

$$\mathbf{B} = \nabla\varphi\times\nabla\psi + \frac{\partial\nu}{\partial\theta}\nabla\theta\times\nabla\psi \tag{1.4}$$

Using the definition of the safety factor, $q(\psi)$, we may deduce

$$q(\psi) \doteq \frac{1}{2\pi}\int_0^{2\pi}\frac{\mathbf{B}\cdot\nabla\varphi}{\mathbf{B}\cdot\nabla\theta}\,d\theta = \frac{1}{2\pi}\int_0^{2\pi}\left(-\frac{\partial\nu}{\partial\theta}\right)\,d\theta = \frac{\nu(\psi,0)-\nu(\psi,2\pi)}{2\pi}\,. \tag{1.5}$$

For concreteness, we choose the following boundary conditions for ν:

$$\nu(\psi,2\pi) = -2\pi\,q(\psi)\,, \tag{1.6}$$

$$\nu(\psi,0) = 0\,. \tag{1.7}$$

By writing $\mathbf{B}$ in the standard form for up-down symmetric equilibria,

$$\mathbf{B} = \nabla\varphi \times \nabla\psi + I(\psi)\nabla\varphi \,, \tag{1.8}$$

we can derive the following integral for ν:

$$\nu(\psi,\theta) = -I(\psi) \int_0^\theta \mathcal{J}_\psi \left|\nabla\varphi\right|^2 d\theta \,. \tag{1.9}$$

We remark that in the case of concentric (unshifted) circular flux surfaces, one will obtain the approximate result $\nu(\psi,\theta) \sim -q(\psi)\theta$.

1.2.2 Periodicity constraints

The periodicity requirements for physical functions are a potential source of confusion. Consider a physical function – for example, potential or density – represented by the (real) field $z(\psi,\theta,\alpha)$. In terms of the physical angle φ, we have

$$z(\psi,\theta,\alpha) = z\left(\psi,\theta,\varphi+\nu[\psi,\theta]\right) \tag{1.10}$$

We impose the following topological requirements on the function z:

1. z is $2\pi/\Delta n$-periodic in φ for fixed ψ and θ,
2. z is 2π-periodic in θ for fixed ψ and φ.

From this point onwards, we will refer to ψ and χ_t simply and the poloidal and toroidal fluxes, respectively.

1.2.3 Toroidal and poloidal flux

We can start from the general forms of the toroidal and poloidal fluxes [DHCS91]

$$\Psi_t \doteq \iint\limits_{S_t} \mathbf{B}\cdot d\mathbf{S} = \frac{1}{2\pi}\iiint\limits_{V_t} \mathbf{B}\cdot\nabla\varphi\, dV \,, \tag{1.11}$$

$$\Psi_p \doteq \iint\limits_{S_p} \mathbf{B}\cdot d\mathbf{S} = \frac{1}{2\pi}\iiint\limits_{V_p} \mathbf{B}\cdot\nabla\theta\, dV \,. \tag{1.12}$$

Explicitly inserting the field-aligned coordinate system of the previous section, and differentiating these with respect to ψ, gives

$$\frac{d\Psi_t}{d\psi} = \frac{1}{2\pi}\int_0^{2\pi} d\varphi \int_0^{2\pi} d\theta\; \mathbf{B}\cdot\nabla\varphi\,\mathcal{J}_\psi \,, \tag{1.13}$$

$$= \frac{1}{2\pi}\int_0^{2\pi} d\varphi \int_0^{2\pi} d\theta\; \frac{\mathbf{B}\cdot\nabla\varphi}{\mathbf{B}\cdot\nabla\theta} \,, \tag{1.14}$$

$$= 2\pi\, q(\psi) \,, \tag{1.15}$$

$$\frac{d\Psi_p}{d\psi} = \frac{1}{2\pi}\int_0^{2\pi} d\varphi \int_0^{2\pi} d\theta\ \mathbf{B}\cdot\nabla\theta\,\mathcal{J}_\psi\ , \tag{1.16}$$

$$= \frac{1}{2\pi}\int_0^{2\pi} d\varphi \int_0^{2\pi} d\theta\ , \tag{1.17}$$

$$= 2\pi\ . \tag{1.18}$$

Thus, ψ is the poloidal flux divided by 2π. For this reason, it is useful to also define the toroidal flux divided by 2π:

$$\chi_t \doteq \frac{1}{2\pi}\Psi_t\ . \tag{1.19}$$

According to these conventions,

$$d\Psi_t = q\,d\Psi_p \quad \text{and} \quad d\chi_t = q\,d\psi\ . \tag{1.20}$$

1.2.4 Flux-surface averaging and the divergence theorem

It is also convenient to define a related Jacobian

$$\mathcal{J}_r = \frac{1}{\nabla r\times\nabla\theta\cdot\nabla\varphi} = \frac{\partial\psi}{\partial r}\mathcal{J}_\psi\ , \tag{1.21}$$

where r is the midplane minor radius. The flux-surface average of a function f can be expressed as

$$\mathcal{F}(f) \doteq \frac{1}{V'}\oint d\theta\,d\varphi\,\mathcal{J}_r\,f \quad \text{where} \quad V'(r) = \oint d\theta\,d\varphi J_r\ . \tag{1.22}$$

The normalizing factor V' is evidently the derivative of the flux-surface volume with respect to r. The element of flux-surface volume can be written as $dV = dn\,dS = dr\,d\theta\,d\varphi\,\mathcal{J}_r$ where dS is the element of surface area on a flux-surface, and n is the length along the normal vector $\mathbf{n}$. The relation between n and r is given by $dr = (\partial r/\partial n)\,dn = |\nabla r|\,dn$. This allows one to write a form of the *divergence theorem* useful for the derivation of transport equations. Integrating the divergence of an arbitrary vector $\mathbf{A}$ over volume gives

$$\int dV\,\nabla\cdot\mathbf{A} = \oint dS\,\mathbf{A}\cdot\mathbf{n} = \oint\frac{dS}{|\nabla r|}\,\mathbf{A}\cdot\nabla r = V'(r)\,\mathcal{F}\left(\mathbf{A}\cdot\nabla r\right)\ , \tag{1.23}$$

where we have used

$$\mathcal{F}(f) = \frac{1}{V'}\oint\frac{dS}{|\nabla r|}\,f \quad \text{and} \quad V'(r) = \oint\frac{dS}{|\nabla r|}\ . \tag{1.24}$$

1.2.5 Additional flux functions

Recall that we have assumed that the coordinates (R, Z) of a each flux-surface are known via a one-dimensional parameterization (the arc length, for example). As a robust measure of the flux-surface elevation, we use the elevation of the centroid, defined as

$$Z_0 \doteq \frac{\oint dZ\,RZ}{\oint dZ\,R}\ . \tag{1.25}$$

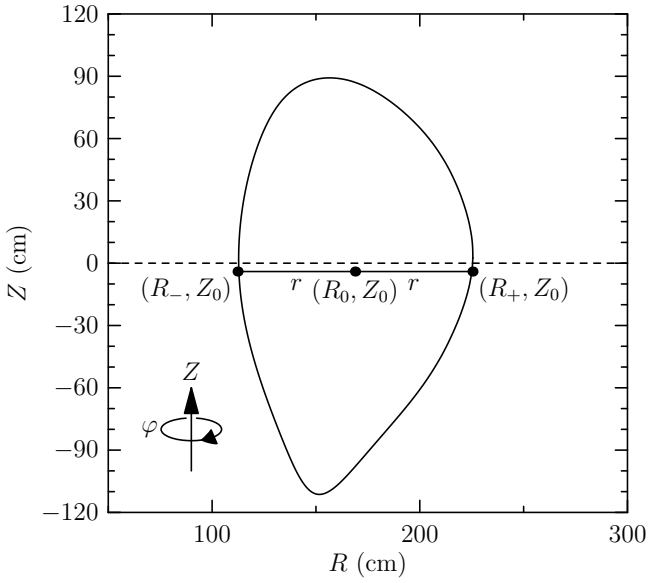

Figure 1.1: Illustration of the centroid elevation, Z_0, the effective major radius, R_0, and the effective minor radius, r, for a near-separatrix flux surface in DIII-D. The orientation of the toroidal angle, φ, is also indicated, such that (R, Z, φ) is a right-handed system.

In terms of the centroid elevation, the *effective minor radius*, r, is defined as the half-width of the flux surface at the elevation, Z_0:

$$r \doteq \frac{R_+ - R_-}{2} \ . \tag{1.26}$$

The quantities R_+ and R_- are the points of intersection of the flux surface with the line $Z = Z_0$, as illustrated in Fig. 1.1. We further define the *effective major radius*, $R_0 = (R_+ + R_-)/2$, and the *effective field strength*, $B_{\rm unit}$, as

$$B_{\rm unit} \doteq \frac{1}{r}\frac{d\chi_t}{dr} = \frac{q}{r}\frac{d\psi}{dr} \ . \tag{1.27}$$

The concept of an effective field was introduced by Waltz [WM99], and represents the equivalent field that would be obtained if the flux surface was deformed to a circle with the penetrating flux held fixed. It is emphasized that one must have access to a global equilibrium, not just the local flux-surface shape, to determine $B_{\rm unit}$. An important feature of the unified approach is that the definitions of r and $B_{\rm unit}$ are the same in both cases; that is, for both the model Grad-Shafranov (i.e., Miller) and general Grad-Shafranov equilibria to be defined shortly.

As an alternative to working with the toroidal flux directly, we introduce a function ρ, with units of length, which parameterizes the toroidal flux:

$$\chi_t = \frac{1}{2\pi}\int \mathbf{B}\cdot d\mathbf{S} = \frac{1}{2}B_{\rm ref}\,\rho(r)^2 \ , \tag{1.28}$$

In the expression above, $B_{\rm ref}$ is some reference field. While this would normally be the vacuum toroidal field, or something similar, it is important to keep in mind that the choice is ultimately arbitrary, but by knowing $B_{\rm ref}$ and ρ, one may calculate χ_t. In terms of ρ, the area enclosed by a

flux surface is approximately given by $A \simeq \pi\rho^2$ so long as $B_{\rm ref}$ is approximately equal to the on-axis toroidal field strength. In this sense, ρ is more intuitive, and so in certain cases more convenient, than χ_t.

1.3 Local Grad-Shafranov equilibria

The aim of this section is to compute convenient, standardized expressions for the common differential and integral operators appearing in the drift-kinetic and gyrokinetic equations.

1.3.1 Required operators

Below we collect, in coordinate-free form, the full set of differential and integral operators which are to be evaluated. In what follows, $\Omega_{ca} = z_a eB/(m_a c)$ is the gyroradius of species a and $p = \sum_a n_a k_B T_a$ is the total plasma pressure.

Perpendicular drift:

$$\mathbf{v}_d \cdot \nabla_\perp = \frac{v_\parallel^2 + v_\perp^2/2}{\Omega_{ca} B^2} \mathbf{B} \times \nabla B \cdot \nabla_\perp + \frac{4\pi v_\parallel^2}{\Omega_{ca} B^2} \mathbf{b} \times \nabla p \cdot \nabla_\perp + \frac{2 v_\parallel \omega_0}{\Omega_{ca}} \mathbf{b} \times \mathbf{s} \cdot \nabla_\perp \,, \tag{1.29}$$

Perpendicular Laplacian: $$\nabla_\perp^2 = (\nabla - \mathbf{b}\mathbf{b} \cdot \nabla)^2 \,, \tag{1.30}$$

Radial gradient of eikonal: $$\frac{\nabla\psi}{|\nabla\psi|} \cdot \nabla\alpha = \frac{\nabla\psi \cdot \nabla\nu}{|\nabla\psi|} \,, \tag{1.31}$$

Binormal gradient of eikonal: $$\mathbf{b} \times \frac{\nabla\psi}{|\nabla\psi|} \cdot \nabla\alpha = -\frac{B}{|\nabla\psi|} \,, \tag{1.32}$$

Parallel gradient: $$\mathbf{b} \cdot \nabla = \frac{1}{\mathcal{J}_\psi B} \frac{\partial}{\partial\theta} \,, \tag{1.33}$$

Flux-surface average: $$\langle f \rangle = \left(\frac{dV}{d\psi}\right)^{-1} \oint d\theta \, d\varphi \, \mathcal{J}_\psi f \,. \tag{1.34}$$

The perpendicular drift operator, Eq. (1.29), is a sum of curvature and grad-B terms. This particular form, which neglects the parallel part of the drift response (see, for example, Eq. (54) of Ref. [HW06] or Eq. (12) of Ref. [BC08]), is sufficient to recover all standard results of gyrokinetic and neoclassical theory. In Eq. (1.34), $\langle f \rangle$ denotes the flux-surface average of the function f, and

$$\frac{dV}{d\psi} = \oint d\theta \, d\varphi \, \mathcal{J}_\psi \,, \tag{1.35}$$

where V is the volume enclosed by the flux surface. In the drift velocity, $\mathbf{s}$ is the following dimensionless vector

$$\mathbf{s} = \frac{1}{\mathcal{J}_\psi B} \frac{\partial R}{\partial\theta} \mathbf{e}_\varphi - \frac{I}{RB} \nabla R \,. \tag{1.36}$$

which is discussed in more detail later.

1.3.2 Metric coefficients

Define a right-handed Cartesian coordinate system (x, y, z) via intermediate (R, Z, φ) coordinates as

$$x = R(r, \theta)\cos(-\varphi) \,, \tag{1.37}$$
$$y = R(r, \theta)\sin(-\varphi) \,, \tag{1.38}$$
$$z = Z(r, \theta) \,. \tag{1.39}$$

In this geometry the covariant basis vectors are

$$\hat{\mathbf{e}}_r \doteq \frac{\partial \mathbf{r}}{\partial r} \quad , \qquad \hat{\mathbf{e}}_\theta \doteq \frac{\partial \mathbf{r}}{\partial \theta} \qquad \text{and} \qquad \hat{\mathbf{e}}_\varphi \doteq \frac{\partial \mathbf{r}}{\partial \varphi} \,, \tag{1.40}$$

where $\mathbf{r} = (x, y, z)$. The corresponding contravariant basis vectors are

$$\hat{\mathbf{e}}^r \doteq \nabla r \quad , \qquad \hat{\mathbf{e}}^\theta \doteq \nabla \theta \qquad \text{and} \qquad \hat{\mathbf{e}}^\varphi \doteq \nabla \varphi \,. \tag{1.41}$$

With this information we can write the covariant and contravariant components of the metric tensor g as $g_{ij} = \hat{\mathbf{e}}_i \cdot \hat{\mathbf{e}}_j$ and $g^{ij} = \hat{\mathbf{e}}^i \cdot \hat{\mathbf{e}}^j$. It is illustrative to write this in matrix form as

$$g_{ij} = \begin{pmatrix} g_{rr} & g_{r\theta} & 0 \\ g_{r\theta} & g_{\theta\theta} & 0 \\ 0 & 0 & g_{\varphi\varphi} \end{pmatrix} \,, \tag{1.42}$$

where

$$g_{rr} = \left(\frac{\partial R}{\partial r}\right)^2 + \left(\frac{\partial Z}{\partial r}\right)^2 \,, \tag{1.43}$$
$$g_{r\theta} = \frac{\partial R}{\partial r}\frac{\partial R}{\partial \theta} + \frac{\partial Z}{\partial r}\frac{\partial Z}{\partial \theta} \,, \tag{1.44}$$
$$g_{\theta\theta} = \left(\frac{\partial R}{\partial \theta}\right)^2 + \left(\frac{\partial Z}{\partial \theta}\right)^2 \,. \tag{1.45}$$
$$g_{\varphi\varphi} = R^2 \tag{1.46}$$

Since we also know that $g_{ij} \cdot g^{ij} = I$, where I is the identity matrix, we can easily determine the contravariant counterpart by calculating the inverse of g_{ij}. This yields

$$g^{ij} = \frac{1}{\mathcal{J}_r^2} \begin{pmatrix} g_{\theta\theta} g_{\varphi\varphi} & -g_{r\theta} g_{\varphi\varphi} & 0 \\ -g_{r\theta} g_{\varphi\varphi} & g_{rr} g_{\varphi\varphi} & 0 \\ 0 & 0 & g_{rr} g_{\theta\theta} - g_{r\theta}^2 \end{pmatrix} \tag{1.47}$$
$$= \begin{pmatrix} (\nabla r)^2 & \nabla r \cdot \nabla \theta & 0 \\ \nabla r \cdot \nabla \theta & (\nabla \theta)^2 & 0 \\ 0 & 0 & (\nabla \varphi)^2 \end{pmatrix} \,. \tag{1.48}$$

Here, the Jacobians are

$$\mathcal{J}_r \doteq \frac{\partial(x, y, z)}{\partial(r, \theta, \varphi)} = \frac{\partial \psi}{\partial r}\mathcal{J}_\psi \quad \text{and} \quad \mathcal{J}_\psi \doteq \frac{\partial(x, y, z)}{\partial(\psi, \theta, \varphi)} \,, \tag{1.49}$$

where explicitly

$$\mathcal{J}_r = \det g_{ij} = R\left(\frac{\partial R}{\partial r}\frac{\partial Z}{\partial \theta} - \frac{\partial R}{\partial \theta}\frac{\partial Z}{\partial r}\right) > 0 \; . \tag{1.50}$$

Metric coefficients can then be computed straightforwardly. For example,

$$|\nabla r| = g_{\theta\theta}^{1/2}\left[\frac{\partial R}{\partial r}\frac{\partial Z}{\partial \theta} - \frac{\partial R}{\partial \theta}\frac{\partial Z}{\partial r}\right]^{-1} \; . \tag{1.51}$$

1.3.3 Mercier-Luc coordinates

Consider a reference flux surface $\psi = \psi_s$ and the corresponding one-dimensional curve $\mathbf{x}(\ell) = (R_s, Z_s)$ defined by the intersection of that surface and the plane $\varphi = 0$. If we choose ℓ to be the arc length along $\mathbf{x}$, then the tangent vector

$$\mathbf{t} \doteq \frac{d\mathbf{x}}{d\ell} = \left(\frac{dR_s(\ell)}{d\ell}, \frac{dZ_s(\ell)}{d\ell}\right) \tag{1.52}$$

is a unit vector. We can further define the unit tangent and unit (inward) normal vectors in terms of a *frame angle* u [Gug77] as

$$\mathbf{t} \doteq (-\sin u, \cos u) \quad \text{and} \quad \mathbf{n} \doteq (-\cos u, -\sin u) \; . \tag{1.53}$$

This definition of the frame angle is different than that used in Ref. [MCG+98] and [WM99]. We believe the present convention is the natural choice, since in the circular limit we have $u = \theta$ and $\ell = r\theta$. The radius of curvature, r_c, satisfies the equation

$$\frac{d\mathbf{t}}{d\ell} = \frac{\mathbf{n}}{r_c} \quad \text{so that} \quad \frac{1}{r_c(\ell)} = \frac{du}{d\ell} \; . \tag{1.54}$$

Some algebra shows that the curvature can be written as

$$r_c(\theta) = g_{\theta\theta}^{3/2}\left(\frac{\partial R}{\partial \theta}\frac{\partial^2 Z}{\partial \theta^2} - \frac{\partial Z}{\partial \theta}\frac{\partial^2 R}{\partial \theta^2}\right)^{-1} \; . \tag{1.55}$$

Following Mercier and Luc [ML74], we introduce a right-handed, orthogonal coordinate system (ϱ, ℓ, φ) which is defined in relation to the reference flux surface $\psi = \psi_s$ through

$$R(r,\theta) = R_s(\ell) + \varrho\cos u \; , \tag{1.56}$$

$$Z(r,\theta) = Z_s(\ell) + \varrho\sin u \; . \tag{1.57}$$

The orientations of ℓ and u are shown in Fig. 1.2. The metric tensor in this case is diagonal, with

$$g_{\varrho\varrho} = 1 \; , \tag{1.58}$$

$$g_{\ell\ell} = \left(1 + \frac{\varrho}{r_c}\right)^2 \; , \tag{1.59}$$

$$g_{\varphi\varphi} = R^2 \; . \tag{1.60}$$

The Jacobian is

$$\mathcal{J}_\varrho = \frac{\partial(x,y,z)}{\partial(\varrho,\ell,\varphi)} = \frac{1}{\nabla\varrho\times\nabla\ell\cdot\nabla\varphi} = R\left(1 + \frac{\varrho}{r_c}\right) > 0 \; . \tag{1.61}$$

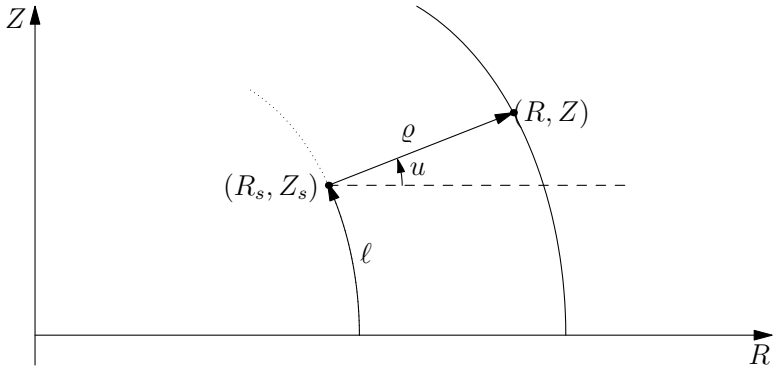

Figure 1.2: Mercier-Luc coordinate system.

By differentiating Eqs. (1.56) and (1.57) with respect to r, and evaluating the result at $\varrho = 0$, we obtain the following identities valid *on the surface* $\psi = \psi_s$:

$$\left.\frac{\partial \rho}{\partial r}\right|_{\psi=\psi_s} = \cos u \, \frac{\partial R}{\partial r} + \sin u \, \frac{\partial Z}{\partial r} \, , \tag{1.62}$$

$$\left.\frac{\partial \ell}{\partial r}\right|_{\psi=\psi_s} = \cos u \, \frac{\partial Z}{\partial r} - \sin u \, \frac{\partial R}{\partial r} \, . \tag{1.63}$$

Differentiation with respect to θ yields

$$\left.\frac{\partial \rho}{\partial \theta}\right|_{\psi=\psi_s} = 0 \, , \tag{1.64}$$

$$\left.\frac{\partial \ell}{\partial \theta}\right|_{\psi=\psi_s} = \sqrt{\left(\frac{\partial Z}{\partial \theta}\right)^2 + \left(\frac{\partial R}{\partial \theta}\right)^2} = \sqrt{g_{\theta\theta}} \, . \tag{1.65}$$

On the surface, the Jacobian is equal to

$$\mathcal{J}_r = \frac{R}{|\nabla r|} \frac{\partial \ell}{\partial \theta} \, . \tag{1.66}$$

1.3.4 Solution of the Grad-Shafranov equation

The solution of Grad-Shafranov equation determines the poloidal flux, ψ, as a function of sources f and p:

$$R^2 \, \nabla \cdot \left(\frac{\nabla \psi}{R^2} \right) = -4\pi R^2 p'(\psi) - II'(\psi) \, . \tag{1.67}$$

The lefthand side can be written as

$$R^2 \, \nabla \cdot \left(\frac{\nabla \psi}{R^2} \right) = \nabla^2 \psi - \frac{2}{R} \, \nabla R \cdot \nabla \psi \, . \tag{1.68}$$

We wish to obtain a solution valid in a neighborhood of $\varrho = 0$ and so expand

$$\psi = \psi_s + \psi_1(\ell) \, \varrho + \psi_2(\ell) \, \varrho^2 + \cdots \, . \tag{1.69}$$

The required operators can then be evaluated to leading order in ϱ as

$$\nabla R = \frac{1}{h_\varrho}\frac{\partial R}{\partial \varrho}\,\hat{\mathbf{e}}_\varrho + \frac{1}{h_\ell}\frac{\partial R}{\partial \ell}\,\hat{\mathbf{e}}_\ell \sim \hat{\mathbf{e}}_\varrho\,\cos u - \hat{\mathbf{e}}_\ell\,\sin u + \mathcal{O}(\varrho)\;, \tag{1.70}$$

$$\nabla \psi = \frac{1}{h_\varrho}\frac{\partial \psi}{\partial \varrho}\,\hat{\mathbf{e}}_\varrho + \frac{1}{h_\ell}\frac{\partial \psi}{\partial \ell}\,\hat{\mathbf{e}}_\ell \sim \psi_1\,\hat{\mathbf{e}}_\varrho + \mathcal{O}(\varrho)\;, \tag{1.71}$$

$$\nabla^2 \psi = \frac{1}{h_\varrho h_\ell h_\varphi}\left[\frac{\partial}{\partial \varrho}\left(\frac{h_\ell h_\varphi}{h_\varrho}\frac{\partial \psi}{\partial \varrho}\right) + \frac{\partial}{\partial \ell}\left(\frac{h_\varrho h_\varphi}{h_\ell}\frac{\partial \psi}{\partial \varrho}\right)\right]\;, \tag{1.72}$$

$$\sim \frac{\partial^2 \psi}{\partial \varrho^2} + \frac{\partial \psi}{\partial \varrho}\frac{1}{h_\ell h_\varphi}\frac{\partial}{\partial \rho}\left(h_\ell h_\varphi\right) + \mathcal{O}(\varrho)\;, \tag{1.73}$$

where $h_i \doteq \sqrt{g_{ii}}$. Combining these results gives

$$R^2\,\nabla\cdot\left(\frac{\nabla\psi}{R^2}\right) \sim \frac{\psi_1}{r_c} - \frac{\psi_1}{R_s}\cos u + 2\psi_2 + \mathcal{O}(\varrho)\;. \tag{1.74}$$

The solution for ψ_1 is obtained from

$$B_p^2 = |\nabla\varphi|^2\,|\nabla\psi|^2 \sim \frac{1}{R_s^2}\left(\frac{\partial\psi}{\partial\rho}\right)^2 + \mathcal{O}(\varrho)\;, \tag{1.75}$$

from which it is evident that

$$\psi_1 = R_s B_{ps}\;, \tag{1.76}$$

where $B_{ps} = B_p(\psi_s)$. The solution of the Grad-Shafranov equation then gives an explicit expression for ψ_2:

$$\psi_2 = \frac{1}{2}\left(B_p\cos u - \frac{B_p R}{r_c} - 4\pi R^2 p' - I I'\right)_{\psi=\psi_s}\;. \tag{1.77}$$

1.3.5 Magnetic field derivatives

We can start with the exact expressions

$$B_p^2 = \frac{1}{R^2}\left[\left(\frac{\partial\psi}{\partial\varrho}\right)^2 + \left(\frac{1}{h_\ell}\frac{\partial\psi}{\partial\ell}\right)^2\right]\;, \tag{1.78}$$

$$B_t^2 = \left(\frac{f(\psi)}{R}\right)^2\;. \tag{1.79}$$

Expanding the poloidal flux gives

$$R^2\,B_t^2 \;\sim I_s^2 + 2\varrho\psi_1 I_s I_s' + \mathcal{O}(\varrho^2)\;, \tag{1.80}$$

$$R^2\,B_p^2 \;\sim \psi_1^2 + 4\varrho\psi_1\psi_2 + \mathcal{O}(\varrho^2)\;, \tag{1.81}$$

where $I_s = I(\psi_s)$. Expanding R and taking derivatives gives

$$\frac{\partial}{\partial\varrho}B_t^2 \;\sim \frac{1}{R_s^2}\left(-2\,\frac{I_s^2}{R_s}\cos u + 2 I_s I_s'\psi_1\right)\;, \tag{1.82}$$

$$\frac{\partial}{\partial\varrho}B_p^2 \;\sim \frac{1}{R_s^2}\left(-2\,\frac{\psi_1^2}{R_s}\cos u + 4\psi_1\psi_2\right)\;. \tag{1.83}$$

Adding these contributions together gives, finally:

$$\frac{\partial}{\partial\varrho}B^2 \sim \left(-2\,\frac{f^2}{R^3}\cos u - 2\,\frac{B_p^2}{r_c} - 8\pi R B_p p'\right)_{\psi=\psi_s} . \tag{1.84}$$

1.3.6 Calculation of the eikonal function

In order to compute radial derivatives required for the evaluation of the drift and Laplacian, we need to determine the radial dependence of ν. Using the expansion, Eq. (1.69), for the poloidal flux, together with the eikonal expansion

$$\nu = \nu_s + \nu_1(\ell)\,\varrho + \cdots , \tag{1.85}$$

we solve the equation

$$\nabla\nu \times \nabla\psi = f\nabla\varphi \tag{1.86}$$

order-by-order in ϱ. First, an expansion of the gradients yields

$$\nabla\psi \ \sim (\psi_1 + 2\varrho\psi_2)\,\nabla\varrho + \varrho\frac{\partial\psi_1}{\partial\ell}\nabla\ell + \mathcal{O}(\varrho^2) , \tag{1.87}$$

$$\nabla\nu \ \sim \nu_1\nabla\varrho + \left(\frac{\partial\nu_s}{\partial\ell} + \varrho\frac{\partial\nu_1}{\partial\ell}\right)\nabla\ell + \mathcal{O}(\varrho^2) . \tag{1.88}$$

Replacing these formulae into Eq. (1.86) and dotting with $\nabla\varphi$ yields

$$-\frac{\partial\nu_s}{\partial\ell}\psi_1 + \varrho\left(\nu_1\frac{\partial\psi_1}{\partial\ell} - \frac{\partial\nu_1}{\partial\ell}\psi_1 - 2\frac{\partial\nu_s}{\partial\ell}\psi_2\right) \sim \frac{I_s + \varrho I_s'\psi_1}{R_s + \varrho\cos u}\left(1 + \frac{\varrho}{r_c}\right) . \tag{1.89}$$

At each order in ϱ, we have

$$\mathcal{O}(1): \quad -\frac{\partial\nu_s}{\partial\ell}\psi_1 = \frac{I_s}{R_s} , \tag{1.90}$$

$$\mathcal{O}(\varrho): \quad -\psi_1\frac{\partial}{\partial\ell}\left(\frac{\nu_1}{\psi_1}\right) = 2\,\frac{\partial\nu_s}{\partial\ell}\,\frac{\psi_2}{\psi_1} + \frac{I_s'}{R_s} + \frac{I_s}{R_s r_c\psi_1} - \frac{I_s\cos u}{R_s^2\psi_1} . \tag{1.91}$$

Thus, the solution for ν_s is

$$\nu_s(\ell) = -\int_0^\ell \frac{d\ell'}{R_s^2 B_{ps}}\,I_s . \tag{1.92}$$

Some additional algebra shows that

$$\nu_1(\ell) = R_s(\ell)B_{ps}(\ell)\left[D_0(\ell) + D_1(\ell)\,II' + D_2(\ell)\,p'\right] , \tag{1.93}$$

where the D_i integrals are:

$$D_0 = -\int_0^\ell \frac{d\ell'}{R_s^2 B_{ps}}\left(\frac{2}{r_c R_s B_{ps}} - \frac{2\cos u}{R_s^2 B_{ps}}\right) I_s \tag{1.94}$$

$$D_1 = -\int_0^\ell \frac{d\ell'}{R_s^2 B_{ps}}\left(\frac{B^2}{B_{ps}^2}\right)\frac{1}{I_s} , \tag{1.95}$$

$$D_2 = -\int_0^\ell \frac{d\ell'}{R_s^2 B_{ps}}\left(\frac{4\pi}{B_{ps}^2}\right) I_s . \tag{1.96}$$

We want to eliminate II' in favour of q'. Writing $\ell(2\pi) \doteq L$, and expanding Eq. (1.6), we find

$$-2\pi(q_s + q_s'\varrho\psi_1) \sim \nu_s(L) + \varrho\nu_1(L) + \mathcal{O}(\varrho^2) \,. \tag{1.97}$$

Therefore, we have the connection

$$-2\pi\, q_s' = D_0(L) + D_1(L)\, II' + D_2(L)\, p' \,. \tag{1.98}$$

1.3.7 Gyrokinetic drift velocity in Mercier-Luc coordinates

In this case, we work out the dominant part of the drift operator acting on a function $f(\psi, \theta, \alpha)$. This limit is appropriate for standard gyrokinetics. We proceed by simplifying Eq. (1.29) in the Miller equilibrium case by beginning from the Mercier-Luc representation. On the surface $\psi = \psi_s$ we have

$$\mathbf{B}_s = B_{ps}\nabla\ell + I_s\nabla\varphi \,. \tag{1.99}$$

Note that Eq. (1.99) cannot be used to obtain $\partial B/\partial\psi$ because the limit $\varrho \to 0$ has already been taken. To evaluate ∇B, we must write

$$\nabla B = \frac{\partial B}{\partial \varrho}\nabla\varrho + \frac{\partial B}{\partial \ell}\nabla\ell \,, \tag{1.100}$$

and then make use of Eq. (1.84). Taking the cross product of the above two quantities gives

$$\mathbf{B}_s \times \nabla B = -B_{ps}\frac{\partial B}{\partial \varrho}\nabla\varrho \times \nabla\ell + I_s\frac{\partial B}{\partial \varrho}\nabla\varphi \times \nabla\varrho + I_s\frac{\partial B}{\partial \ell}\nabla\varphi \times \nabla\ell \,. \tag{1.101}$$

Then, the perpendicular gradient operator, accurate to $\mathcal{O}(\varrho)$, can be written as

$$\nabla_\perp \sim \nabla\varrho\,\frac{\partial}{\partial\varrho} + \left(\nabla\varphi + \frac{\partial\nu_s}{\partial\ell}\,\nabla\ell + \nu_1\nabla\varrho + \mathcal{O}(\varrho)\right)\frac{\partial}{\partial\alpha} \,. \tag{1.102}$$

The final result, valid on the surface $\psi = \psi_s$, is

$$\mathbf{B} \times \nabla B \cdot \nabla = -I_s B_{ps}\,\frac{\partial B}{\partial \ell}\frac{\partial}{\partial\psi} + \left(-\frac{B^2}{R_s B_{ps}}\frac{\partial B}{\partial\varrho} - \frac{I_s\nu_1}{R_s}\frac{\partial B}{\partial\ell}\right)\frac{\partial}{\partial\alpha} \,. \tag{1.103}$$

1.3.8 Perpendicular Laplacian in Mercier-Luc coordinates

To evaluate the perpendicular Laplacian, we square Eq. (1.102) and simplify, where it is sufficiently accurate to ignore variation of coefficients

$$\nabla_\perp^2 \sim \frac{\partial^2}{\partial\varrho^2} + 2\nu_1\frac{\partial}{\partial\varrho}\frac{\partial}{\partial\alpha} + \left[\frac{1}{R^2} + \nu_1^2 + \left(\frac{\partial\nu_0}{\partial\ell}\right)^2\right]\frac{\partial^2}{\partial\alpha^2} \,. \tag{1.104}$$

1.3.9 Coriolis drift terms

Some algebra show that

$$\mathbf{b} \times \mathbf{s} \cdot \nabla_\perp = -\sin u\frac{\partial}{\partial\rho} + \left(\frac{I}{R^2 B_p}\cos u - \nu_1 \sin u\right)\frac{\partial}{\partial\alpha} \,, \tag{1.105}$$

where we have used the relation

$$\sin u = -\frac{\partial R}{\partial\theta}\left(\frac{\partial\ell}{\partial\theta}\right)^{-1} \,. \tag{1.106}$$

1.3.10 Detailed catalogue of shape functions

For convenience, we give a complete summary of the equations needed to compute all the relevant shape functions. In the expressions below, R and Z are taken to be functions of r and θ, and the subscript s can be safely omitted.

$$\frac{\partial \ell}{\partial \theta} = \sqrt{\left(\frac{\partial R}{\partial \theta}\right)^2 + \left(\frac{\partial Z}{\partial \theta}\right)^2} \,, \tag{1.107}$$

$$\mathcal{J}_r = R\left(\frac{\partial R}{\partial r}\frac{\partial Z}{\partial \theta} - \frac{\partial R}{\partial \theta}\frac{\partial Z}{\partial r}\right) \,, \tag{1.108}$$

$$|\nabla r| = \frac{R}{\mathcal{J}_r}\frac{\partial \ell}{\partial \theta} \,, \tag{1.109}$$

$$r_c(\theta) = \left(\frac{\partial \ell}{\partial \theta}\right)^3 \left(\frac{\partial R}{\partial \theta}\frac{\partial^2 Z}{\partial \theta^2} - \frac{\partial Z}{\partial \theta}\frac{\partial^2 R}{\partial \theta^2}\right)^{-1} \,, \tag{1.110}$$

$$\frac{f(r)}{B_{\rm unit}} = 2\pi\, r \left(\int_0^L \frac{d\ell'}{R|\nabla r|}\right)^{-1} \,, \tag{1.111}$$

$$\frac{B_t(r,\theta)}{B_{\rm unit}(r)} = \frac{f}{RB_{\rm unit}} \,, \tag{1.112}$$

$$\frac{B_p(r,\theta)}{B_{\rm unit}(r)} = \frac{r}{R}\frac{|\nabla r|}{q} \,, \tag{1.113}$$

$$\frac{B(r,\theta)}{B_{\rm unit}(r)} = {\rm sgn}(B_{\rm unit})\sqrt{\left(\frac{B_p}{B_{\rm unit}}\right)^2 + \left(\frac{B_t}{B_{\rm unit}}\right)^2} \,, \tag{1.114}$$

$${\rm gsin}(r,\theta) \doteq \frac{B_t}{B}\left(\frac{R_0}{B}\frac{\partial B}{\partial \ell}\right) \,, \tag{1.115}$$

$${\rm gcos}(r,\theta) \doteq -\frac{R_0}{B}\frac{\partial B}{\partial \varrho} = {\rm gcos}_1 + {\rm gcos}_2 \,, \tag{1.116}$$

$${\rm gcos}_1(r,\theta) = \frac{B_t^2}{B^2}\frac{R_0}{R}\cos u + \frac{B_p^2}{B^2}\frac{R_0}{r_c} \,, \tag{1.117}$$

$${\rm gcos}_2(r,\theta) = -\frac{1}{2}\frac{B_{\rm unit}^2}{B^2}R_0\,|\nabla r|\,\beta^* \,, \tag{1.118}$$

$${\rm usin}(r,\theta) = \sin u \,, \tag{1.119}$$

$${\rm ucos}(r,\theta) = \frac{B_t}{B}\cos u \,, \tag{1.120}$$

$$E_1(r,\theta) = 2\int_0^{\ell(\theta)} \frac{d\ell'}{R|\nabla r|}\frac{B_t}{B_p}\left(\frac{r}{r_c} - \frac{r}{R}\cos u\right) \tag{1.121}$$

$$E_2(r,\theta) = \int_0^{\ell(\theta)} \frac{d\ell'}{R|\nabla r|}\left(\frac{B^2}{B_p^2}\right) \,, \tag{1.122}$$

$$E_3(r,\theta) = \frac{1}{2}\int_0^{\ell(\theta)} \frac{d\ell'}{R}\frac{B_t}{B_p}\left(\frac{B_{\rm unit}^2}{B_p^2}\right) , \tag{1.123}$$

$$f^*(r) = \frac{1}{E_2(r,2\pi)}\left[2\pi\frac{qs}{r} - \frac{1}{r}E_1(r,2\pi) + \beta^* E_3(r,2\pi)\right] \tag{1.124}$$

$$\Theta(r,\theta) \doteq -\left(\frac{RB_p}{B}\right)\nu_1 = \frac{RB_p}{B}|\nabla r|\left(\frac{1}{r}E_1 + f^* E_2 - \beta^* E_3\right) \tag{1.125}$$

$$G_q(r,\theta) \doteq \frac{1}{q}\left(\frac{rB}{RB_p}\right) , \tag{1.126}$$

$$G_\theta(r,\theta) \doteq \frac{\mathcal{J}_\psi B}{qR_0} = \frac{B}{B_{\rm unit}}\frac{R}{R_0}\frac{1}{r|\nabla r|}\frac{\partial \ell}{\partial\theta} . \tag{1.127}$$

1.3.11 Required operators in terms of shape functions

Perpendicular drift:

$$\begin{aligned}\mathbf{v}_d\cdot\nabla_\perp = {} & -ik_\theta G_q\left(\frac{v_\parallel^2+\mu B}{\Omega_{ca}R_0}\right)\,[\mathrm{gcos}_1 + \mathrm{gcos}_2 + \Theta\,\mathrm{gsin}] \\ & + ik_\theta G_q\left(\frac{v_\parallel^2}{\Omega_{ca}R_0}\right)\,\mathrm{gcos}_2 - \left(\frac{v_\parallel^2+\mu B}{\Omega_{ca}R_0}\right)|\nabla r|\,\mathrm{gsin}\,\frac{\partial}{\partial r} , \\ -ik_\theta G_q\left(\frac{2v_\parallel\omega_0 R_0}{\Omega_{ca}R_0}\right)\,[\mathrm{ucos} + \Theta\,\mathrm{usin}] & - \left(\frac{2v_\parallel\omega_0 R_0}{\Omega_{ca}R_0}\right)|\nabla r|\,\mathrm{usin}\,\frac{\partial}{\partial r} ,\end{aligned} \tag{1.128}$$

Perpendicular Laplacian:

$$\nabla_\perp^2 = |\nabla r|^2\frac{\partial^2}{\partial r^2} + 2i\Theta k_\theta G_q|\nabla r|\frac{\partial}{\partial r} - k_\theta^2 G_q^2\left(1+\Theta^2\right) , \tag{1.129}$$

Radial gradient of eikonal:
$$n\frac{\nabla\psi}{|\nabla\psi|}\cdot\nabla\alpha = -k_\theta G_q\Theta , \tag{1.130}$$

Binormal gradient of eikonal:
$$n\,\mathbf{b}\times\frac{\nabla\psi}{|\nabla\psi|}\cdot\nabla\alpha = -k_\theta G_q , \tag{1.131}$$

Parallel gradient:
$$\mathbf{b}\cdot\nabla = \frac{1}{G_\theta}\frac{1}{qR_0}\frac{\partial}{\partial\theta} , \tag{1.132}$$

Flux-surface average:
$$\langle f\rangle = \frac{\displaystyle\int_0^{2\pi} d\theta\,\frac{G_\theta}{B}\,f(\theta)}{\displaystyle\int_0^{2\pi} d\theta\,\frac{G_\theta}{B}} . \tag{1.133}$$

Above, we have introduced the binormal wavenumber, $k_\theta = i(q/r)\partial/\partial\alpha$.

1.3.12 Pressure-gradient effects in the drift velocity

In cases where compressional magnetic perturbations are neglected, one may also wish to ignore finite-pressure effects in the drift velocity [WM99]. This is done by setting $\mathrm{gcos}_2 = 0$ in Eq. (1.128).

1.4 Specification of the plasma shape

It is assumed throughout that we have access to a global equilibrium for which the poloidal and toroidal fluxes are known over the entire range of r. Then, we consider two general ways in which to specify the plasma shape via a closed contour in the (R, Z) plane: (1) a model parameterization, and (2) a general Fourier expansion.

In addition to the plasma shape, we also need to know the plasma pressure gradient, which we will define via the effective inverse beta-gradient scale length:

$$\beta^*(r) \doteq -\frac{8\pi}{B_{\rm unit}^2}\frac{\partial p}{\partial r} > 0 \; . \tag{1.134}$$

The safety factor $q = d\psi/d\chi_t$ and the magnetic shear $s = (r/q)dq/dr$ can be obtained directly via numerical differentiation.

1.4.1 Model flux-surface shape

A popular model for the flux-surface shape in (R, Z) coordinates was introduced by Miller [MCG+98]. We generalize that model to include the effects of elevation and squareness. In particular, finite elevation is required very close to $r = 0$, where the flux surface may lie entirely above the midplane at $Z = 0$. Specifically, let

$$R(r,\theta) = R_0(r) + r\cos(\theta + \arcsin\delta\sin\theta) \; , \tag{1.135}$$

$$Z(r,\theta) = Z_0(r) + \kappa(r) r \sin(\theta + \zeta\sin 2\theta) \; , \tag{1.136}$$

where κ is the elongation, δ is the triangularity, ζ is the squareness and Z_0 is the elevation [TLLM+99]. In order to evaluate the required quantities $\partial R/\partial r$ and $\partial Z/\partial r$, we also need to know the radial derivatives of R_0, Z_0, δ, κ and ζ. To this end, we define the associated shape functions

$$s_\kappa \doteq \frac{r}{\kappa}\frac{\partial\kappa}{\partial r} \; , \quad s_\delta \doteq r\frac{\partial\delta}{\partial r} \; , \quad s_\zeta \doteq r\frac{\partial\zeta}{\partial r} \; . \tag{1.137}$$

Note that this definition of s_δ differs slightly from Refs. [MCG+98] and [WM99]. Thus, to compute the shape functions for the flux-surface at r according to this model, we require the 10 parameters

$$\left\{R_0, \frac{dR_0}{dr}, Z_0, \frac{dZ_0}{dr}, \kappa, s_\kappa, \delta, s_\delta, \zeta, s_\zeta\right\} \; . \tag{1.138}$$

1.4.2 General flux-surface shape

In this case the flux-surface shape is an expansion of the form

$$R(r,\theta) = \frac{1}{2}a_0^R(r) + \sum_{n=1}^{N}\left[a_n^R(r)\cos(n\theta) + b_n^R(r)\sin(n\theta)\right] \; , \tag{1.139}$$

$$Z(r,\theta) = \frac{1}{2}a_0^Z(r) + \sum_{n=1}^{N}\left[a_n^Z(r)\cos(n\theta) + b_n^Z(r)\sin(n\theta)\right] \; . \tag{1.140}$$

Here, N is an integer which evidently controls the accuracy of the expansion, and is in principle arbitrary. If (R, Z) are known as functions of arc length, then one can simply set $\theta = 2\pi\ell/L$. To compute the shape functions for the flux-surface at r, we require the $8(N+1)$ parameters

$$\left\{ a_n^R, b_n^R, a_n^Z, b_n^Z, \frac{da_n^R}{dr}, \frac{db_n^R}{dr}, \frac{da_n^Z}{dr}, \frac{db_n^Z}{dr} \right\} . \tag{1.141}$$

1.4.3 A measure of the error

It is beyond the scope of the present paper to give a detailed assessement of the error in neoclassical or turbulent transport calculations caused by errors in the flux-surface shape. Nevertheless, we can define the error in the flux-surface approximation of the discrete data $\{R_i, Z_i\}_{i=1}^{n_d}$ as

$$\varepsilon \doteq \frac{1}{n_d\, r} \sum_{i=1}^{n_d} \min_{\theta} \sqrt{[R(\theta) - R_i]^2 + [Z(\theta) - Z_i]^2} \, . \tag{1.142}$$

Figure 1.3 shows the flux-surface fitting error for DIII-D discharge 132010. This discharge is part of a series of experiments designed to accurately measure profiles across the entire confined plasma, including the edge barrier region. Discharge 132010 is a standard DIII-D H-mode plasma, with typical values of the magnetic field ($B_t = 2.1T$), current ($I_p = 1.2MA$), elongation ($\kappa = 1.8$) and triangularity ($\delta = 0.3$). The width of the edge barrier ($\sim 3\%$ in r/a), height of the edge barrier ($\sim 11kPa$), and global pressure ($\beta_N \sim 2$) are all fairly typical of DIII-D H-Modes. The Grad-Shafranov equillbrium was computed by EFIT using a 129×129 mesh, and then mapped to very-high-resolution (R, Z)-contours (400 flux surfaces, each with 512 points equally-spaced in arc length along the surface) using the ELITE code. The Miller-type model equilibrium is seen to be significantly less accurate, according to the metric defined in Eq. 1.142, at all radii than even the $N = 4$ Fourier expansion (red curve). The $N = 8$ (solid black curve) and $N = 12$ (green curve) results are also shown. In the region $r/a < 0.4$, the accuracy of the Fourier expansion probably exceeds the accuracy of the original equilibrium solution, and is therefore limited by it. This result shows that $N > 12$ is probably a good default choice for N. A further comparison of actual flux surface shapes at $r/a = 0.99$ (i.e., very close to the separatrix) is shown in Fig. 1.4.

For core plasma parameters, our limited experience is that the difference, with respect to linear growth rates, between general and model flux-surfaces is insignificant in moderately-shaped DIII-D plasmas (roughly 5% at $r/a = 0.9$, and less than that deeper in the core). However, this relies on the accuracy of the fitting procedure used to obtain the model parameters κ, δ, etc. If the model flux-surface shape is poorly calculated, the absolute error can be significant.

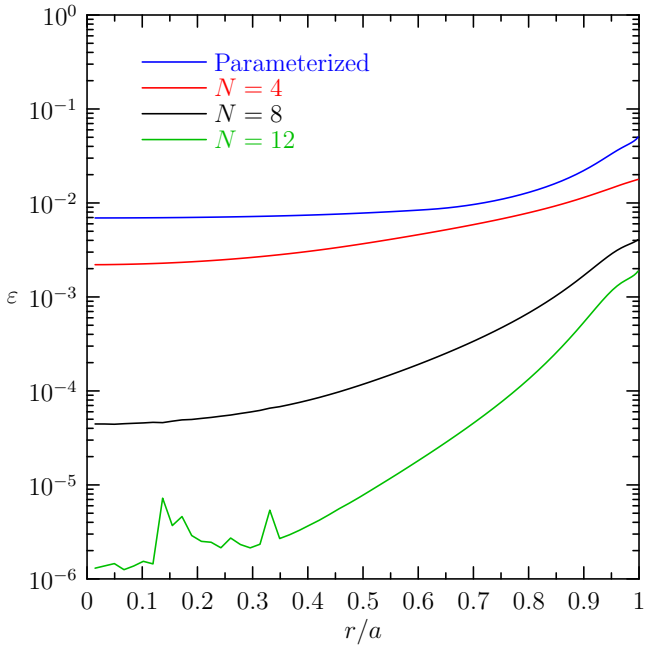

Figure 1.3: Error, ε, in the flux-surface fits for DIII-D discharge 132010. The Miller-type model equilibrium is seen to be significantly less accurate at all radii than even the $N = 4$ Fourier expansion (red curve). The $N = 8$ (solid black curve) and $N = 12$ (green curve) results are also shown. In the region $r/a < 0.4$, the accuracy of the Fourier expansion probably exceeds the accuracy of the original equilibrium solution, and is therefore limited by it.

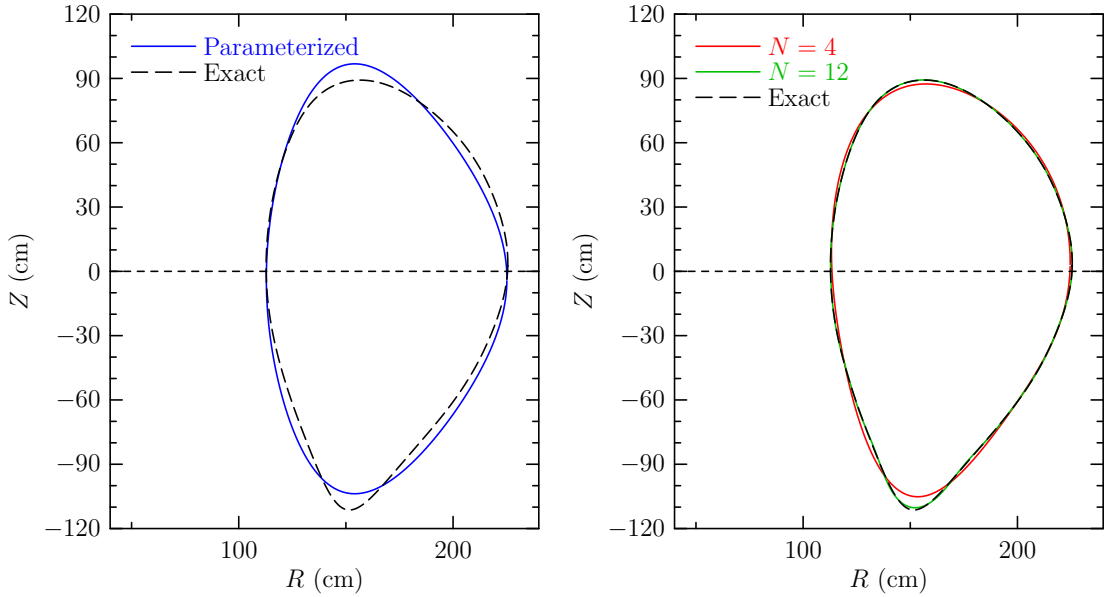

Figure 1.4: Comparison of exact flux-surface (dashed curve) to parameterized (left) and general Fourier expansion (right) at $r/a = 0.99$.

Appendix A: Large-aspect-ratio expansion

Consider a shifted-circle (Shafranov) flux-surface shape:

$$R(r,\theta) = R_0 + \Delta(r) + r\cos\theta \,, \tag{1.143}$$

$$Z(r,\theta) = r\sin\theta \,. \tag{1.144}$$

Let $\Delta(r) = ar^2/(2R_0)$ be the Shafranov shift, with a an $\mathcal{O}(1)$ constant, so that $\partial\Delta/\partial r = a\,(r/R_0)$. It is instructive to calculate the shape functions as Taylor series in the small parameter r/R_0. To first order in r/R_0, we find

$$|\nabla r| \sim 1 - a\,\frac{r}{R_0}\cos\theta \,, \tag{1.145}$$

$$\frac{B_t(r,\theta)}{B_{\rm unit}(r)} \sim 1 - \frac{r}{R_0}\cos\theta \,, \tag{1.146}$$

$$\frac{B_p(r,\theta)}{B_{\rm unit}(r)} \sim \frac{r}{qR_0}\left[1 - (a+1)\frac{r}{R_0}\cos\theta\right] \,, \tag{1.147}$$

$$\frac{B(r,\theta)}{B_{\rm unit}(r)} \sim 1 - \frac{r}{R_0}\cos\theta \,, \tag{1.148}$$

$$\mathrm{gsin}(r,\theta) \sim \sin\theta\left[1 - \frac{r}{R_0}\cos\theta\right] \,, \tag{1.149}$$

$$\mathrm{gcos}_1(r,\theta) \sim \cos\theta - \frac{r}{R_0}\left(\cos^2\theta - \frac{1}{q^2}\right) \,, \tag{1.150}$$

$$\Theta(r,\theta) \sim s\theta - q^2R_0\beta^*\sin\theta + \ \Theta_1\frac{r}{R_0} \,, \tag{1.151}$$

$$G_q(r,\theta) \sim 1 + (a-1)\frac{r}{R_0}\cos\theta \,, \tag{1.152}$$

$$G_\theta(r,\theta) \sim 1 + a\,\frac{r}{R_0}\cos\theta \,. \tag{1.153}$$

Here, Θ_1 is the function

$$\Theta_1 = (1-2a)s\theta\sin\theta + \sin\theta\left[(3a-1)s - 2(1+a) + \frac{1}{2}(a-3)q^2R_0\beta^*\cos\theta\right] \,. \tag{1.154}$$

Since the formulae do not represent an exact Grad-Shafranov equilibrium, but rather an equilibrium accurate only first order in r/R_0, they should not be used for simulation purposes. However, they can be used to provide a convenient asymptotic check of the numerical routines used to compute the shape functions in the general case.

Finally, for completeness, we can make contact with the popular s-α equilibrium model [CHT78]. First, recall that

$$\alpha_{\rm MHD} \doteq q^2R_0\beta^* = -q^2R_0\frac{8\pi}{B_{\rm unit}^2}\frac{dp}{dr} \,. \tag{1.155}$$

To recover the usual s-α formulae, we must take the limit $r/R_0 \to 0$ in all the expressions above, except for B, which is taken to be $B/B_{\rm unit} = R_0/R$. Evidently, the result is not a Grad-Shafranov equilibrium (not even to first order in r/R_0). In practice, simulation results obtained using a model circular equilibrium (sometimes called a "Miller circle") can differ significantly from the corresponding s-α result. For example, Kinsey [KWC07] has shown that the nonlinear electron energy flux increases by more than a factor of 1.5 when using a Miller circle instead of s-α geometry.

Chapter 2

The Gyrokinetic Model

2.1 Foundations and Notation

The definitive works in terms of the complete derivation of the gyrokinetic-Maxwell equations for evolution of fluctuations, and the neoclassical equations for evaluation of collisional transport, are due to Sugama and coworkers [SH97, SH98]. For historical reasons, the notation and presentation here differ in some respects from these papers. Nevertheless, what is documented here should be completely consistent with the formulae given in Ref. [SH98]. We prefer when applicable to use Gaussian CGS units[1]. Roughly speaking, the gyrokinetic approach [AL80, CTB81, FC82] is based on the assumption that equilibrium quantities are slowly varying, while perturbations are smaller but more rapidly varying in space. To describe this ordering, it is convenient to introduce the parameters

$$c_s = \sqrt{\frac{T_e}{m_i}} \qquad \text{ion-sound speed} \tag{2.1}$$

$$\rho_s = \frac{c_s}{\Omega_{ci}} \qquad \text{ion-sound gyroradius} \tag{2.2}$$

where Ω_{ci} is the ion cyclotron frequency. The derivation of the gyrokinetic equation proceeds by expanding the primitive Fokker-Planck equation in the small parameter, $\rho_* \doteq \rho_s/a$, where a is the plasma minor radius.

2.2 Reduction of the Fokker-Planck Equation

The details of the derivation of the gyrokinetic (and neoclassical) equations is beyond the scope of this manual. Still, we attempt to sketch the essential details. The Fokker-Planck equation provides the fundamental theory for plasma equilibrium, fluctuations, transport. In this section, we use Sugama's notation. The FP equations is written as

$$\left[\frac{\partial}{\partial t} + \mathbf{v}\cdot\nabla + \frac{e_a}{m_a}\left((\mathbf{E}+\hat{\mathbf{E}}) + \frac{\mathbf{v}}{c}\times(\mathbf{B}+\hat{\mathbf{B}})\right)\cdot\frac{\partial}{\partial\mathbf{v}}\right](f_a+\hat{f}_a) = C_a(f_a+\hat{f}_a) + S_a \tag{2.3}$$

[1] See `http://wwwppd.nrl.navy.mil/nrlformulary/NRL_FORMULARY_06.pdf`

where f_a is the ensemble-averaged distribution, $\hat{f}_a$ is the fluctuating distribution, S_a are sources (beams, RF, etc), and

$$C_a = \sum_b C_{ab}(f_a + \hat{f}_a, f_b + \hat{f}_b) \tag{2.4}$$

is the nonlinear collision operator. The general approach is to separate the FP equation into ensemble-averaged, $\mathcal{A}$, and fluctuating, $\mathcal{F}$, components:

$$\mathcal{A} = \left.\frac{d}{dt}\right|_{\rm ens} f_a - \langle C_a \rangle_{\rm ens} - D_a - S_a \ , \tag{2.5}$$

$$\mathcal{F} = \left.\frac{d}{dt}\right|_{\rm ens} \hat{f}_a + \frac{e_a}{m_a}\left(\hat{\mathbf{E}} + \frac{\mathbf{v}}{c}\times\hat{\mathbf{B}}\right)\cdot\frac{\partial}{\partial \mathbf{v}}(f_a + \hat{f}_a) - C_a + \langle C_a\rangle_{\rm ens} + D_a \ , \tag{2.6}$$

where

$$\left.\frac{d}{dt}\right|_{\rm ens} \doteq \frac{\partial}{\partial t} + \mathbf{v}\cdot\nabla + \frac{e_a}{m_a}\left(\mathbf{E} + \frac{\mathbf{v}}{c}\times\mathbf{B}\right)\cdot\frac{\partial}{\partial \mathbf{v}} \ , \tag{2.7}$$

$$D_a \doteq -\frac{e_a}{m_a}\left\langle \left(\hat{\mathbf{E}} + \frac{\mathbf{v}}{c}\times\hat{\mathbf{B}}\right)\cdot\frac{\partial \hat{f}_a}{\partial \mathbf{v}}\right\rangle_{\rm ens} \ . \tag{2.8}$$

such that D_a is the *fluctuation-particle interaction operator*. Ensemble averages are expanded in powers of ρ_* as

$$f_a = f_{a0} + f_{a1} + f_{a2} + \dots \ , \tag{2.9}$$

$$S_a = \qquad\qquad S_{a2} + \dots \text{ (transport ordering)}, \tag{2.10}$$

$$\mathbf{E} = \mathbf{E}_0 + \mathbf{E}_1 + \mathbf{E}_2 + \dots \ , \tag{2.11}$$

$$\mathbf{B} = \mathbf{B}_0 \ . \tag{2.12}$$

Fluctuations are also expanded in powers of ρ_* as

$$\hat{f}_a = \hat{f}_{a1} + \hat{f}_{a2} + \dots \ , \tag{2.13}$$

$$\hat{\mathbf{E}} = \hat{\mathbf{E}}_1 + \hat{\mathbf{E}}_2 + \dots \ , \tag{2.14}$$

$$\hat{\mathbf{B}} = \hat{\mathbf{B}}_1 + \hat{\mathbf{B}}_2 + \dots \ . \tag{2.15}$$

2.2.1 Lowest-order constraints

The lowest-order ensemble-averaged equation gives the constraints

$$\mathcal{A}_{-1} = 0: \qquad \mathbf{E}_0 + \frac{1}{c}\mathbf{V}_0\times\mathbf{B} = 0 \qquad \text{and} \qquad \frac{\partial f_{a0}}{\partial \xi} = 0 \tag{2.16}$$

where ξ is the gyroangle. The only zeroth-order flow (i.e., sonic) flow that persists on the fluctuation timescale is a purely toroidal flow [HW85], which we write as

$$\mathbf{V}_0 = V_0\mathbf{e}_\varphi = R\,\omega_0(\psi)\mathbf{e}_\varphi \quad \text{where} \quad \omega_0 \doteq -c\frac{\partial \phi_{-1}}{\partial \psi} \ . \tag{2.17}$$

The first-order flow $\mathbf{V}_1$ contains both toroidal and poloidal components which are self-consistenly calculated by as moments of the ensemble averaged first-order distribution, f_{a1} (that is, they are computed within the context of neoclassical theory).

2.2.2 Equilibrium equation and solution

The gyrophase average of the zeroth order ensemble-averaged equation gives the collisional equilibrium equation:

$$\int_0^{2\pi} \frac{d\xi}{2\pi} \mathcal{A}_0 = 0 : \qquad \left(\mathbf{V}_0 + v'_\parallel \mathbf{b}\right) \cdot \nabla f_{a0} = C_a(f_{a0}) \tag{2.18}$$

where $\mathbf{v}' = \mathbf{v} - \mathbf{V}_0$ is the deviation from the mean flow velocity. The exact solution for f_{a0} is a Maxwellian in the rotating frame, such that the centrifugal force causes the density to vary on the flux surface:

$$f_{a0} = \frac{n_a(\psi,\theta)}{(2\pi T_a/m_a)^{3/2}} \exp\left(-\frac{m_a(v')^2}{2T_a}\right) = n_a F_{Ma} \ . \tag{2.19}$$

It is important to note here that to account for sonic rotation in the equilibrium, we **do not** use the shifted Maxwellian approach [WSCH07]. Although the use of a shifted Maxwellian gives rise to errors which are probably not significant for typical operating parameters, the approach is conceptually incorrect. Instead, we work in the shifted velocity frame $\mathbf{v}' = \mathbf{v} - \mathbf{V}_0$. The latter approach was first used in the context of neoclassical transport by Hinton and Wong [HW85].

Beyond this point, we limit our attention to the *moderate flow regime*, such that $\rho_* \ll V_0/c_s \ll 1$. Operationally, this means that we will ignore terms quadratic in V_0/c_s, whilst retaining all terms which are linear in V_0/c_s. Physically, this approach will not capture centrifugal effects like the poloidal variation of density, since

$$n_a(\psi,\theta) \sim n_a(\psi) + \mathcal{O}(V_0^2/c_s^2) \ , \tag{2.20}$$

but will correctly retain the symmetry-breaking effects of radial electric field shear, rotation shear drive, and the Coriolis drift.

2.2.3 The drift-kinetic equation

Taking a gyroaverage of the first-order ensemble-averaged component $\mathcal{A}_1$ gives expressions for the gyroangle-dependent and independent distributions, $\tilde{f}_{a1}$ and $\bar{f}_{a1}$:

$$\int_0^{2\pi} \frac{d\xi}{2\pi} \mathcal{A}_1 = 0 : \qquad f_{a1} = \tilde{f}_{a1} + \bar{f}_{a1} \ , \quad \tilde{f}_{a1} = \frac{1}{\Omega_a} \int^\xi d\xi \, \widetilde{\mathcal{L} f_{a0}} \tag{2.21}$$

The function $\bar{f}_{a1}$ is determined by the solution of the *drift kinetic equation.*

2.2.4 The gyro-kinetic equation

The gyroaverage of first-order $\mathcal{F}_1$ gives an expression for first-order fluctuating distribution, $\hat{f}_{a1}$, in terms of the distribution of the gyrocenters, $H_a(\mathbf{R})$:

$$\int_0^{2\pi} \frac{d\xi}{2\pi} \mathcal{F}_1 = 0 : \qquad \hat{f}_{a1}(\mathbf{x}) = -\frac{e_a \delta\phi(\mathbf{x})}{T_a} f_{a0} + H_a(\mathbf{R}) \ , \tag{2.22}$$

where $\mathbf{x} = \mathbf{R} + \boldsymbol{\rho}$ is the particle position, $\boldsymbol{\rho} = \mathbf{b} \times \mathbf{v}'/\Omega_{ca}$ is the gyroradius vector, $\Omega_{ca} = e_a B/(m_a c)$ is the cyclotron frequency, and $\mathbf{R}$ ($\mathbf{X}$ in Ref. [SH98]) is the guiding-center position. The function $H_a(\mathbf{R})$ ($h_a(\mathbf{R})$ in Ref. [SH98]) is determined by solution of the nonlinear gyrokinetic equation. Also note that the perturbed potential $\delta\phi$ appears as $\hat{\phi}$ in Ref. [SH98].

2.3 The Gyrokinetic Equation in Detail

In what follows, we will drop the prime notation in reference to the velocity coordinates. To bring the gyrokinetic equation into a form convenient for numerical integration, we introduce the function $h_a(\mathbf{R})$:

$$H_a(\mathbf{R}) = \frac{e_a f_{a0}}{T_a}\,\Psi_a(\mathbf{R}) + h_a(\mathbf{R}) \tag{2.23}$$

where Ψ_a ($\hat{\psi}_a$ in Ref. [SH98]) is the following gyrophase average (or, more simply, gyroaverage) at fixed $\mathbf{R}$:

$$\Psi_a(\mathbf{R}) \doteq \left\langle \delta\phi(\mathbf{R}+\boldsymbol{\rho}) - \frac{1}{c}(\mathbf{V}_0+\mathbf{v})\cdot\delta\mathbf{A}(\mathbf{R}+\boldsymbol{\rho})\right\rangle_{\mathbf{R}} . \tag{2.24}$$

The gyroaverage can be defined formally as

$$\langle z(\mathbf{R},\xi)\rangle_{\mathbf{R}} \doteq \oint \frac{d\xi}{2\pi}\, z(\mathbf{R},\xi)\ , \tag{2.25}$$

for any function, z. Also, we note the following identities

$$\mathbf{b}\cdot\nabla\mathbf{V}_0 = \omega_0\mathbf{s} \tag{2.26}$$

$$\mathbf{b}\cdot\nabla\mathbf{V}_0 + \nabla\mathbf{V}_0\cdot\mathbf{b} = \frac{I}{B}\nabla\omega_0\ , \tag{2.27}$$

where $\mathbf{s}$ is the dimensionless vector

$$\mathbf{s} = \frac{1}{\mathcal{J}_\psi B}\frac{\partial R}{\partial\theta}\mathbf{e}_\varphi - \frac{I}{RB}\nabla R\ . \tag{2.28}$$

We use a form of the gyrokinetic equation which can be obtained, after some rearrangement, from Eq. (46) of Ref. [SH98].

$$\frac{\partial h_a}{\partial t} + \left(v_\parallel\mathbf{b}+\mathbf{v}_d\right)\cdot\nabla H_a + \mathbf{v}_{\mathrm{E}0}\cdot\nabla h_a + \delta\mathbf{v}_a\cdot\nabla h_a + \delta\mathbf{v}_a\cdot\left(\nabla f_{a0} + \frac{m_a v_\parallel f_{a0}}{T_a}\frac{I}{B}\nabla\omega_0\right) = C_a^{GL}\left[H_a\right]\ . \tag{2.29}$$

The velocities are

$$\mathbf{v}_d \doteq \frac{v_\parallel^2+\mu B}{\Omega_{ca}B}\,\mathbf{b}\times\nabla B + \frac{2v_\parallel\omega_0}{\Omega_{ca}}\,\mathbf{b}\times\mathbf{s} + \frac{4\pi v_\parallel^2}{\Omega_{ca}B^2}\,\mathbf{b}\times\nabla p \tag{2.30}$$

$$\mathbf{v}_{\mathrm{E}0} \doteq \frac{c}{B}\,\mathbf{b}\times\nabla\phi_{-1}\ , \tag{2.31}$$

$$\delta\mathbf{v}_a \doteq \frac{c}{B}\,\mathbf{b}\times\nabla\Psi_a\ . \tag{2.32}$$

In this result, $\mathbf{s}$ is a dimensionless vector which is **not** exactly in the grad-B direction. The correct form of s cannot be obtained using the shifted Maxwellian model. This form of the drift matches Brizard's result, and the resulting expression for $\mathbf{v}_d\cdot\nabla\psi$ matches the familiar result from Hinton

and Wong [HW85]. By setting $\omega_0 = 0$, we recover the usual diamagnetic rotation ordering. For normalization purposes it is useful to note that

$$\int d^3v \, F_{Ma} = 1 \, . \tag{2.33}$$

Various terms can be simplified without refering to the geometry model. Within the accuracy of the gyrokinetic ordering, we have

$$\mathbf{v}_{\mathrm{E}0} \cdot \nabla h_a = \frac{c}{B} \, \mathbf{b} \times \nabla \phi_{-1} \cdot \nabla h_a \sim \omega_0 \frac{\partial h_a}{\partial \alpha} \, , \tag{2.34}$$

$$\delta \mathbf{v}_a \cdot \nabla f_{a0} = \frac{c}{B} \, \mathbf{b} \times \nabla \Psi_a \cdot \nabla f_{a0} \sim c \, \frac{\partial f_{a0}}{\partial \psi} \frac{\partial \Psi_a}{\partial \alpha} \, , \tag{2.35}$$

$$\delta \mathbf{v}_a \cdot \nabla h_a = \frac{c}{B} \, \mathbf{b} \times \nabla \Psi_a \cdot \nabla h_a \sim c \, \frac{\partial h_a}{\partial \psi} \frac{\partial \Psi_a}{\partial \alpha} - c \, \frac{\partial h_a}{\partial \alpha} \frac{\partial \Psi_a}{\partial \psi} \, . \tag{2.36}$$

Using these expression, we find

$$\begin{aligned} \frac{\partial h_a}{\partial t} + \frac{v_\parallel}{\mathcal{J}_\psi B} \frac{\partial H_a}{\partial \theta} + \mathbf{v}_d \cdot \nabla H_a + \omega_0 \frac{\partial h_a}{\partial \alpha} + c \, [h_a, \Psi_a]_{\psi,\alpha} \\ + c \left(\frac{\partial f_{a0}}{\partial \psi} + \frac{m_a v_\parallel}{T_a} \frac{I}{B} \frac{\partial \omega_0}{\partial \psi} f_{a0} \right) \frac{\partial \Psi_a}{\partial \alpha} = C_a^{GL} \left[H_a \right] \, . \end{aligned} \tag{2.37}$$

The expansion and simplification of the remaining operators has been treated in Chap. 1.

2.3.1 Ordering

We remark that the gyrokinetic ordering requires that

$$\frac{e_a \Psi_a}{T_a} \sim \frac{h_a}{f_{a0}} \sim \frac{\omega - \mathbf{k}_\perp \cdot \mathbf{V}_0}{\Omega_{ca}} \sim k_\parallel \rho_s \sim \rho_* \, . \tag{2.38}$$

2.3.2 Rotation and rotation shear parameters

Recalling the definition of the rotation frequency:

$$\omega_0 \doteq -c \frac{\partial \phi_{-1}}{\partial \psi} \, , \tag{2.39}$$

we define the *Mach number*, the E_r *shearing rate* and the *rotation shearing rate* respectively as

$$M \doteq \frac{\omega_0 R_0}{c_s} \, , \tag{2.40}$$

$$\gamma_E \doteq \frac{r}{q} \frac{\partial \omega_0}{\partial r} \, , \tag{2.41}$$

$$\gamma_p \doteq R_0 \frac{\partial \omega_0}{\partial r} \, . \tag{2.42}$$

These parameters are defined in this way for legacy reasons and are not independent; rather, we have the constraint

$$\gamma_p = \frac{R_0}{qr} \gamma_E \, . \tag{2.43}$$

2.3.3 Comment on the Hahm-Burrell shearing rate

Note that the shearing rate defined in Eq. (2.41) is not in general equal to the familiar *Hahm-Burrell shearing rate* [Bur97]

$$\gamma_{\rm E}^{\rm HB} \doteq \frac{(RB_p)^2}{B}\frac{\partial}{\partial\psi}\left(\frac{E_r}{RB_p}\right) , \tag{2.44}$$

where E_r is the radial electric field

$$E_r \doteq -\hat{\mathbf{e}}_r\cdot\nabla\phi_{-1} = -|\nabla r|\,\frac{\partial\phi_{-1}}{\partial r} . \tag{2.45}$$

In terms of the Miller geometry coefficients, $\gamma_{\rm E}^{\rm HB}$ can be written as

$$\gamma_{\rm E}^{\rm HB} = \frac{|\nabla r|}{G_q}\frac{r}{q}\frac{\partial}{\partial r}\left(\frac{c}{B_{\rm unit}}\frac{q}{r}\frac{\partial\phi_{-1}}{\partial r}\right) = \frac{|\nabla r|}{G_q}\,\gamma_{\rm E} . \tag{2.46}$$

2.4 Maxwell equations

Defining the scalar electromagnetic fields $\delta A_\parallel \doteq \mathbf{b}\cdot\delta\mathbf{A}$ and $\delta B_\parallel \doteq \mathbf{b}\cdot\nabla\times\delta\mathbf{A}$, we can write an equation for each of the fields $(\delta\phi, \delta A_\parallel, \delta B_\parallel)$ (see Appendix A, [SH98]). In each case, the species summation runs over all species a (ions and electrons).

Poisson equation

$$-\nabla_\perp^2\delta\phi(\mathbf{x}) = 4\pi\sum_a ez_a\,\delta n_a = 4\pi\sum_a e_a\int d^3v\,\hat{f}_{a1}(\mathbf{x}) . \tag{2.47}$$

Parallel Ampère's Law

$$-\nabla_\perp^2\delta A_\parallel(\mathbf{x}) = \frac{4\pi}{c}\sum_a \delta j_{\parallel,a} = \frac{4\pi}{c}\sum_a e_a\int d^3v\,v_\parallel\,\hat{f}_{a1}(\mathbf{x}) . \tag{2.48}$$

Perperdicular Ampère's Law

$$\nabla_\perp\delta B_\parallel(\mathbf{x})\times\mathbf{b} = \frac{4\pi}{c}\sum_a \delta\mathbf{j}_{\perp,a} = \frac{4\pi}{c}\sum_a e_a\int d^3v\,\mathbf{v}_\perp\hat{f}_{a1}(\mathbf{x}) \tag{2.49}$$

The righthand sides can be written in terms of H_a according to

$$\int d^3v\,\hat{f}_{a1}(\mathbf{x}) = -\frac{n_a e_a}{T_a}\,\delta\phi(\mathbf{x}) + \int d^3v\,H_a(\mathbf{x}-\boldsymbol{\rho}) , \tag{2.50}$$

$$\int d^3v\,v_\parallel\,\hat{f}_{a1}(\mathbf{x}) = \int d^3v\,v_\parallel\,H_a(\mathbf{x}-\boldsymbol{\rho}) \tag{2.51}$$

$$\int d^3v\,\mathbf{v}_\perp\,\hat{f}_{a1}(\mathbf{x}) = \int d^3v\,\mathbf{v}_\perp\,H_a(\mathbf{x}-\boldsymbol{\rho}) \tag{2.52}$$

2.5 Transport Fluxes and Heating

For each species separately, we define a *particle flux*, a *toroidal angular momentum flux*, an *energy flux*, and an *exchange power density*:

$$\Gamma_a(r) = \mathcal{F}\int d^3v\, H_a^*(\mathbf{R})\,\delta\mathbf{v}_a\cdot\nabla r\ , \tag{2.53}$$

$$Q_a(r) = \mathcal{F}\int d^3v\ H_a^*(\mathbf{R})\,\delta\mathbf{v}_a\cdot\nabla r\,\frac{1}{2}m_a v^2\ , \tag{2.54}$$

$$\Pi_a(r) = \mathcal{F}\int d^3v\, H_a^*(\mathbf{R}) \left\langle [m_a R(\mathbf{V}_0+\mathbf{v})\cdot\mathbf{e}_\varphi]\,\frac{c}{B}\mathbf{b}\times\nabla\left[\delta\phi(\mathbf{x})-\frac{1}{c}(\mathbf{V}_0+\mathbf{v})\cdot\delta\mathbf{A}(\mathbf{x})\right]\cdot\nabla r\right\rangle_{\mathbf{R}} \tag{2.55}$$

$$S_a(r) = \mathcal{F}\int d^3v\, H_a^*(\mathbf{R})\, e_a \left\langle\left(\frac{\partial}{\partial t}+\mathbf{V}_0(\mathbf{x})\cdot\frac{\partial}{\partial\mathbf{x}}\right)\left[\delta\phi(\mathbf{x})-\frac{1}{c}(\mathbf{V}_0+\mathbf{v})\cdot\delta\mathbf{A}(\mathbf{x})\right]\right\rangle_{\mathbf{R}} \tag{2.56}$$

2.5.1 Ambipolarity and Exchange Symmetries

By summing the particle fluxes over species and using the Maxwell equations, one can prove the exact ambipolarity property

$$\sum_a e_a\bar{\Gamma}_a = 0\ , \tag{2.57}$$

where an overbar denotes a perpendicular spatial and time average taken in the flux-tube limit. Similarly, summing the exchange power density over species and using the Maxwell equations, one can prove the net heating is zero:

$$\sum_a e_a\bar{S}_a = 0\ . \tag{2.58}$$

Note that the time-average is only required to prove the exchange property, not the ambipolarity property. Both these conditions are in general violated if profile variation is allowed.

2.6 Entropy production

The balance equation for entropy production is given by

$$\sigma_a - \mathcal{F}\int d^3v\,\frac{H_a^*}{f_{a0}}\frac{\partial H_a}{\partial t} + \mathcal{F}\int d^3v\,\frac{H_a^*}{f_{a0}}\,C_a^{GL} + \mathcal{F}\int d^3v\,\frac{H_a^*}{f_{a0}}\,D_\tau + \mathcal{F}\int d^3v\,\frac{H_a^*}{f_{a0}}\,D_r \to 0\ , \tag{2.59}$$

where D_τ and D_r represent the (artificial) upwind dissipation terms added in the numerical discretization. The function σ_a is

$$\sigma_a \doteq \left(\frac{1}{L_{na}}-\frac{3}{2}\frac{1}{L_{Ta}}\right)\Gamma_a + \frac{1}{L_{Ta}}\frac{Q_a}{T_a} + \frac{\partial\omega_0}{\partial r}\frac{\Pi_a}{T_a} + S_a\frac{1}{T_a}\ . \tag{2.60}$$

On taking a radial average, and the time-average over sufficiently long times, the sum of terms should approach zero.

2.7 Simplified fluxes and field equations with operator notation

2.7.1 Operator notation

It useful at this point to discuss the general spectral representation of fields and operators. First, expanding an arbitrary field in a spectral (Fourier) basis gives

$$z(\mathbf{R}) \doteq \sum_{\mathbf{k}_\perp} e^{iS(\mathbf{R})}\, \tilde{z}(\mathbf{k}_\perp) \;, \tag{2.61}$$

where $\mathbf{k}_\perp = -i\nabla_\perp$. In this case, the gyrophase dependence in Fourier space is harmonic

$$z(\mathbf{R}+\boldsymbol{\rho}) = \sum_{\mathbf{k}_\perp} e^{iS(\mathbf{R})} e^{i\mathbf{k}_\perp\cdot\boldsymbol{\rho}}\, \tilde{z}(\mathbf{k}_\perp) \;, \tag{2.62}$$

and the gyroaverage becomes

$$\langle z(\mathbf{R}+\boldsymbol{\rho})\rangle_{\mathbf{R}} = \sum_{\mathbf{k}_\perp} e^{iS(\mathbf{R})} J_0(k_\perp\rho_a)\, \tilde{z}(\mathbf{k}_\perp) \;, \tag{2.63}$$

where $\rho_a \doteq v_\perp/\Omega_{ca}$. Thus, in real space, the gyroaverage can be represented as a linear operator $\mathcal{G}_{0a}$ whose spectral representation is $J_0(k_\perp\rho_a)$.

Now, we can write the field defined in Eq. 2.24 using operator notation. Moreover, we also define a new field which is useful for calculation of momentum transport coefficients. These are

$$\Psi_a(\mathbf{R}) \doteq \mathcal{G}_{0a}\left[\delta\phi(\mathbf{R}) - \frac{v_\parallel}{c}\delta A_\parallel(\mathbf{R})\right] + \frac{v_\perp^2}{\Omega_{ca}c}\mathcal{G}_{1a}\,\delta B_\parallel(\mathbf{R}) \;, \tag{2.64}$$

$$\mathcal{X}_a(\mathbf{R}) \doteq \mathcal{G}_{2a}\left[\delta\phi(\mathbf{R}) - \frac{v_\parallel}{c}\delta A_\parallel(\mathbf{R})\right] + 0\cdot\delta B_\parallel(\mathbf{R}) \;, \tag{2.65}$$

where for simplicity we neglect the effect of magnetic compression on $\mathcal{X}$ (which as we will show is connected with perpendicular momentum transport). Although we will construct explicit discrete approximations to the operators $\mathcal{G}_{0a}$, $\mathcal{G}_{1a}$ and $\mathcal{G}_{2a}$ in the next chapter, it can be shown that they have the following spectral representations:

$$\mathcal{G}_{0a} \to J_0(k_\perp\rho_a) \;, \tag{2.66}$$

$$\mathcal{G}_{1a} \to \frac{1}{2}\left[J_0(k_\perp\rho_a) + J_2(k_\perp\rho_a)\right] \;, \tag{2.67}$$

$$\mathcal{G}_{2a} \to \frac{i}{2}k_x\rho_a\left[J_0(k_\perp\rho_a) + J_2(k_\perp\rho_a)\right] \;. \tag{2.68}$$

2.7.2 Maxwell equations

In terms of the function h_a the field equations can be written these can be written as:

Poisson equation

$$-\frac{1}{4\pi}\nabla_\perp^2\delta\phi + \sum_a n_a\frac{e_a^2}{T_a}\int d^3v\, F_{Ma}\,(1-\mathcal{G}_{0a}^2)\delta\phi$$
$$-\sum_a n_a\frac{e_a^2}{T_a}\int d^3v\, F_{Ma}\mathcal{G}_{0a}\mathcal{G}_{1a}\frac{v_\perp^2}{\Omega_{ca}c}\delta B_\parallel = \sum_a e_a\int d^3v\,\mathcal{G}_{0a}h_a \tag{2.69}$$

Parallel Ampère's Law

$$-\frac{1}{4\pi}\nabla_\perp^2\delta A_\parallel + \sum_a n_a \frac{e_a^2}{T_a}\int d^3v\,\frac{v_\parallel^2}{c^2}F_{Ma}\mathcal{G}_{0a}^2\delta A_\parallel = \sum_a ez_a\int d^3v\,\frac{v_\parallel}{c}\mathcal{G}_{0a}h_a \tag{2.70}$$

Perperdicular Ampère's Law

$$\frac{1}{4\pi}\delta B_\parallel + \sum_a n_a\frac{e_a^2}{T_a}\int d^3v\,F_{Ma}\left(\frac{v_\perp^2}{\Omega_{ca}c}\mathcal{G}_{1a}\right)^2\delta B_\parallel + \sum_a n_a\frac{e_a^2}{T_a}\int d^3v\,F_{Ma}\frac{v_\perp^2}{\Omega_{ca}c}\mathcal{G}_{1a}\mathcal{G}_{0a}\delta\phi = -\sum_a e_a\int d^3v\,\mathcal{G}_{1a}\frac{v_\perp^2}{\Omega_{ca}c}h_a \tag{2.71}$$

2.7.3 Transport coefficients

Some algebra yields the simplifications:

$$\Gamma_a(r) = \frac{c}{\psi'}\mathcal{F}\int d^3v\,H_a^*(\mathbf{R})\,\frac{\partial\Psi_a}{\partial\alpha}\,, \tag{2.72}$$

$$Q_a(r) = \frac{c}{\psi'}\mathcal{F}\int d^3v\,H_a^*(\mathbf{R})\,\frac{1}{2}m_a v^2\,\frac{\partial\Psi_a}{\partial\alpha}\,, \tag{2.73}$$

$$\Pi_a(r) = \frac{c}{\psi'}\mathcal{F}\int d^3v\,H_a^*(\mathbf{R})m_aR\left[\left(V_0 + v_\parallel\frac{B_t}{B}\right)\frac{\partial\Psi_a}{\partial\alpha} + v_\perp\frac{B_p}{B}\frac{\partial\mathcal{X}_a}{\partial\alpha}\right]\,, \tag{2.74}$$

$$S_a(r) = \frac{c}{\psi'}\mathcal{F}\int d^3v\,H_a^*(\mathbf{R})\,e_a\left(\frac{\partial}{\partial t} + \omega_0\frac{\partial}{\partial\alpha}\right)\Psi_a\,. \tag{2.75}$$

Chapter 3

Normalization of Fields and Equations

3.1 Dimensionless fields and profiles

For consistency, we will use an overbar to denote *reference quantities*; that is, quantities which are evaluated at the *reference radius*, $\bar{r}$. Explicitly,

$$\bar{T}_e = T_e(\bar{r}) \tag{3.1}$$

$$\bar{n}_e = n_e(\bar{r}) \tag{3.2}$$

$$\bar{c}_s = \sqrt{\frac{\bar{T}_e}{m_i}} \tag{3.3}$$

Here, m_i is the mass of the main ion species (in practice, this will often be deuterium). Next, we introduce the *normalized fields*

$$\hat{h}_a \doteq \frac{h_a}{\bar{n}_e F_{Ma}(r)} \tag{3.4}$$

$$\delta\hat{\phi} \doteq \frac{e\delta\phi}{\bar{T}_e} \tag{3.5}$$

$$\delta\hat{A}_\parallel \doteq \frac{\bar{c}_s}{c}\frac{e\delta A_\parallel}{\bar{T}_e} \ , \tag{3.6}$$

$$\delta\hat{B}_\parallel \doteq \frac{\delta B_\parallel}{B_{\rm unit}(r)} \ , \tag{3.7}$$

and the *normalized profiles*

$$\hat{n}_a(r) \doteq \frac{n_a(r)}{\bar{n}_e} \ , \tag{3.8}$$

$$\hat{T}_a(r) \doteq \frac{T_a(r)}{\bar{T}_e} \ , \tag{3.9}$$

$$\hat{\omega}_0(r) \doteq \frac{a}{\bar{c}_s}\omega_0(r) \ , \tag{3.10}$$

$$\hat{\gamma}_E(r) \doteq \frac{a}{\bar{c}_s}\gamma_E(r) \ , \tag{3.11}$$

$$\hat{\gamma}_p(r) \doteq \frac{a}{\bar{c}_s}\gamma_p(r) \ . \tag{3.12}$$

We also have the additional normalized quantities

$$\hat{B} \doteq \frac{B(r,\theta)}{B_{\rm unit}(r)} \tag{3.13}$$

$$\hat{v}_{\|a} \doteq \frac{v_\|}{\bar{c}_s} \tag{3.14}$$

For quantities which depend on the magnetic field strength, it is necessary to define *unit quantities*:

$$\rho_{s,{\rm unit}}(r) = \frac{\bar{c}_s}{eB_{\rm unit}(r)/(m_i c)} \ , \tag{3.15}$$

$$\beta_{e,{\rm unit}}(r) = \frac{8\pi n_e T_e}{B_{\rm unit}^2} \ . \tag{3.16}$$

At the reference radius, these are written as $\bar{\rho}_{s,{\rm unit}}$ and $\bar{\beta}_{e,{\rm unit}}$. To measure the radial variation of $B_{\rm unit}$, we introduce the parameter

$$G_r(r) = \frac{B_{\rm unit}(r)}{B_{\rm unit}(\bar{r})} \ . \tag{3.17}$$

3.2 Velocity space normalization

3.2.1 Velocity variables

We also use the normalized velocity-space coordinates $(\varepsilon, \lambda, \varsigma)$, defined as

$$\varepsilon = \frac{m_a v^2}{2T_a} \ , \tag{3.18}$$

$$\lambda = \frac{v_\perp^2}{v^2\,\hat{B}} \ , \tag{3.19}$$

$$\varsigma = {\rm sgn}(\hat{v}_{\|a}) \ . \tag{3.20}$$

Let us also note the identities

$$v_\|^2 = v^2\left(1 - \lambda\hat{B}\right) \ , \tag{3.21}$$

$$v_\perp^2 = v^2\lambda\hat{B} = 2\mu B \ . \tag{3.22}$$

The pair (ε, λ) are unperturbed constants of motion. The sign of the parallel velocity, ς, is required to separate two populations of trapped particles for each value of λ. With these definitions, the normalized parallel velocity becomes

$$\hat{v}_{\|a} = \pm\sqrt{\frac{m_i}{m_a}}\sqrt{2\varepsilon\hat{T}_a(1-\lambda\hat{B})}\,. \tag{3.23}$$

3.2.2 Dimensionless velocity-space integration

At this point, we must introduce the *dimensionless velocity-space integration operator* $V[\cdot]$

$$V[z] \doteq \sum_{\varsigma=\pm1}\frac{1}{2\sqrt{\pi}}\int_0^\infty d\varepsilon\, e^{-\varepsilon}\sqrt{\varepsilon}\int_0^1\frac{d(\lambda\hat{B})}{\sqrt{1-\lambda\hat{B}}}\,z(\mathbf{R},\lambda,\varepsilon,\varsigma)\,, \tag{3.24}$$

where $\varsigma = \mathrm{sgn}\,(\hat{v}_{\|a}) = \pm1$. It can be verified that $V[1] = 1$. In writing Eq. (3.24), we explicitly rule out consideration of non-Maxwellian particle distributions.

3.3 Dimensionless equations

3.3.1 Normalized gyrokinetic equation

The normalized gyrokinetic equation is

$$\begin{aligned}\frac{\partial\hat{h}_a}{\partial\hat{t}} + \frac{\hat{v}_{\|a}}{G_\theta q(R_0/a)}\frac{\partial\hat{H}_a}{\partial\theta} + \frac{\mathbf{v}_d}{\bar{c}_s}\cdot\hat{\nabla}\hat{H}_a + \hat{\omega}_0\frac{\partial\hat{h}_a}{\partial\alpha} + \frac{q\bar{\rho}_{s,\mathrm{unit}}}{rG_r}a[\hat{h}_a,\hat{\Psi}_a]_{r,\alpha}\\ - \hat{n}_a\frac{q\bar{\rho}_{s,\mathrm{unit}}}{rG_r}\left[\frac{a}{L_{na}} + (\varepsilon-3/2)\frac{a}{L_{Ta}} - \frac{m_a\hat{v}_{\|a}}{m_i\hat{T}_a}\frac{B_tR}{BR_0}\hat{\gamma}_p\right]\frac{\partial\hat{\Psi}_a}{\partial\alpha} = \hat{C}_a^{GL}\left[\hat{H}_a\right]\,,\end{aligned} \tag{3.25}$$

where

$$\hat{H}_a = \hat{h}_a + z_a\alpha_a\hat{\Psi}_a\,, \tag{3.26}$$

$$\hat{\Psi}_a = \mathcal{G}_{0a}\left(\delta\hat{\phi} - \hat{v}_{\|a}\delta\hat{A}_\|\right) + \frac{2\varepsilon\lambda\hat{T}_a}{z_a}\mathcal{G}_{1a}\delta\hat{B}_\|\,, \tag{3.27}$$

$$\alpha_a = \hat{n}_a/\hat{T}_a\,, \tag{3.28}$$

and $e_a = ez_a$. The inverse gradient scale lengths are defined as

$$\frac{1}{L_{na}} = -\frac{1}{n_a}\frac{\partial n_a}{\partial r}\,, \tag{3.29}$$

$$\frac{1}{L_{Ta}} = -\frac{1}{T_a}\frac{\partial T_a}{\partial r}\,. \tag{3.30}$$

3.3.2 Normalized Maxwell equations

Poisson equation:

$$-\bar{\lambda}_D^2\nabla_\perp^2\delta\hat{\phi} + \sum_a\alpha_a z_a^2 V\left[\left(1-\mathcal{G}_{0a}^2\right)\delta\hat{\phi}\right] - 2\sum_a z_a\hat{n}_a V\left[\mathcal{G}_{0a}\mathcal{G}_{1a}\varepsilon\lambda\delta\hat{B}_\|\right] = \sum_a z_a V[\mathcal{G}_{0a}\hat{h}_a]\,. \tag{3.31}$$

Above, $\bar{\lambda}_D$ is the *Debye length* at the reference radius

$$\bar{\lambda}_D = \left(\frac{\bar{T}_e}{4\pi \bar{n}_e e^2} \right)^{1/2} . \tag{3.32}$$

Parallel Ampère's Law

$$-\frac{2\bar{\rho}_{s,\mathrm{unit}}^2}{\bar{\beta}_{e,\mathrm{unit}}} \nabla_\perp^2 \delta\hat{A}_\parallel + \sum_a \alpha_a z_a^2 \, V[\hat{v}_{\parallel a}^2 \mathcal{G}_{0a}^2 \delta\hat{A}_\parallel] = \sum_a z_a V[\hat{v}_{\parallel a} \mathcal{G}_{0a} \hat{h}_a] \, . \tag{3.33}$$

We remind the reader that the *Ampère cancellation problem* [CW03] will occur if one attempts to set $V[\hat{v}_{\parallel a}^2] = 1$ rather than evaluate it numerically.

Perperdicular Ampère's Law

$$G_r^2 \frac{\delta\hat{B}_\parallel}{\bar{\beta}_{e,\mathrm{unit}}} + 2\sum_a \hat{n}_a \hat{T}_a V\left[\mathcal{G}_{1a}^2 \varepsilon^2 \lambda^2 \delta\hat{B}_\parallel\right] + \sum_a z_a \hat{n}_a V\left[\mathcal{G}_{1a}\mathcal{G}_{0a}\varepsilon\lambda\delta\hat{\phi}\right] = -\sum_a \hat{T}_a V\left[\mathcal{G}_{1a}\varepsilon\lambda\hat{h}_a\right] \, . \tag{3.34}$$

3.3.3 Normalized Transport Fluxes

The normalized particle flux is

$$\hat{\Gamma}_a(r) = \frac{\Gamma_a}{\bar{n}_e \bar{c}_s} = \frac{q\bar{\rho}_{s,\mathrm{unit}}}{r\, G_r} \mathcal{F}V\left[\hat{H}_a^* \frac{\partial\hat{\Psi}_a}{\partial\alpha}\right] \, . \tag{3.35}$$

The normalized energy flux is

$$\hat{Q}_a(r) = \frac{Q_a}{\bar{n}_e \bar{T}_e \bar{c}_s} = \hat{T}_a \frac{q\bar{\rho}_{s,\mathrm{unit}}}{r\, G_r} \mathcal{F}V\left[\hat{H}_a^* \frac{\partial\hat{\Psi}_a}{\partial\alpha}\,\varepsilon\right] \, . \tag{3.36}$$

The normalized toroidal momentum flux is

$$\hat{\Pi}_a(r) \;= \frac{\Pi_a}{\bar{n}_e m_i \bar{c}_s^2 a} \, , \tag{3.37}$$

$$= \frac{m_a}{m_i} \frac{q\bar{\rho}_{s,\mathrm{unit}}}{r\, G_r} \mathcal{F}V\left[\hat{H}_a^* \frac{R}{a}\left\{\left(\frac{V_0}{\bar{c}_s} + \hat{v}_{\parallel a}\frac{B_t}{B}\right)\frac{\partial\hat{\Psi}_a}{\partial\alpha} + \hat{v}_\perp \frac{B_p}{B}\frac{\partial\hat{\mathcal{X}}_a}{\partial\alpha}\right\}\right] \tag{3.38}$$

Finally, the normalized anomalous energy exchange is

$$\hat{S}_a(r) = \frac{S_a}{\bar{n}_e \bar{T}_e \bar{c}_s / a} = z_a \frac{1}{G_r} \frac{q\bar{\rho}_{s,\mathrm{unit}}}{r\, G_r} \mathcal{F}V\left[\hat{H}_a^*\left(\frac{\partial}{\partial\hat{t}} + \hat{\omega}_0 \frac{\partial}{\partial\alpha}\right)\hat{\Psi}_a\right] \, . \tag{3.39}$$

Above, $\mathcal{F}V$ represents the flux-surface average of the dimensionless velocity-space integration operator. The discrete respresentation of the product $\mathcal{F}V$ will be described in detail in the next chapter.

3.3.4 Diffusivities

In terms of the fluxes, we further define a *particle diffusivity* D_a according to

$$\Gamma_a = -D_a \frac{\partial n_a}{\partial r} \ , \tag{3.40}$$

and an *energy diffusivity* χ_a according to

$$Q_a = -n_a \chi_a \frac{\partial T_a}{\partial r} \ . \tag{3.41}$$

3.3.5 GyroBohm normalization

In GYRO, the output fluxes and diffusivites also carry the so-called *gyroBohm* normalization. That is, for output, we use

$$\frac{\Gamma_a}{\Gamma_{\rm GB}} \quad \text{where} \quad \Gamma_{\rm GB} \doteq \bar{n}_e \bar{c}_s (\bar{\rho}_{s,\rm unit}/a)^2 \ , \tag{3.42}$$

$$\frac{\Pi_a}{\Pi_{\rm GB}} \quad \text{where} \quad \Pi_{\rm GB} \doteq \bar{n}_e a \bar{T}_e (\bar{\rho}_{s,\rm unit}/a)^2 \ , \tag{3.43}$$

$$\frac{Q_a}{Q_{\rm GB}} \quad \text{where} \quad Q_{\rm GB} \doteq \bar{n}_e \bar{c}_s \bar{T}_e (\bar{\rho}_{s,\rm unit}/a)^2 \ , \tag{3.44}$$

$$\frac{S_a}{S_{\rm GB}} \quad \text{where} \quad S_{\rm GB} \doteq \bar{n}_e (\bar{c}_s/a) \bar{T}_e (\bar{\rho}_{s,\rm unit}/a)^2 \ , \tag{3.45}$$

$$\frac{\chi_a}{\chi_{\rm GB}} \ , \ \frac{D_a}{\chi_{\rm GB}} \quad \text{where} \quad \chi_{\rm GB}, \doteq \bar{\rho}^2_{s,\rm unit} \bar{c}_s / a \ . \tag{3.46}$$

Chapter 4

Spatial Discretization

4.1 Foreword

The original explicit version of GYRO has been partially documented in a previous article [CW03]. This report supercedes that document in all respects. Among many other changes and improvements over [CW03], the current version of GYRO includes

1. the option to treat the fast electron parallel motion implicitly,
2. an improved and simplified treatment of boundary conditions,
3. a fully Arakawa-like nonlinear discretization scheme,
4. a generalization to an arbitrary number of kinetic impurities.

For an exhaustive, chronological list of changes, always refer to the `CHANGES` file with each GYRO release.

4.2 Spectral Decomposition in Toroidal Direction

4.2.1 Expansion of fields

We expand the perturbed quantities $(\delta\hat{\phi}, \delta\hat{A}_{\parallel}, \delta\hat{B}_{\parallel}, \hat{h}_a)$ as Fourier series in α. For example, the potential is written as

$$\delta\hat{\phi}(r,\theta,\alpha) = \sum_{j=-N_n+1}^{N_n-1} \delta\phi_n(r,\theta)\, e^{-in\alpha} e^{in\overline{\omega_0}t} \quad \text{where} \quad n = j\Delta n \; . \tag{4.1}$$

In GYRO,

$$N_n \rightarrow \texttt{TOROIDAL\_GRID}$$
$$\Delta n \rightarrow \texttt{TOROIDAL\_SEP}$$

The hat is omitted on n-space quantities for brevity. Here, $\overline{\omega_0}$ is a suitably-averaged rotation frequency. In GYRO, this is taken to be the rotation frequency at the domain center. The θ-periodicity condition (see condition 2, Sec. 1.2.2) requires that

$$\delta\hat{\phi}\left(r, 0, \varphi + \nu[\psi, 0]\right) = \delta\hat{\phi}\left(r, 2\pi, \varphi + \nu[\psi, 2\pi]\right) \; . \tag{4.2}$$

So, although the physical field, $\delta\hat{\phi}$, is 2π-periodic in θ, the Fourier representation has the implication that the coefficients, $\delta\phi_n$, are nonperiodic, and satisfy the phase condition

$$\delta\phi_n(r,0) = e^{2\pi i n q(r)}\delta\phi_n(r,2\pi) \; . \tag{4.3}$$

Since $\delta\hat{\phi}$ is real, the Fourier coefficients satisfy the relation $\delta\phi_n^* = \delta\phi_{-n}$. The spectral form given in Eq. (4.1) is

1. $(2\pi/\Delta n)$-periodic in α at fixed (r,θ)
2. $(2\pi/\Delta n)$-periodic in φ at fixed (r,θ).

4.2.2 Poloidal wavenumber

We choose to define the *poloidal wavenumber* so that it is a proper flux-surface function:

$$k_\theta = \frac{nq(r)}{r} \; . \tag{4.4}$$

4.3 Operator Discretization Methods

4.3.1 Finite-difference operators for derivatives

The *differential band width* in the radial direction is denoted by the parameter i_d. First and second derivatives can be discretized using n_d-point centered differences, where $n_d \doteq 2i_d + 1$. These are

$$\mathcal{D}_1^{ii'}(n_d,\Delta x)f^{i'} = \frac{1}{\Delta x}\sum_{\nu=-i_d}^{i_d} c_{1\nu} f^{i+\nu} \; , \tag{4.5}$$

$$\mathcal{D}_2^{ii'}(n_d,\Delta x)f^{i'} = \frac{1}{(\Delta x)^2}\sum_{\nu=-i_d}^{i_d} c_{2\nu} f^{i+\nu} \; , \tag{4.6}$$

where

$$c_{1\nu} = \sum_{p\neq\nu}\frac{1}{\nu-p}\prod_{j\neq\nu,p}\frac{(-j)}{\nu-j} \; , \tag{4.7}$$

$$c_{2\nu} = \sum_{p\neq\nu}\frac{1}{\nu-p}\sum_{q\neq\nu,p}\frac{1}{\nu-q}\prod_{j\neq\nu,q,p}\frac{(-j)}{\nu-j} \; . \tag{4.8}$$

The argument n_d in the operators refers to the *number of points* in the stencil, not the order or accuracy of the stencil. The formal truncation error for both $\mathcal{D}_1$ and $\mathcal{D}_2$ is $\mathcal{O}\left[(\Delta x)^{n_d-1}\right]$; in other words, these stencils are said to be order-(n_d-1) accuracte. A typical case would be $n_d = 5$; that is, 5-point, 4th-order

4.3.2 Upwind schemes

To construct an arbitrary-order upwind scheme, we begin by writing the centered (n_d-1)th derivative as

$$\mathcal{D}_*^{ii'}(n_d,\Delta x)f^{i'} = -\frac{1}{(\Delta x)^{n_d-1}}\sum_{\nu=-i_d}^{i_d}(-1)^\nu\binom{n_d-1}{\nu+i_d}f^{i+\nu}\ . \tag{4.9}$$

The (n_d-2)th-order upwind discretization (we will lose one order in accuracy because of the added dissipation) of an advective derivative is then written as

$$v\,\frac{\partial}{\partial x} \to v\,\mathcal{D}_1^{ii'}(n_d,\Delta x) - \gamma|v|\mathcal{D}_*^{ii'}(n_d,\Delta x) \quad \text{where} \quad \gamma \doteq |c_{1i_d}|\,(\Delta r)^{n_d-2}\ . \tag{4.10}$$

The choice above for the dissipation, γ, recovers the usual first, third and higher-order upwind schemes. For a more complete discussion of the discretization given in Eq. (4.10), see [CW03]. So, we define a smoothing stencil

$$\mathcal{S}^{ii'}(n_d,\Delta x) \doteq |c_{1i_d}|\,(\Delta r)^{n_d-2}\mathcal{D}_*^{ii'}(n_d,\Delta x)\ . \tag{4.11}$$

In GYRO, we add an adjustable parameter c to the upwind scheme:

$$v\,\frac{\partial}{\partial x} \to v\,\mathcal{D}_1^{ii'}(n_d,\Delta x) - c|v|\mathcal{S}^{ii'}(n_d,\Delta x)\ , \tag{4.12}$$

such that $c=1$ gives the standard 1st-order and 3rd-order upwind schemes in the case $n_d=3$ and $n_d=5$, respectively.

4.3.3 Banded pseudospectral gyro-orbit integral operators

In this section, we derive explicit forms for the gyroaverage and associated operators which were introduced in Sec. 2.7.1. The gyroaverage of a function $z(\mathbf{x})$ is defined as

$$\mathcal{G}_{0a}z(\mathbf{R}) = \int_0^{2\pi}\frac{d\xi}{2\pi}z\left[\mathbf{R}+\boldsymbol{\rho}_a(\xi)\right]\ . \tag{4.13}$$

To perform the loop integral, we write the velocity and gyrovector as

$$\boldsymbol{\rho}_a = \frac{v_\perp}{\Omega_{ca}}\left(\mathbf{e}_x\cos\xi + \mathbf{e}_y\sin\xi\right) \tag{4.14}$$

$$\mathbf{v}_\perp = v_\perp\left(\mathbf{e}_x\sin\xi - \mathbf{e}_y\cos\xi\right) \tag{4.15}$$

where $\mathbf{e}_x = \nabla r/|\nabla r|$ and $\mathbf{e}_y = \mathbf{b}\times\mathbf{e}_x$. Then, we write z in spectral form

$$z(\mathbf{R}) = \sum_n\sum_{p=-n_r/2}^{n_r/2-1} z_{np}(\theta)e^{2\pi ipr/L}e^{-in\alpha}\ , \tag{4.16}$$

$$z(\mathbf{R}+\boldsymbol{\rho}_a) = \sum_n\sum_{p=-n_r/2}^{n_r/2-1} z_{np}(\theta)e^{2\pi ipr/L}e^{-in\alpha}e^{2\pi ip\boldsymbol{\rho}_a\cdot\nabla r/L}e^{-in\boldsymbol{\rho}_a\cdot\nabla\alpha}\ . \tag{4.17}$$

We have neglected the θ-variation of the integrand, consistent with the gyrokinetic ordering (i.e., low parallel wavenumber). Some algebra shows

$$\boldsymbol{\rho}_a \cdot \nabla r = \frac{v_\perp}{\Omega_{ca}} |\nabla r| \cos\xi \ , \tag{4.18}$$

$$\boldsymbol{\rho}_a \cdot \nabla \alpha = \frac{v_\perp}{\Omega_{ca}} \left(\mathbf{e}_x \cdot \nabla\alpha \cos\xi + \mathbf{e}_y \cdot \nabla\alpha \sin\xi \right) \ . \tag{4.19}$$

In terms of local equilibrium functions, we have

$$\mathbf{e}_x \cdot \nabla\alpha = \ -\frac{q}{r} G_q \Theta \ , \tag{4.20}$$

$$\mathbf{e}_y \cdot \nabla\alpha = \ -\frac{q}{r} G_q \ . \tag{4.21}$$

So, if we define

$$k_x = 2\pi p \frac{|\nabla r|}{L} + \frac{nq}{r} G_q \Theta \ , \tag{4.22}$$

$$k_y = \frac{nq}{r} G_q \tag{4.23}$$

with $\rho_a = v_\perp / \Omega_{ca}$, then the gyroaveraged potential for a single harmonic becomes

$$\mathcal{G}_{0a,n} z_n = \sum_{p=-n_r/2}^{n_r/2-1} z_{np}(\theta) e^{2\pi i p r/L} e^{-in\alpha} \int_0^{2\pi} \frac{d\xi}{2\pi} e^{i(k_x \rho_a \cos\xi + k_y \rho_a \sin\xi)} \ , \tag{4.24}$$

$$= \sum_{p=-n_r/2}^{n_r/2-1} z_{np}(\theta) e^{2\pi i p r/L} e^{-in\alpha} J_0(k_\perp \rho_a) \ , \tag{4.25}$$

where $k_\perp = \sqrt{k_x^2 + k_y^2}$. To evaluate the gyroaverage explicitly, we assume that z is known on a uniform mesh $r_j = j\Delta r$:

$$(z_n)^j = \sum_{p=-J}^{J-1} z_{np} \, e^{2\pi i p r_j / L} \ , \tag{4.26}$$

where L is the *radial domain size*. The radial domain and boundary conditions are described in more detail in Sec. 6.1. The Fourier decomposition is easily inverted to yield

$$z_{np} = \frac{1}{n_r} \sum_{j=-n_r/2}^{n_r/2-1} (z_n)^j \, e^{-2\pi i p r_j / L} \ , \tag{4.27}$$

so that

$$\mathcal{G}^{jj'}_{0a,n} z^{j'}_n = \sum_{p=-J}^{J-1} e^{2\pi i p r_j / L} J_0 \left(k_\perp \rho_a \right)_{r=r_j} \, z_{np} \ , \tag{4.28}$$

where J_0 is a Bessel function of the first kind, and

$$k_\perp = \sqrt{(2\pi p |\nabla r|/L + k_\theta G_q \Theta)^2 + (k_\theta G_q)^2} \ . \tag{4.29}$$

The result gives the **pseudospectral** forms of the gyroaverage operator:

$$\mathcal{G}_{0a,n}^{jj'} = \frac{1}{n_r} \sum_{p=-n_r/2}^{n_r/2-1} w_p^{j-j'} J_0\left(k_\perp \rho_a\right)_{r=r_j} \ , \tag{4.30}$$

where indices $\{j, j'\}$ run from $-n_r/2$ to $n_r/2-1$, and

$$w_p \doteq \exp(2\pi i p/n_r) \ . \tag{4.31}$$

In terms of normalized quantities,

$$\rho_a = \bar{\rho}_{s,\mathrm{unit}} \sqrt{\frac{m_a}{m_i}} \frac{\sqrt{2\varepsilon \hat{T}_a \lambda \hat{B}}}{z_a \hat{B} G_r} \tag{4.32}$$

Additional required operators are

$$(\mathcal{G}^2)_{0a,n}^{jj'} = \frac{1}{n_r} \sum_{p=-n_r/2}^{n_r/2-1} w_p^{j-j'} J_0^2\left(k_\perp \rho_a\right) \ , \tag{4.33}$$

$$\mathcal{G}_{1a,n}^{jj'} = \frac{1}{n_r} \sum_{p=-n_r/2}^{n_r/2-1} w_p^{j-j'} \frac{1}{2} \left[J_0\left(k_\perp \rho_a\right) + J_2\left(k_\perp \rho_a\right)\right] \ , \tag{4.34}$$

$$\mathcal{G}_{2a,n}^{jj'} = \frac{1}{n_r} \sum_{p=-n_r/2}^{n_r/2-1} w_p^{j-j'} \frac{i}{2} k_x \rho_a \left[J_0\left(k_\perp \rho_a\right) + J_2\left(k_\perp \rho_a\right)\right] \ , \tag{4.35}$$

4.3.4 Banded Approximations

The matrix $\mathcal{G}_{0a,n}^{jj'}$ is diagonally-dominant, such that elements $\{j, j'\}$ for which $|j-j'| > j_g$, where j_g is some sufficiently large integer, can be neglected. Thus, to convert the operators in Eqs. (4.30) to banded form, it is enough to set

$$\widehat{\mathcal{G}}_{0a,n}^{jj'} = \begin{cases} \mathcal{G}_{0a,n}^{jj'} & \text{if } |j-j'| \le j_g \\ 0 & \text{if } |j-j'| > j_g \end{cases} \tag{4.36}$$

For $n = 0$, an additional correction is required. One must ensure that the long-wavelength limit is asymptotically correct:

$$\mathcal{G}_{0a,0} \cdot 1 = 1 \ . \tag{4.37}$$

This is accomplished by making a small correction to the diagonal term

$$\widehat{\mathcal{G}}_{0a,0}^{jj} \to \widehat{\mathcal{G}}_{0a,0}^{jj} + 1 - \sum_{j'=j-j_g}^{j+j_g} \mathcal{G}_{0a,0}^{jj'} \tag{4.38}$$

The size of this correction (the sum above) decreases rapidly as i_g is increased. We have observed excellent results using these banded approximations for the various averaging operators, even when the radial domain is nonperiodic. Physically, the validity of this method relies on the observation that the numerical contribution to the averages decays rapidly at distances beyond a few gyroradii from the gyrocenter. For linear benchmarks, when the radial domain is only one period of the ballooning mode, we generally use full pseudospectral representations.

4.4 Discretization of the gyrokinetic equation

Upon spectral decomposition, the gyrokinetic equation finally takes the form which is solved in GYRO. We write this symbolically as

$$\frac{\partial h_{a,n}}{\partial \hat{t}} - i\widehat{\omega_\theta} H_{a,n} - i\widehat{\omega_d} H_{a,n} - i\widehat{\omega_E} h_{a,n} - i\widehat{\omega_*}\Psi_{a,n} + \frac{q\bar{\rho}_{s,\mathrm{unit}}}{rG_r} a\{\hat{h}_a, \hat{\Psi}_a\} = \hat{C}_a^{GL}[H_{a,n}] \;, \tag{4.39}$$

where the various toroidal harmonics are given by

$$H_{a,n} = h_{a,n} + z_a \alpha_a \Psi_{a,n} \;, \tag{4.40}$$

$$\Psi_{a,n} = \mathcal{G}_{0a,n}\left(\delta\phi_n - \hat{v}_{\parallel a}\delta A_{\parallel n}\right) + \frac{2\varepsilon\lambda \hat{T}_a}{z_a}\mathcal{G}_{1a,n}\delta B_{\parallel n} \;. \tag{4.41}$$

The Poisson bracket $\{\cdot,\cdot\}$ is defined in Eq. (4.60) of Sec. 4.4.5, the geometry functions G_θ, G_q, gsin, gcos and Θ are defined in Sec. 1.3.10, and the profile function G_r is defined in Eq. (3.17).

4.4.1 Parallel motion on an orbit-time grid

The parallel advection term is written

$$-i\widehat{\omega_\theta} H_{a,n} = \frac{\hat{v}_{\parallel a}}{G_\theta q(R_0/a)}\frac{H_{a,n}}{\partial\theta} \;. \tag{4.42}$$

The presence of field quantities in the definition of $H_{a,n}$ complicates the matter of poloidal discretization as we will discuss shortly. Equation (4.42) is subject to short-wavelength instability in regions where the variation of $\hat{v}_{\parallel a}(\theta)$ is sufficiently strong. This property is well-known [Dur99], and time-explicit schemes must normally include dissipative smoothing if a solution is sought on an equally-spaced θ-grid. Moreover, at bounce points θ_b, where $v_\parallel(\theta_b) = 0$, the distribution function may develop cusps, bringing into question the accuracy of any finite-difference scheme on such a grid.

This leads us to the observation that the poloidal angle, θ, is a potentially poor variable for numerical solution of the GK equation. The obvious solution is to remove these cusps analytically using the normalized *orbit time* for discretization in the poloidal direction. To this end, define

$$\tau_0(\lambda,\theta) \doteq \begin{cases} \displaystyle\int_{-\theta_b}^{\theta} \frac{G_\theta(\theta)\,d\theta'}{\sqrt{1-\lambda\hat{B}(\theta')}} & \text{if } \lambda \le \dfrac{1}{\hat{B}(\pi)} \text{ (trapped)} \;, \\ \displaystyle\int_{-\pi}^{\theta} \frac{G_\theta(\theta)\,d\theta'}{\sqrt{1-\lambda\hat{B}(\theta')}} & \text{if } \lambda > \dfrac{1}{\hat{B}(\pi)} \text{ (passing)} \;, \end{cases} \tag{4.43}$$

where θ_b is the solution of $\hat{B}(\theta_b) = 1/\lambda$. $\tau_0(\lambda,\theta)$ must be computed numerically for general plasma equilibria — a tedious but straightforward exercise in numerical analysis. Note that in Eq. (4.43), and in the rest of this section, we suppress the radial dependence of $\tau_0(\lambda, r, \theta)$, $\hat{B}(r,\theta)$ and $G_\theta(r,\theta)$ for brevity.

Next, we introduce a normalized orbit time, τ, which runs from 0 to 2 for a given λ and describes *both signs of velocity*. In this way τ parameterizes the solution on both Riemann sheets

by subsuming the two signs of velocity:

$$\tau(\lambda,\theta) \doteq \begin{cases} \tau_0(\lambda,\theta)/\bar{\tau} & \text{for } 0 \le \tau \le 1 \quad (\varsigma = 1)\ , \\ 2 - \tau_0(\lambda,\theta)/\bar{\tau} & \text{for } 1 < \tau \le 2 \quad (\varsigma = -1)\ , \end{cases} \tag{4.44}$$

where $\bar{\tau} = \tau_0(\lambda,\theta_b)$ for trapped particles, and $\bar{\tau} = \tau_0(\lambda,\pi)$ for passing particles. The parallel advection operator is reduced to one with constant velocity

$$\frac{\hat{v}_{\|a}}{G_\theta q(R_0/a)}\frac{H_{a,n}}{\partial\theta} = \Omega_a(\varepsilon,\lambda)\,\frac{\partial H_{a,n}}{\partial\tau}\ , \quad \text{where} \quad \Omega_a(\varepsilon,\lambda) \doteq \sqrt{\frac{m_i}{m_a}}\frac{1}{q(R_0/a)}\frac{\sqrt{2\hat{T}_a\varepsilon}}{\bar{\tau}}\ . \tag{4.45}$$

High-accuracy numerical discretization schemes for this form of the equation are well-documented. Boundary conditions on physical distributions can be stated very simply:

- trapped are periodic on the interval $[0,2)$;
- co-passing are periodic on $[0,1)$;
- counter-passing are periodic on $[1,2)$.

However, the Fourier representation of Eq. (4.3)] requires that the functions h describing the passing population are not periodic, but subject to phase conditions: $h(1) = \mathcal{P}\,h(0)$ for co-passing, and $h(2) = \mathcal{P}\,h(1)$ for counter-passing. The important result is that as a function of τ, the trapped distribution will be not only continuous, but also smooth, across bounce points no matter what order difference scheme is used. The obvious physical interpretation of the location of orbit-time gridpoints is that they are equally spaced in time, not space, along an orbit. In particular, because they are highly stagnant near $\theta = \pm\pi$, particles close to the trapped-passing boundary benefit from equal-time spacing.

For finite-n modes, we write the continuous derivative as the sum of a centered 4th-order 1st derivative plus a 4th derivative smoother:

$$\left(\Omega_a\frac{\partial H_{a,n}}{\partial\tau}\right)_j = \Omega_a\mathcal{D}_1^{jj'}(5,\Delta\tau)H_{a,n}^{j'} - c|\Omega_a|\mathcal{S}^{jj'}(5,\Delta\tau)h_{a,n}^{j'}\ . \tag{4.46}$$

The grid spacing for the parallel motion is taken to be $\Delta\tau \doteq 2/n_\tau$, and c is a parameter which measures the amount of numerical disipation. When $c = 1$ (and $\Psi_{a,n} = 0$) we are left with the usual third-order upwind method. We have shown previously that in this scheme finite dissipation is required to give proper Landau damping of $n = 0$ GAMs [CW03]. Conversely, dissipation-free schemes suffer from recurrence problems. Note that the dissipation, above, acts on $h_{a,n}$ but not $H_{a,n}$. In fact, attempting to add upwind diffusion to $H_{a,n}$ (that is, also to fields) will generate numerical modes with growth rate proportional to the square of the radial box size. The difference scheme given in Eq. (4.46) is applied only if the species is to be integrated in time explicitly. When implicit integration is used, we set $c = 0$.

4.4.2 E_r shear

Since we have already shifted to a frame rotating with the mean frequency $\bar{\omega_0}$, the remaining shearing term is

$$-i\widehat{\omega_E}h_{a,n} = -in\left[\omega_0(r) - \overline{\omega_0}\right]h_{a,n}\ . \tag{4.47}$$

In a simulation with fixed shearing rate, this can be approximated as

$$-i\widehat{\omega_E}h_{a,n} \to -in\frac{\partial\omega_0}{\partial r}(r-\bar{r})h_{a,n} = -ik_\theta\gamma_E(r-\bar{r})h_{a,n}\ . \tag{4.48}$$

4.4.3 Drift motion

Using the geometry formulae presented in Sec. 1.3.11, we write the drift operator as

$$\begin{aligned}
-i\widehat{\omega_d}H_{a,n} = &-iG_qk_\theta(R_\parallel+R_\perp)\left(\mathrm{gcos}_1+\mathrm{gcos}_2+\Theta\mathrm{gsin}\right)H_{a,n} &(4.49)\\
&+iG_qk_\theta R_\parallel \mathrm{gcos}_2 H_{a,n} &(4.50)\\
&-iG_qk_\theta R_c\left(\mathrm{ucos}+\Theta\mathrm{usin}\right)H_{a,n} &(4.51)\\
&-|\nabla r|(R_\parallel+R_\perp)\mathrm{gsin}\,\frac{\partial H_{a,n}}{\partial r} &(4.52)\\
&-|\nabla r|R_c\mathrm{usin}\,\frac{\partial H_{a,n}}{\partial r}\ , &(4.53)
\end{aligned}$$

where the dimensionless quantities $R_\parallel/a$, $R_\perp/a$ and R_c/a are defined as

$$\frac{R_\parallel}{a} \doteq \frac{v_\parallel^2}{\bar{c}_a\Omega_{ca}R_0} = \frac{\bar{\rho}_{s,\mathrm{unit}}}{R_0}\frac{2\varepsilon\hat{T}_a}{z_aG_r\hat{B}}\left(1-\lambda\hat{B}\right)\ , \tag{4.54}$$

$$\frac{R_\perp}{a} \doteq \frac{\mu B}{\bar{c}_a\Omega_{ca}R_0} = \frac{\bar{\rho}_{s,\mathrm{unit}}}{R_0}\frac{2\varepsilon\hat{T}_a}{z_aG_r\hat{B}}\left(\frac{\lambda\hat{B}}{2}\right)\ , \tag{4.55}$$

$$\frac{R_c}{a} \doteq \frac{2v_\parallel\omega_0R_0}{\bar{c}_a\Omega_{ca}R_0} = \frac{\bar{\rho}_{s,\mathrm{unit}}}{R_0}\frac{m_a}{m_i}\frac{2\hat{v}_{\parallel a}(\omega_0R_0/\bar{c}_s)}{z_aG_r\hat{B}}\ . \tag{4.56}$$

The derivative operator is discretized according to:

$$\left(\mathrm{gsin}\,a\frac{\partial H_{a,n}}{\partial r}\right)_i = \mathrm{gsin}\,\mathcal{D}_1^{ii'}(n_d,\Delta r/a)H_{a,n}^{i'} - c|\mathrm{gsin}|\mathcal{S}^{ii'}(n_d,\Delta r/a)h_{a,n}^{i'}\ , \tag{4.57}$$

where

$$n_d = 2\times\texttt{RADIAL\_DERIVATIVE\_BAND}+1 \tag{4.58}$$

4.4.4 Diamagnetic effects

The spectral form of the diamagnetic term is simply

$$-i\widehat{\omega_*}\Psi_{a,n} = i\hat{n}_a\frac{k_\theta\bar{\rho}_{s,\mathrm{unit}}}{G_r}\left[\frac{a}{L_{na}}+(\varepsilon-3/2)\frac{a}{L_{Ta}}-\frac{m_a\hat{v}_{\parallel a}}{m_i\hat{T}_a}\frac{B_tR}{BR_0}\hat{\gamma}_p\right]\Psi_{a,n}\ . \tag{4.59}$$

4.4.5 Poisson bracket nonlinearity

Numerical discretizations of the nonlinear $\mathbf{E}\times\mathbf{B}$ motion (including electrstatic, flutter and compressional components) are subject to short-wavelength instabilities. A numerical scheme which preserves continuous conservation laws for domain-integrated number, energy and enstrophy (and thereby prevents both instability and a cascade to short wavelengths) was proposed by Arakawa in

1966 [Ara66]. We adapt this scheme to a semi-spectral variant suitable for use with GYRO. First, let us begin by writing the continuous form of the bracket appearing in the gyrokinetic equation:

$$\{F, G\} = \frac{\partial F}{\partial \alpha}\frac{\partial G}{\partial r} - \frac{\partial G}{\partial \alpha}\frac{\partial F}{\partial r} \; . \tag{4.60}$$

Eq. (4.60) can be recast into the following alternative but equivalent forms

$$\{F, G\} = \frac{\partial}{\partial \alpha}\left(F\,\frac{\partial G}{\partial r}\right) - \frac{\partial}{\partial r}\left(F\,\frac{\partial G}{\partial \alpha}\right) \; , \tag{4.61}$$

and

$$\{F, G\} = -\frac{\partial}{\partial \alpha}\left(G\,\frac{\partial F}{\partial r}\right) + \frac{\partial}{\partial r}\left(G\,\frac{\partial F}{\partial \alpha}\right) \; . \tag{4.62}$$

The trick, first proposed by Arakawa, is to sum these and divide by 3 to yield

$$\{F, G\} = \frac{1}{3}\left[\frac{\partial}{\partial \alpha}\left(F\,\frac{\partial G}{\partial r} - G\,\frac{\partial F}{\partial r}\right) + \frac{\partial}{\partial r}\left(G\,\frac{\partial F}{\partial \alpha} - F\,\frac{\partial G}{\partial \alpha}\right) + \frac{\partial F}{\partial \alpha}\frac{\partial G}{\partial r} - \frac{\partial G}{\partial \alpha}\frac{\partial F}{\partial r}\right] \; . \tag{4.63}$$

Using the spectral decomposition of the bracket together with the discrete form of the derivative operator, $\mathcal{D}_N^{ii'}(\Delta r/a)$, gives the final discrete form

$$\{F, G\}_n^i = \frac{1}{3}\sum_{n'}(n+n')\left(F_{n'}^i\,\mathcal{D}_1^{ii'}G_{n-n'}^{i'} - G_{n'}^i\,\mathcal{D}_1^{ii'}F_{n-n'}^{i'}\right) + \frac{1}{3}\sum_{n'} n'\mathcal{D}_1^{ii'}\left(G_{n-n'}^{i'}F_{n'}^{i'} - F_{n-n'}^{i'}G_{n'}^{i'}\right) \; . \tag{4.64}$$

This is the expression used in GYRO. Now, let us assume, in what follows, that the radial domain is periodic. Deviations from the results below will as a consequence be solely limited to boundary effects.

Lowest order invariant

The lowest integral invariant, which measures the rate of change of the distribution along the nonlinear flow, is

$$\int d\alpha \int dr\,\{F, G\} = \sum_i \{F, G\}_0^i = 0 \; . \tag{4.65}$$

Using Eq. (4.64), the sum above vanishes for all $\mathcal{D}_N$ which satisfy $\sum_i \mathcal{D}_N^{ii'}a^{i'} = 0$ for all vectors a. Centered-difference formulae of all orders for $\mathcal{D}_N$ will satsify this condition.

Higher-order invariants

Some algebra shows that the additional quantities vanish:

$$\int d\alpha \int dr\, G\,\{F, G\} = \sum_n \sum_i G_n^i\,\{F, G\}_{-n}^i = 0 \; , \tag{4.66}$$

$$\int d\alpha \int dr\, F\,\{F, G\} = \sum_n \sum_i F_n^i\,\{F, G\}_{-n}^i = 0 \; . \tag{4.67}$$

4.5 Blending-function expansion for fields

Since the distribution function $h_{a,n}$ is computed at a different set of points $\{\theta_j\}$ for each discrete value of λ, there is no natural way to solve the Maxwell equations using finite-difference methods on a fixed poloidal grid. Instead, we adopt a *function-space* approach, and expand the fields $(\delta\phi_n, \delta A_{\parallel n}, \delta B_{\parallel n})$ in series of *uniform polynomial blending functions*. We will show that basis functions which incorporate the complex phase conditions [see Eq. (4.3)] at $-\pi$ and π can be constructed from pairs of these blending functions. Equations for the expansion coefficients are then obtained using the well-known Galerkin method.

In computing the poloidal dependence of the fields, there are a number of separate discretization effects to consider. Since the fields are sums (integrals in the continuum limit) of distribution functions, low velocity-space resolution will lead to poor poloidal accuracy — even if the there are no other sources of discretization error. Conversely, even when a very large number of velocity-space grids are used, discretization error in the orbit-time integration of $h_{a,n}$ will lead to poor poloidal accuracy — even if the function-space method of the present section was exact. Thus, achieving an absolute level of accuracy in the θ-dependence of the fields requires sufficient convergence in both velocity-space and in orbit-time.

Examples of blending functions

A finite number of blending functions, $N_m(s)$, are used to provide a basis for the field expansion. An important feature of the N_m, however, is that they are all translates of a single function $N(s)$, such that $N(s-m) = N_m(s)$. In practise, we use one of the following three types of blending functions:

Piecewise linear:

$$N^{(2)}(s) \doteq \begin{cases} s & \text{if } 0 \le s \le 1 \,, \\ 2-s & \text{if } 1 \le s \le 2 \,. \end{cases} \tag{4.68}$$

Piecewise quadratic:

$$N^{(3)}(s) \doteq \begin{cases} s^2/2 & \text{if } 0 \le s \le 1 \,, \\ -(3/2) + 3s - s^2 & \text{if } 1 \le s \le 2 \,, \\ (3-s)^2/2 & \text{if } 2 \le s \le 3 \,. \end{cases} \tag{4.69}$$

Piecewise cubic:

$$N^{(4)}(s) \doteq \begin{cases} (1/6)s^3 & \text{if } 0 \le s \le 1 \,, \\ (2/3) - 2s + 2s^2 - (1/2)s^3 & \text{if } 1 \le s \le 2 \,, \\ -(22/3) + 10s - 4s^2 + (1/2)s^3 & \text{if } 2 \le s \le 3 \,, \\ (1/6)(4-s)^3 & \text{if } 3 \le s \le 4 \,. \end{cases} \tag{4.70}$$

Representation of a quasi-periodic function

It remains to construct meaningful set of *basis* vectors from the prototype blending functions given above. Let us begin by considering a function $z(\theta)$ which is not periodic in θ, but satisfies a phase

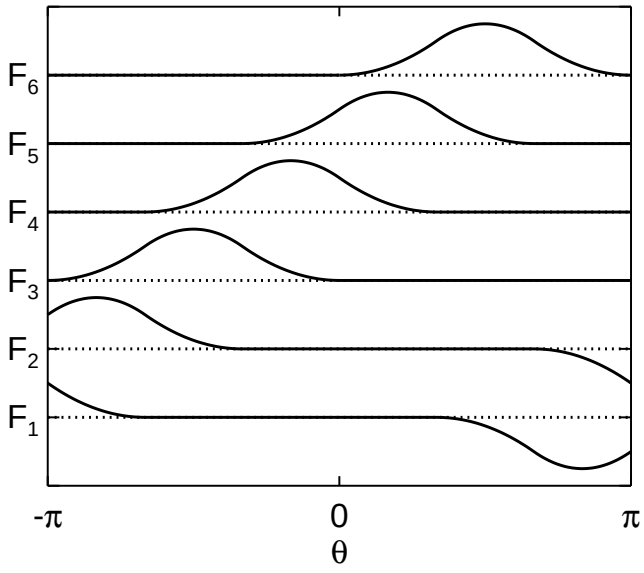

Figure 4.1: Quadratic basis functions, $F_m(\theta)$, for $n_{\text{blend}} = 6$ and phase $\mathcal{P} = -1$.

condition $z(\theta + 2\pi) = \mathcal{P} z(\theta)$. On the infinite domain $(-\infty, \infty)$ we can write

$$z(\theta) = \sum_{m=-\infty}^{\infty} c_m \, N_m(\theta/\Delta\theta) \; , \tag{4.71}$$

$$= \sum_{m=1}^{n_{\text{blend}}} \left[\cdots + c_{m-n_{\text{blend}}} N_{m-n_{\text{blend}}} + c_m N_m + c_{m+n_{\text{blend}}} N_{m+n_{\text{blend}}} + \cdots \right] \; , \tag{4.72}$$

where $N_m(\theta/\Delta\theta) = N(\theta/\Delta\theta - m)$, $\Delta\theta \doteq 2\pi/n_{\text{blend}}$, and n_{blend} is the number of basis functions used to represent one 2π-segment of the function z. The phase condition in θ translates into an equivalent phase condition for the blending coefficients themselves; namely $c_{m+n_{\text{blend}}} = \mathcal{P}\, c_m$. The function z is therefore completely described by the coefficients $\{c_1, \ldots, c_{n_{\text{blend}}}\}$ and basis functions $\{F_1, \ldots, F_{n_{\text{blend}}}\}$ according to

$$z(\theta) = \sum_{m=1}^{n_{\text{blend}}} c_m F_m(\theta) \quad \text{where} \quad F_m(\theta) = N(\theta/\Delta\theta - m) + \mathcal{P} N(\theta/\Delta\theta - m - n_{\text{blend}}) \; . \tag{4.73}$$

In choosing a value of the parameter n_{blend}, one is constrained by the number of points used in the orbit time discretization, n_τ. Given that a passing particle is described by $n_\tau/2$ orbit points, choosing values of n_{blend} larger than $n_\tau/2$ will lead to a breakdown of the method since there will be less than one orbit point per blending function segment. For the simulations presented in this paper, we have found that $n_{\text{blend}} = 6$ and $n_\tau = 20$ are efficient choices. However, we expect that the simulation of plasmas with strong equilibrium shaping, will require a simultaneous increase of both n_{blend} and n_τ.

Figure 4.1 shows the $n_{\text{blend}} = 6$ quadratic basis functions $\{F_1, \ldots, F_6\}$ for $\mathcal{P} = -1$. We remark that since $\mathcal{P}$ is generally a complex number, and is a function of radius, the basis functions are also

complex and functions of radius. Knowing this, we can write the expansion of fields in terms of the basis functions, with explicit radial dependence indicated, as

$$\delta\phi_n(r_i,\theta) = \sum_{m=1}^{n_b} \tilde{\phi}^i_m F^i_m(\theta) \tag{4.74}$$

$$\delta A_{\|n}(r_i,\theta) = \sum_{m=1}^{n_b} \tilde{A}^i_m F^i_m(\theta) \tag{4.75}$$

$$\delta B_{\|n}(r_i,\theta) = \sum_{m=1}^{n_b} \tilde{B}^i_m F^i_m(\theta) \tag{4.76}$$

Although the blending expansion coefficients $\tilde{\phi}$ and $\tilde{A}$ depend on the toroidal mode number n, we supress this dependence for brevity. A few well-known but important observations concerning the approximation properties of the linear, quadratic and cubic functions should be stated. In a region of extremely rapid field variation, the cubic approximation is the least robust — suffering from overshoot/undershoot oscillations. Conversely, as the fields become progressively smoother, the linear approximation will give the poorest interpolation accuracy. A further undesireable property of the linear approximation is its discontinuous first derivative. Although there is no general rule or obviously best interpolation order for all situations, we find that the piecewise quadratic functions are sufficiently accurate and robust for all cases studied to date.

4.6 Velocity-Space Discretization

To solve the Maxwell equations, and to compute the transport fluxes, we will need to develop a discrete representation of the operator $\mathcal{F}V$. In the present section, we discuss quadrature methods for evaluation of these operators. Since the techniques which follow apply independently to all species, we omit species indices for brevity.

4.6.1 Decomposition of $\mathcal{F}V$

Since $V[1] = 1$, it follows automatically that $\mathcal{F}V[1] = 1$. An equivalent statement of this result is embodied in the identity

$$\frac{1}{2\sqrt{\pi}} \int_0^\infty d\varepsilon\, e^{-\varepsilon} \sqrt{\varepsilon} \int_0^{\lambda^*} d\lambda\, \bar{\tau} \oint d\tau = \mathcal{J}_0 \ , \tag{4.77}$$

with $\lambda^* = 1/\hat{B}(r,0)$ the maximum possible value of λ, and $\mathcal{J}_0$ defined in Sec. 1.2.4. Above, we have used the integral identity

$$\sum_\sigma \int_{-\pi}^{\pi} d\theta\, G_\theta(r,\theta) \int_0^{1/\hat{B}(r,\theta)} \frac{d\lambda}{\sqrt{1-\lambda\hat{B}(r,\theta)}} = \int_0^{\lambda^*} d\lambda\, \bar{\tau} \oint d\tau \ . \tag{4.78}$$

Since the numerical evaluation of integrals of this type will involve separate integration weights in each of the variables ε, λ and τ, it is useful to make the decomposition

$$\mathcal{F}V = V_\varepsilon \times V_\lambda \times V_\tau \ , \tag{4.79}$$

with factors

$$V_\varepsilon[h] \doteq \frac{2}{\sqrt{\pi}} \int_0^\infty d\varepsilon\, e^{-\varepsilon} \sqrt{\varepsilon}\, h \,, \tag{4.80}$$

$$V_\lambda[h] \doteq \frac{1}{2\,\mathcal{J}_0} \int_0^{\lambda^*} d\lambda\, \bar{\tau}\, h \,, \tag{4.81}$$

$$V_\tau[h] \doteq \frac{1}{2} \oint d\tau\, h \,. \tag{4.82}$$

These are normalized so that $V_\varepsilon[1] = V_\lambda[1] = V_\tau[1] = 1$. The task at hand, now, is the construction of discrete forms of these operators, and therefore of $\mathcal{F}V$.

4.6.2 Energy Integration

To develop a quadrature method for the energy integral, we split the interval of integration in V_ε — defined in Eq. (4.80) — into two regions: $[0, \varepsilon^*)$ and $[\varepsilon^*, \infty)$, where ε^* is the maximum energy gridpoint (input). Integration over the first interval is done by changing variables according to

$$x(\varepsilon) \doteq \frac{2}{\sqrt{\pi}} \int_0^\varepsilon d\varepsilon\, e^{-\varepsilon} \sqrt{\varepsilon} \,. \tag{4.83}$$

We let $x_0 \doteq x(\varepsilon^*)$, and evaluate the integral using Gauss-Legendre integration [BF85] over $n_\varepsilon - 1$ points:

$$\int_0^{x_0} dx\, h[\varepsilon(x)] \simeq \sum_{i=1}^{n_\varepsilon - 1} w_i\, h[\varepsilon(x_i)] \,. \tag{4.84}$$

The abscissae and weights (x_i, w_i) are the usual Gauss-Legendre ones. Note that we must solve the nonlinear equations $x_i = x(\varepsilon_i)$ for ε_i to obtain the energy gridpoints. With the dominant part of the energy integration done, we evaluate the remaining, infinite integral according to

$$\frac{2}{\sqrt{\pi}} \int_{\varepsilon^*}^\infty d\varepsilon\, e^{-\varepsilon} \sqrt{\varepsilon}\, h(\varepsilon) \simeq h(\varepsilon^*)\, \frac{2}{\sqrt{\pi}} \int_{\varepsilon^*}^\infty d\varepsilon\, e^{-\varepsilon} \sqrt{\varepsilon} = (1 - x_0) h(\varepsilon^*) \,. \tag{4.85}$$

This gives the final weight $1 - x_0$ at the energy gridpoint ε^*, for a total of n_ε gridpoints. We remark that this method has the desireable property

$$\sum_{i=1}^{n_\varepsilon} w_i = 1 \quad \text{such that} \quad \forall i,\, w_i > 0 \,. \tag{4.86}$$

Some sample abscissae and weights are given in Table 4.1 to limited precision (10 significant digits). Note that it is straightforward to generate these, and thus to enforce the sum in Eq. (4.86), to machine precision. The abcissae and weights are unique for a given n_ε and ε^*. Outside of this section, to avoid ambiguity, we will use index i_ε and weight $w_{i_\varepsilon}^{(\varepsilon)}$ to refer to energy integration.

4.6.3 λ Integration

The λ integration follows essentially the same strategy as the energy integration, with only minor differences. First, introduce the integration variable

$$x(\lambda) \doteq \frac{1}{\mathcal{J}_0} \int_0^\lambda d\lambda' \bar{\tau}(\lambda') \,. \tag{4.87}$$

	$n_\varepsilon = 4$, $\varepsilon^* = 3.0$		$n_\varepsilon = 6$, $\varepsilon^* = 4.0$	
i	ε_i	w_i	ε_i	w_i
1	0.2924572707	0.2467749375	0.1625303849	0.1130127375
2	1.0404041729	0.3948399000	0.5442466206	0.2283030745
3	2.2531263847	0.2467749375	1.1228428641	0.2713566704
4	3.0000000000	0.1116102251	1.9784353093	0.2283030745
5			3.2361246631	0.1130127375
6			4.0000000000	0.0460117057

Table 4.1: Sample energy abscissae and weights

i	x_i	λ_i	w_i
1	0.0701916516	0.1353809983	0.1730025988
2	0.3114046777	0.5237287429	0.2768041580
3	0.5526177038	0.7871934230	0.1730025988
4	0.6653193692	0.8581589333	0.1047751790
5	0.8114046777	0.9778736670	0.1676402866
6	0.9574899862	1.1217887702	0.1047751790

Table 4.2: Sample λ weights for $n_{\text{pass}} = n_{\text{trap}} = 3$.

Then, then V_λ can be expressed as

$$V_\lambda[h] = \int_0^1 dx\, h[x(\lambda)] \,. \tag{4.88}$$

Because h is rapidly-varying across the trapped-passing boundary at $x_t = x(\lambda_t)$, where $\lambda_t = 1/B(\pi)$, it is wise to split the previous integral into two regions:

$$\int_0^1 dx\, h[x(\lambda)] = \int_0^{x_t} dx\, h[x(\lambda)] + \int_{x_t}^1 dx\, h[x(\lambda)] \,. \tag{4.89}$$

Gauss-Legendre rules are then applied to each integral separately to determine abscissae and weights (x_i, w_i). Then, as before, the equations $x_i = x(\lambda_i)$ must be inverted numerically to obtain the gridpoints λ_i.

We emphasize that there is no assumption of continuity across the trapped passing boundary. In fact, in the collisionless limit, we do not expect the distribution to be continuous there. With weak collisions, we expect the formation of of a boundary layer around $x = x_t$. In the latter case, we expect good layer resolution because the Gauss-Legendre scheme puts integration abcissae very close to (but not on) x_t. When combined with the orbit-time grid, the λ integration abcissae provide the $(\theta, v_\parallel/v)$ gridpoint distribution shown in Fig. 7.1.

Sample values of abscissae and weights are given in Table 3 for a circular equilibrium with $r/R_0 = 1/6$. Outside of this section, to avoid ambiguity, we will use index i_λ and weight $w_{i_\lambda}^{(\lambda)}$ to refer to pitch-angle integration.

4.6.4 Discretization Summary

Our methods for solution of the Maxwell equations have the implication that it is not V but $\mathcal{F}V$ for which a discrete form is required. But we have already done enough to show that the discretization takes the form

$$\mathcal{F}V[h] \to \sum_{i_\varepsilon=1}^{n_\varepsilon} w_{i_\varepsilon}^{(\varepsilon)} \sum_{i_\lambda=1}^{n_\lambda} w_{i_\lambda}^{(\lambda)} \sum_{i_\tau=1}^{n_\tau} w_{i_\tau}^{(\tau)} \, h_{i_\varepsilon i_\lambda i_\tau} \ , \tag{4.90}$$

where, so far, no radial discretization has been employed. The τ-weights are simply $w_{i_\tau}^{(\tau)} = (1/2)\Delta\tau = 1/n_\tau$. The numerical representation of the weights is such that when $h = 1$, the sum in Eq. (4.90) is unity to machine precision.

4.7 Connection to Ballooning Modes

In what follows, we limit our discussion to $s - \alpha$ geometry. Recall the form of a toroidal harmonic when expanded in a radial Fourier series

$$\delta\phi_n(r,\theta)e^{-in\alpha} = e^{-in[\varphi - q(r)\theta]} \sum_p e^{2\pi i p r/L} \delta\phi_{np}(\theta) \tag{4.91}$$

where L, the radial domain size, is written as a multiple, M, of the natural quantization length, $1/(nq_0')$, of the ballooning mode:

$$L \doteq M \, \frac{1}{nq_0'} = M \, \frac{r_0}{nq_0 s_0} \ . \tag{4.92}$$

So we can write

$$\delta\phi_n(r,\theta)e^{-in\alpha} = e^{-in[\varphi - q(r)\theta]} \sum_p e^{2\pi i p r (nq_0'/M)} \, \delta\phi_{np}(\theta) \ , \tag{4.93}$$

$$= e^{-in[\varphi - q(r)\theta]} \sum_p e^{2\pi i p (nq/M)} \, \Phi_B^\ell(\theta + 2\pi p') \ . \tag{4.94}$$

where we have introduced the *ballooning potential* Φ_B^ℓ via

$$\delta\phi_{np}(\theta) = \Phi_B^\ell(\theta + 2\pi p') e^{2\pi i n q_0 p/M} \ . \tag{4.95}$$

This transformation is motivated by the fact that the function $\delta\phi_n(r,\theta)$ is not periodic but instead satisfies the phase condition in Eq. (4.3). The meanings of p' and ℓ are not yet specified. Writing $p = Mp' + \ell$, and breaking the sum into parts yields

$$\delta\phi_n(r,\theta)e^{-in\alpha} = e^{-in[\varphi - q(r)\theta]} \sum_{\ell=0}^{M-1} \sum_{p'} e^{inq(\theta_B^\ell + 2\pi p')} \, \Phi_B^\ell(\theta + 2\pi p') \ , \tag{4.96}$$

$$= e^{-in\varphi} \sum_{\ell=0}^{M-1} \sum_{p'} e^{inq(\theta + \theta_B^\ell + 2\pi p')} \, \Phi_B^\ell(\theta + 2\pi p') \ , \tag{4.97}$$

where the function $\Phi_B^\ell(\theta)$ is continuous and bounded over the domain $-\infty < \theta < \infty$. The usual equation for Φ_B^ℓ can be obtained by substituting Eq. (4.97) into the gyrokinetic equation, and then solving for Φ_B^ℓ for a given value of ℓ on the infinite θ-domain. Here, $\theta_B^\ell = 2\pi(\ell/M)$ is the *ballooning angle*. In GYRO, we have

$$M = \texttt{BOX\_MULTIPLIER} \; . \tag{4.98}$$

On a discrete grid, the indices have the following ranges of variation:

$$p = -\frac{n_r}{2}, \ldots, \frac{n_r}{2} - 1 \; , \tag{4.99}$$

$$p' = -\frac{n_r}{2M}, \ldots, \frac{n_r}{2M} - 1 \; , \tag{4.100}$$

$$\ell = 0, \ldots, M-1 \; . \tag{4.101}$$

such that the discrete Fourier transform of the potential is

$$\delta\phi_{np}(\theta) = \frac{1}{n_r} \sum_{j=-n_r/2}^{n_r/2-1} \delta\phi_n(r_j, \theta) e^{-2\pi i p j / n_r} \; . \tag{4.102}$$

In conclusion, over the interval

$$-\pi \left(\frac{n_r}{M} + 1 \right) \leq \theta < \pi \left(\frac{n_r}{M} - 1 \right) \; , \tag{4.103}$$

we have the reconstruction algorithm

$$\ell = 0: \quad \Phi_B^0(\theta + 2\pi p') = \delta\phi_{n,Mp'}(\theta) e^{-2\pi i n q_0 p'} \; , \tag{4.104}$$

$$\ell = 1: \quad \Phi_B^1(\theta + 2\pi p') = \delta\phi_{n,Mp'+1}(\theta) e^{-2\pi i n q_0 p'} e^{-2\pi i n q_0 (1/M)} \; , \tag{4.105}$$

$$\ell = 2: \quad \Phi_B^2(\theta + 2\pi p') = \delta\phi_{n,Mp'+2}(\theta) e^{-2\pi i n q_0 p'} e^{-2\pi i n q_0 (2/M)} \; , \tag{4.106}$$

$$\vdots \tag{4.107}$$

$$\ell = M-1: \quad \Phi_B^{M-1}(\theta + 2\pi p') = \delta\phi_{n,Mp'+M-1}(\theta) e^{-2\pi i n q_0 p'} e^{-2\pi i n q_0 (M-1)/M} \; . \tag{4.108}$$

Chapter 5

Temporal Discretization

The gyrokinetic treatment of electrons is problematic in simulations because of the emergence of a host of numerical instabilities connected with the discretization of the electron parallel motion. The presence of the electrostatic and magnetic potentials in the advection term,

$$\frac{\partial \hat{h}_a}{\partial \hat{t}} + \frac{\hat{v}_{\parallel a}}{G_\theta q(R_0/a)} \frac{\partial}{\partial \theta} \left(\hat{h}_a + z_a \alpha_a \hat{\Psi}_a \right) + \cdots \tag{5.1}$$

for $a = e$ give rise to stability considerations much more troublesome than the simple electron parallel Courant limit. Physically, the parallel term gives rise to the high-frequency *electrostatic Alfvén* wave [LLHL01] at $\beta = 0$. In the slab limit, one can show

$$\omega_{\rm H} = \frac{k_\parallel}{k_r} \sqrt{\frac{m_i}{m_e}}\, \Omega_{ci} \ . \tag{5.2}$$

This mode is physically pathological, because the frequency increases indefinitely as m_e decreases, and also as k_r decreases – that is, as the radial box size grows. While nonzero β provides a cutoff, the stable numerical treatment of this term is nontrivial.[1] To overcome this severe and intrinsic simulation difficulty, we were persuaded to treat the electron advection implicitly. We experimented with a variety of implicit-explicit (IMEX) Runge-Kutta (RK) schemes that were popular in the period 2001-2003 [ARW95, ARS97, PR00, PR02, KC03], settling on an IMEX-SSP scheme of Pareschi and Russo [PR02].

5.0.1 Reduction to canonical form

For brevity, we suppress the toroidal harmonic index and abbreviate $h_{a,n}$ as h_a. With all spatial operators discretized, the GKM system has the form

$$\dot{h}_a = \widetilde{H}_a(\{h_a\}, h_e) \ , \quad a = 1, \ldots, n_{\rm ion} \tag{5.3}$$

$$\dot{h}_e = \widetilde{H}_e(\{h_a\}, h_e) + H_e(\{\hat{h}_a\}, h_e) \ , \tag{5.4}$$

where $\{h_a\} = h_1, \ldots, h_{n_{\rm ion}}$. In Eqs. (5.3) and (5.4), the use of a tilde on the RHS represents a *nonstiff* term, while the absence of a tilde indicates a *stiff* term. The IMEX-RK schemes are written

[1] The ability of Eulerian codes to treat this term both accurately and stably has been a major contributor to the relative success of Eulerian solvers in comparison to their PIC counterparts.

for equations in the canonical form

$$\dot{y} = \widetilde{Y}(y) + Y(y) \ , \tag{5.5}$$

with $\widetilde{Y}$ the explicit RHS and Y the implicit RHS. Thus, we have the connection

$$y = \begin{bmatrix} \{\hat{h}_a\} \\ h_e \end{bmatrix} \quad \widetilde{Y} = \begin{bmatrix} \{\widetilde{H}_a\} \\ \widetilde{H}_e \end{bmatrix} \quad Y = \begin{bmatrix} 0 \\ H_e \end{bmatrix} \ . \tag{5.6}$$

Now, there is some hidden complexity in how we have written the GKM equations, as the functions H depend on the distribution function h both directly, and indirectly through the fields. We emphasize that it is only the fast electron advection term, H_e, which we wish to (or are able to) treat implicitly:

$$H_e \doteq -\hat{v}_{\|e}(r,\theta,\varepsilon)\frac{a}{qR_0G_\theta}\frac{\partial}{\partial\theta}\left[\hat{h}_e - \alpha_e\left(\delta\hat{\phi} - \hat{v}_{\|e}\delta\hat{A}_\| - \varepsilon\lambda\hat{T}_e\delta\hat{B}_\|\right)\right] \tag{5.7}$$

$$= -\Omega(r,\theta,\varepsilon)\partial_\tau\left[\hat{h}_e - \alpha_e\left(\delta\hat{\phi} - \hat{v}_{\|e}\delta\hat{A}_\| - \varepsilon\lambda\hat{T}_e\delta\hat{B}_\|\right)\right] \ , \tag{5.8}$$

where from this point forward we suggest that the reader consider the object ∂_τ as a matrix.

5.0.2 IMEX-RK-SSP schemes of Pareschi and Russo

The second-order IMEX schemes we consider can be summarized in Butcher tableau form as

Explicit

0		
$\tilde{a}_{21}$	0	
$\tilde{a}_{31}$	$\tilde{a}_{32}$	0
$\tilde{w}_1$	$\tilde{w}_2$	$\tilde{w}_3$

Implicit

a_{11}		
a_{21}	a_{22}	
a_{31}	a_{32}	a_{33}
w_1	w_2	w_3

This notation corresponds to the following explicit evolution equations:

$$y_1 = y + \Delta t\, a_{11} Y_1 \tag{5.9}$$

$$y_2 = y + \Delta t(\tilde{a}_{21}\widetilde{Y}_1 + a_{21}Y_1) + \Delta t\, a_{22} Y_2 \tag{5.10}$$

$$y_3 = y + \Delta t(\tilde{a}_{31}\widetilde{Y}_1 + \tilde{a}_{32}\widetilde{Y}_2 + a_{31}Y_1 + a_{32}Y_2) + \Delta t\, a_{33} Y_3 \tag{5.11}$$

$$\bar{y} = y + \Delta t \sum_{k=1}^{3} \tilde{w}_k \widetilde{Y}_k + \Delta t \sum_{k=1}^{3} w_k Y_k \ . \tag{5.12}$$

Above, y is the old field vector (time t) and $\bar{y}$ is the new field vector (time $t + \Delta t$). In GYRO, we currently use the SSP2(3,2,2) scheme:

SSP2(3,2,2)

Explicit

0		
0	0	
0	1	0
0	1/2	1/2

Implicit

1/2		
−1/2	1/2	
0	1/2	1/2
0	1/2	1/2

Since the diagonal coefficients of the implicit stages are equal, we need to solve the same implicit system at each stage. It would be good at some point to implement the SSP2(3,3,2) scheme, which requires the solution of two different implicit problems, but has half the advective Courant limit in explicit part.

SSP2(3,3,2)

Explicit

0		
1/2	0	
1/2	1/2	0
1/3	1/3	1/3

Implicit

1/4		
0	1/4	
1/3	1/3	1/3
1/3	1/3	1/3

5.0.3 Implementation in GYRO

The complication which arisese when applying these methods to GYRO are connected with the field solve. For all the so-called SDIRK methods, the implicit equations at each stage have a generic form. In the present case, at each integrator stage ($k = 1, 2, 3$), we are faced with:

$$(h_a)_k = h_a + \Delta t \sum_{p<k} \tilde{a}_{kp} (\widetilde{H}_a)_p \ , \tag{5.13}$$

$$(h_e)_k = h_e + \Delta t \sum_{p<k} \tilde{a}_{kp} (\widetilde{H}_e)_p + \Delta t \sum_{p<k} a_{kp} (H_e)_p + \Delta t \, a_{kk} (H_e)_k \ . \tag{5.14}$$

Because H_e depends on the fields, we must advance the Maxwell equations at each stage before determining the $(h_e)_k$. However, we can compute all $(h_a)_k$ for $a = 1, \ldots, n_{\rm ion}$ before solving the implicit problem. First, solve formally for $(h_e)_k$:

$$(h_e)_k = (\delta h_e)_k + \alpha_e \frac{c_0 \Delta t \, \Omega \, \partial_\tau}{1 + c_0 \Delta t \, \Omega \, \partial_\tau} \left(\delta\hat{\phi} - \hat{v}_{\parallel e} \delta\hat{A}_\parallel - \varepsilon \lambda \hat{T}_e \delta\hat{B}_\parallel \right)_k \tag{5.15}$$

where $(\delta h_e)_k$ is the explicitly-known quantity

$$(\delta h_e)_k = \frac{1}{1 + c_0 \Delta t \, \Omega \, \partial_\tau} \left[h_e + \Delta t \sum_{p<k} \tilde{a}_{kp} (\widetilde{H}_e)_k + \Delta t \sum_{p<k} a_{kp} (H_e)_k \right] \ . \tag{5.16}$$

Now, substitute the analytic expression for $(h_e)_k$ into the Maxwell equations. This substitution gives a version of the Maxwell equations that looks like the standard explicit forms, but with added field terms arising from the second term on the RHS of Eq. (5.15). If we multiply the Maxwell equations by $F^{*i}_m(\theta)$, and operate with the bounce-velocity summation operator $\mathcal{F}V$ (noting that $VV = V$), we obtain Δt-coupled Poisson-Ampère equations.

$$(M_{PP})^{ii'}_{mm'} \tilde{\phi}^{i'}_{m'} + (M_{PB})^{ii'}_{mm'} \tilde{B}^{i'}_{m'} = (S_P)^i_m + (\mathrm{I}_{\rm PP})^i_{mm'} \tilde{\phi}^i_{m'} + (\mathrm{I}_{\rm PA})^i_{mm'} \tilde{A}^i_{m'} + (\mathrm{I}_{\rm PB})^i_{mm'} \tilde{B}^i_{m'} \tag{5.17}$$

$$(M_{AA})^{ii'}_{mm'} \tilde{A}^{i'}_{m'} = (S_A)^i_m + (\mathrm{I}_{\rm AP})^i_{mm'} \tilde{\phi}^i_{m'} + (\mathrm{I}_{\rm AA})^i_{mm'} \tilde{A}^i_{m'} + (\mathrm{I}_{\rm AB})^i_{mm'} \tilde{B}^i_{m'} \tag{5.18}$$

$$(M_{BP})^{ii'}_{mm'} \tilde{\phi}^{i'}_{m'} + (M_{BB})^{ii'}_{mm'} \tilde{B}^{i'}_{m'} = (S_B)^i_m + (\mathrm{I}_{\rm BP})^i_{mm'} \tilde{\phi}^i_{m'} + (\mathrm{I}_{\rm BA})^i_{mm'} \tilde{A}^i_{m'} + (\mathrm{I}_{\rm BB})^i_{mm'} \tilde{B}^i_{m'} \tag{5.19}$$

Here the *field matrices* are:

$$(M_{PP})^{ii\prime}_{mm'} = \mathcal{F}V\left[F^{*i}_m(\theta(\tau_q))\mathcal{L}^{ii\prime}_{PP}(\theta(\tau_q))F^{i\prime}_{m\prime}(\theta(\tau_q))\right] \tag{5.20}$$

$$(M_{PB})^{ii\prime}_{mm'} = \mathcal{F}V\left[F^{*i}_m(\theta(\tau_q))\mathcal{L}^{ii\prime}_{PB}(\theta(\tau_q))F^{i\prime}_{m\prime}(\theta(\tau_q))\right] \tag{5.21}$$

$$(M_{AA})^{ii\prime}_{mm'} = \mathcal{F}V\left[F^{*i}_m(\theta(\tau_q))\mathcal{L}^{ii\prime}_{AA}(\theta(\tau_q))F^{i\prime}_{m\prime}(\theta(\tau_q))\right] \tag{5.22}$$

$$(M_{BB})^{ii\prime}_{mm'} = \mathcal{F}V\left[F^{*i}_m(\theta(\tau_q))\mathcal{L}^{ii\prime}_{BB}(\theta(\tau_q))F^{i\prime}_{m\prime}(\theta(\tau_q))\right] \tag{5.23}$$

$$(M_{BP})^{ii\prime}_{mm'} = \mathcal{F}V\left[F^{*i}_m(\theta(\tau_q))\mathcal{L}^{ii\prime}_{BP}(\theta(\tau_q))F^{i\prime}_{m\prime}(\theta(\tau_q))\right] \tag{5.24}$$

where

$$\mathcal{L}_{PP} = \bar{\lambda}_D^2\nabla_\perp^2 + \alpha_e + \sum_{a=1}^{n_{ion}}\alpha_a z_a^2 V\left[1-\mathcal{G}_{0a}^2\right] \tag{5.25}$$

$$\mathcal{L}_{PB} = \sum_{a=1}^{n_{ion}} -2z_a\hat{n}_a V[\varepsilon\lambda\mathcal{G}_{0a}\mathcal{G}_{1a}] \tag{5.26}$$

$$\mathcal{L}_{AA} = \frac{-2\bar{\rho}^2_{s,\text{unit}}}{\bar{\beta}_{e,\text{unit}}}\nabla_\perp^2 + \sum_{a=1}^{n_{ion}}\alpha_a z_a^2 V[\hat{v}_\parallel^2\mathcal{G}_{0a}^2] \tag{5.27}$$

$$\mathcal{L}_{BB} = \frac{1}{\bar{\beta}_{e,\text{unit}}} + \sum_{a=1}^{n_{ion}} 2\hat{n}_a\hat{T}_a V[\lambda^2\mathcal{G}_{1a}^2\varepsilon^2] \tag{5.28}$$

$$\mathcal{L}_{BP} = \sum_{a=1}^{n_{ion}} z_a\hat{n}_a V[\varepsilon\lambda\mathcal{G}_{1a}\mathcal{G}_{0a}]\,. \tag{5.29}$$

The *advection matrices* are:

$$(I_{PP})^i_{mm\prime} = \alpha_e^i\mathcal{F}V\left[F^{*i}_m(\theta(\tau_q))\mathcal{O}^i_{qq\prime}F^i_{m\prime}(\theta(\tau_{q\prime}))\right] \tag{5.30}$$

$$(I_{PA})^i_{mm\prime} = -\alpha_e^i\mathcal{F}V\left[F^{*i}_m(\theta(\tau_q))\mathcal{O}^i_{qq\prime}F^i_{m\prime}(\theta(\tau_{q\prime}))\hat{v}_{\parallel e}(\theta(\tau_{q\prime}))\right] \tag{5.31}$$

$$(I_{PB})^i_{mm\prime} = -\alpha_e^i\hat{T}_e^i\mathcal{F}V\left[F^{*i}_m(\theta(\tau_q))\mathcal{O}^i_{qq\prime}F^i_{m\prime}(\theta(\tau_{q\prime}))\varepsilon\lambda\right] \tag{5.32}$$

$$(I_{AP})^i_{mm\prime} = \alpha_e^i\mathcal{F}V\left[\hat{v}_{\parallel e}(\theta(\tau_q))F^{*i}_m(\theta(\tau_q))\mathcal{O}^i_{qq\prime}F^i_{m\prime}(\theta(\tau_{q\prime}))\right] \tag{5.33}$$

$$(I_{AA})^i_{mm\prime} = -\alpha_e^i\mathcal{F}V\left[\hat{v}_{\parallel e}(\theta(\tau_q))F^{*i}_m(\theta(\tau_q))\mathcal{O}^i_{qq\prime}F^i_{m\prime}(\theta(\tau_{q\prime}))\hat{v}_{\parallel e}(\theta(\tau_{q\prime}))\right] \tag{5.34}$$

$$(I_{AB})^i_{mm\prime} = -\alpha_e^i\hat{T}_e^i\mathcal{F}V\left[\hat{v}_{\parallel e}(\theta(\tau_q))F^{*i}_m(\theta(\tau_q))\mathcal{O}^i_{qq\prime}F^i_{m\prime}(\theta(\tau_{q\prime}))\varepsilon\lambda\right] \tag{5.35}$$

$$(I_{BP})^i_{mm\prime} = \frac{1}{2}\alpha_e^i\hat{T}_e^i\mathcal{F}V\left[F^{*i}_m(\theta(\tau_q))\mathcal{O}^i_{qq\prime}F^i_{m\prime}(\theta(\tau_{q\prime}))\varepsilon\lambda\right] \tag{5.36}$$

$$(I_{BA})^i_{mm\prime} = -\frac{1}{2}\alpha_e^i\hat{T}_e^i\mathcal{F}V\left[F^{*i}_m(\theta(\tau_q))\mathcal{O}^i_{qq\prime}F^i_{m\prime}(\theta(\tau_{q\prime}))\hat{v}_{\parallel e}(\theta(\tau_{q\prime}))\varepsilon\lambda\right] \tag{5.37}$$

$$(I_{BB})^i_{mm\prime} = -\frac{1}{2}\alpha_e^i(\hat{T}_e^i)^2\mathcal{F}V\left[F^{*i}_m(\theta(\tau_q))\mathcal{O}^i_{qq\prime}F^i_{m\prime}(\theta(\tau_{q\prime}))\varepsilon^2\lambda^2\right] \tag{5.38}$$

Next, the *source matrices* are

$$(S_P)^i_m = \mathcal{F}V\left[F^{*i}_m(\theta(\tau_q))H^i_P(\theta(\tau_q))\right] - \mathcal{F}V\left[F^{*i}_m(\theta(\tau_q))\delta\hat{h}^i_e(\theta(\tau_q))\right] \tag{5.39}$$

$$(S_A)^i_m = \mathcal{F}V\left[F^{*i}_m(\theta(\tau_q))H^i_A(\theta(\tau_q))\right] - \mathcal{F}V\left[\hat{v}_{\parallel e}(\theta(\tau_q))F^{*i}_m(\theta(\tau_q))\delta\hat{h}^i_e(\theta(\tau_q))\right] \tag{5.40}$$

$$(S_B)^i_m = \mathcal{F}V\left[F^{*i}_m(\theta(\tau_q))H^i_B(\theta(\tau_q))\right] - \frac{1}{2}\hat{T}_e\mathcal{F}V\left[\varepsilon\lambda F^{*i}_m(\theta(\tau_q))\delta\hat{h}^i_e(\theta(\tau_q))\right] \tag{5.41}$$

where

$$H_P \doteq \sum_{a=1}^{n_{ion}} z_a \mathcal{G}_{\prime a} \hat{h}_a \tag{5.42}$$

$$H_A \doteq \sum_{a=1}^{n_{ion}} z_a \hat{v}_{\parallel} \mathcal{G}_{\prime a} \hat{h}_a \tag{5.43}$$

$$H_B \doteq \sum_{a=1}^{n_{ion}} -\hat{T}_a \mathcal{G}_{\infty a} \hat{h}_a \varepsilon \lambda \; . \tag{5.44}$$

In the preceeding expressions, we have omitted the stage number, k, for brevity. The advection matrix $\mathcal{O}_{qq'}$ is defined as

$$\mathcal{O}_{qq'}(r, \lambda, \varepsilon) \doteq \left(\frac{1}{1 + c_0 \Delta t \, \Omega \, \partial_\tau} \right)_{qq'} . \tag{5.45}$$

We reorganize the equations into a single partitioned system suitable for solution with a direct sparse solver (the current implementation uses UMFPACK). Solve the system with UMFPACK (S_P, S_A and S_B need to be computed at each step).

$$\begin{bmatrix} M_{PP} & 0 & M_{PB} \\ 0 & M_{AA} & 0 \\ M_{BP} & 0 & M_{BB} \end{bmatrix} \begin{bmatrix} \tilde{\phi} \\ \tilde{A} \\ \tilde{B} \end{bmatrix} = \begin{bmatrix} S_P \\ S_A \\ S_B \end{bmatrix} + \begin{bmatrix} I_{PP} & I_{PA} & I_{PB} \\ I_{AP} & I_{AA} & I_{AB} \\ I_{BP} & I_{BA} & I_{BB} \end{bmatrix} \begin{bmatrix} \tilde{\phi} \\ \tilde{A} \\ \tilde{B} \end{bmatrix} \tag{5.46}$$

5.0.4 Procedural summary

Having precomputed the matrices M and I, for $k = 1, \ldots, 3$:

1. Evaluate $(h_a)_k$ using Eq. (5.13).
2. Evaluate $(\delta h_e)_k$ using Eq. (5.16).
3. Evaluate S_P, S_A and S_B using Eqs. (5.39) through (5.41), respectively.
4. Solve Eq. (5.46) for $\tilde{\phi}$, $\tilde{A}$ and $\tilde{B}$.
5. Evaluate $(h_e)_k$ using Eq. (5.15).

With all stage values, $k = 1, 2, 3$, computed, evaluate $\bar{y} = (\{\bar{h}_a\}, \bar{h}_e)^{\mathrm{T}}$ using Eq. (5.12). Then, synchronize the fields using an explicit field update.

5.0.5 Time-Integration Considerations

Ad-hoc semi-implicit schemes (for example, first order splitting) are normally a mixed-blessing, offering improved stability of stiff terms at the expense of accuracy and/or stability loss for the explicit terms. Higher order splittings can be constructed but are susceptible to a severe accuracy loss in the stiff limit. The IMEX schemes we describe herein [PR00] are:

- **Asymptotic Preserving**: the difference scheme is asymptotically correct in the stiff limit.
- **Asymptotically Accurate**: the explicit integrator retains its order for the limiting differential-algebraic system in the stiff limit.
- **Strong-Stability-Preserving**: we recover an SSP-ERK [GST] scheme in the stiff limit.

Chapter 6

Source and Boundary Conditions

6.1 Radial Domain and Boundary Conditions

GYRO has the option of treating periodic (variously called flux-tube, or local) or nonperiodic (global) boundary conditions on $(\delta\phi_n, \delta A_{\parallel n}, h_{\sigma,n})$.

$$r_i = \bar{r} - \frac{L}{2} + \Delta r(i-1) \quad \text{for} \quad i = 1, \ldots, n_r \ . \tag{6.1}$$

where

$$\Delta r \doteq \begin{cases} L/n_r & \text{periodic; } \texttt{BOUNDARY\_METHOD=1} \ , \\ L/(n_r - 1) & \text{nonperiodic; } \texttt{BOUNDARY\_METHOD=2} \ . \end{cases} \tag{6.2}$$

The central radius, $\bar{r}$, is specified by the INPUT parameter `RADIUS`.

6.1.1 Periodic

Flux-tube boundary conditions effectively eliminate the inner and outer radial boundaries by making the quantities periodic in r. For example,

$$\delta\phi_n(r_1, \theta) = \delta\phi_n(r_{n_r}, \theta) \ . \tag{6.3}$$

Use of this boundary condition is very useful for local linear analyses (all the linear results presented in this report use flux-tubes) and computationally efficient for restricted nonlinear studies. However, the flux-tube mode of operation is incompatible with variation of the equilibrium profiles.

6.1.2 Nonperiodic

In order to study physical effects associated with profile variation and rotation shear, it is necessary to abandon flux-tubes and use some type of nonperiodic radial boundary condition. In the design of nonperiodic end conditions, we have attempted to minimize as much as possible the effect of the boundaries on the interior dynamics. To this extent, our goal was to construct "benign" rather

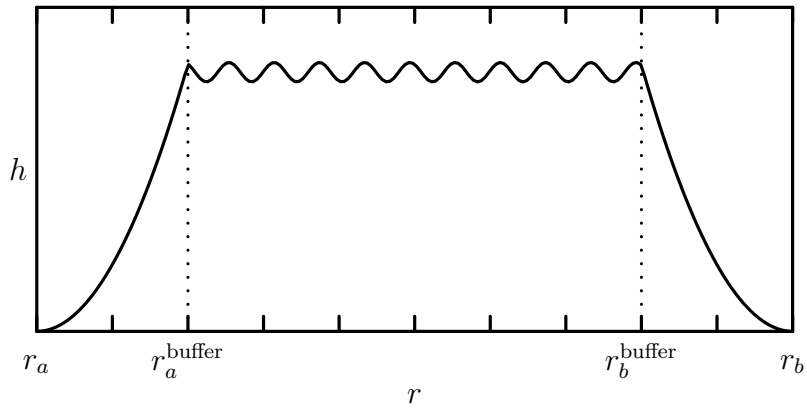

Figure 6.1: Illustration of placement of boundary *buffer* regions.

than physical end conditions. First, to make the notation less cumbersome, let us write

$$r_a \rightarrow r_1 \,, \tag{6.4}$$
$$r_a^{\text{buffer}} \rightarrow r_p \,, \tag{6.5}$$
$$r_b^{\text{buffer}} \rightarrow r_{n_r-p+1} \,, \tag{6.6}$$
$$r_b \rightarrow r_{n_r} \,, \tag{6.7}$$

where the width of the buffer region, p, is set by the input parameter `EXPLICIT_DAMP_GRID`. Experience shows that this number (which is an integer number of gridpoints) should be no smaller than about $8\rho_i$. GYRO has a diagnostic to warn the user if this condition is not satisfied.

First, at the extreme edges of the computational domain, $r = r_a$ and $r = r_b$, we impose Dirichlet boundary conditions on all toroidal harmonics.

$$h_{a,n}(r_a, \theta) = \delta\phi_n(r_a, \theta) = 0 \,, \tag{6.8}$$
$$h_{a,n}(r_b, \theta) = \delta\phi_n(r_b, \theta) = 0 \,. \tag{6.9}$$

Experience shows that these boundary conditions, in the absence of any other tricks, will give rise to strong oscillations at the boundaries. The effect of these oscillations will be felt well into the interior of the computational domain and so various techniques were explored in an effort to mitigate the corruption of the interior solution. One solution that works well is the imposition of a "buffer" region; that is, a region near the boundary where we impose an explicit damping on the $n = 0$ evolution equation. Generally speaking, we modify the normalized gyrokinetic equation, Eq. (4.39), according to

$$\frac{\partial h_{\sigma,0}}{\partial \hat{t}} = \text{RHS}_0 - \frac{a\nu_\sigma(r)}{\bar{c}_s} H_{\sigma,0} \,, \tag{6.10}$$

where

$$\nu_\sigma(r) \doteq \begin{cases} \nu_\sigma^{\text{buffer}} & \text{if } r_a \le r \le r_a^{\text{buffer}} \,, \\ 0 & \text{if } r_a^{\text{buffer}} < r < r_b^{\text{buffer}} \,, \\ \nu_\sigma^{\text{buffer}} & \text{if } r_b^{\text{buffer}} \le r \le r_b \,. \end{cases} \tag{6.11}$$

An illustration of the effect of this technique on computed fields is given in Fig. 6.1. In GYRO, the strength of the damping in the buffer is controlled by the following INPUT parameters

$$\texttt{EXPLICIT\_DAMP} \rightarrow \frac{a\nu_i^{\text{buffer}}}{\bar{c}_s} \ , \tag{6.12}$$

$$\texttt{EXPLICIT\_DAMP\_ELECTRON} \rightarrow \frac{a\nu_e^{\text{buffer}}}{\bar{c}_s} \ . \tag{6.13}$$

6.2 Long-wavelength Source

One dramatic benefit of flux-tube simulations is that no special techniques are required to keep the equilibrium from evolving. In this case, the equilibrium is analytically separable from the fluctuations and there is no coupling between them. In a global simulation there is no such possibility for separability and short-wavelength radial fluctuations are coupled to long-wavelength equilibrium-scale dynamics. In this note we propose a method to partially decouple equilibrium from fluctuations so as to keep the equilibrium profiles from changing.

6.2.1 Formulation of the problem

As in the previous section, we write the $n = 0$ component of the gyrokinetic equation for fluctuations as

$$\frac{\partial h_{\sigma,0}}{\partial \hat{t}} = \text{RHS}_0(r) \ . \tag{6.14}$$

If the system were periodic in r, we could write the Fourier space expression

$$\frac{\partial \widetilde{h}_p}{\partial \hat{t}} = \widetilde{\text{RHS}}_p \ , \tag{6.15}$$

where

$$h_{\sigma,0}(r) = \sum_p \widetilde{h}_p \, e^{-2\pi i p r/L} \ . \tag{6.16}$$

Then, in a flux-tube simulation, we would simply set $\widetilde{h}_0 = 0$, which corresponds to zero radial average of the $n = 0$ fluctuations. Since the $p = 0$ equations decouples from the rest of the problem (the $p = 0$ component of the $\mathbf{E} \times \mathbf{B}$ nonlinearity is identically zero), this is allowed. However, in a global simulation, there is no way to cleanly separate the equilibrium from the fluctuations, because there is no exact analogue of $\widetilde{h}_0$.

6.2.2 Solution by damping

Instead of ignoring $p = 0$ as in a flux-tube simulation, we can instead damp the long-wavelength components. This will drain, in a nonconservative fashion, any pumping that the equilibrium-scale distribution receives from nonlinear coupling. In real space, then, we modify the gyrokinetic equation according to

$$\frac{\partial h_{\sigma,0}}{\partial \hat{t}} = \text{RHS}_0 - \frac{a\nu_{\text{source}}}{\bar{c}_s} \langle h_{\sigma,0} \rangle \ , \tag{6.17}$$

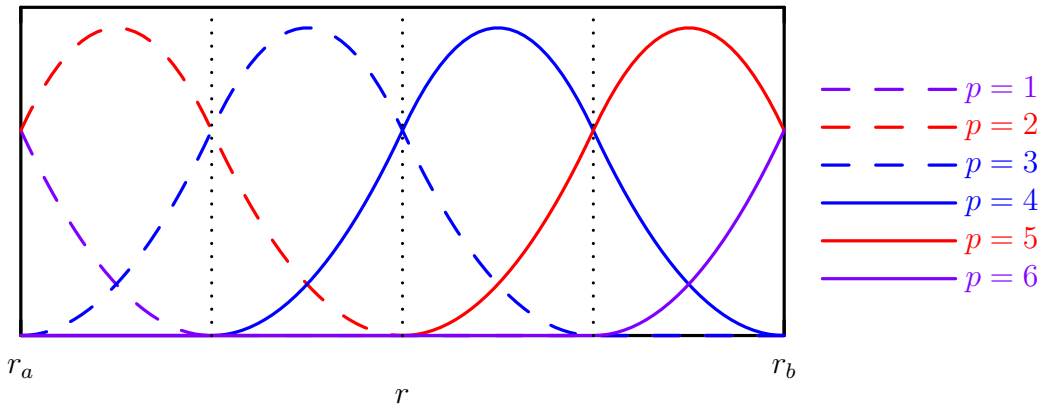

Figure 6.2: Illustration of quadratic finite-element basis for `N_SOURCE=2`. Note that $p = 1, 2$ and $p = 5, 6$ are partial elements.

where the angle brackets denote a projection onto long wavelengths only. For example,

$$\langle h_{\sigma,0}(r)\rangle = \sum_{p=1}^{\texttt{N\_SOURCE}+4} c_p F_p(r) \; . \tag{6.18}$$

The expansion coefficients satisfy $M_{pp'}c_{p'} = S_p$ where

$$M_{pp'} = \int_{r_a}^{r_b} dr\, F_p(r) F_{p'}(r) \quad \text{and} \quad S_p = \int_{r_a}^{r_b} dr\, h_{\sigma,0}(r) F_p(r) \; . \tag{6.19}$$

In GYRO, we take the F_p to be quadratic finite elements. These are defined as scaled translates of the function $N^{(3)}$ given in Eq. (4.69). We also include partial elements in order to satisfy *general nonperiodic boundary conditions*, rather than Dirichlet boundary conditions. The reason for doing this is to most gracefully accomodate the rapid variation of h in the buffer regions. The choice of `N_SOURCE` is somewhat arbitrary but should be small enough to hold only the longest wavelengths fixed (i.e., between 1 and 3).

Note that if the time rate of change is slow, $\partial_t \to 0$, and the steady-state solution for the long-wavelength component is

$$\langle h_{\sigma,0}(r)\rangle = \langle \mathrm{RHS}_0\rangle / \nu_{\mathrm{source}} \; , \tag{6.20}$$

which can be made arbitrarily small by increasing ν_{source}. In GYRO, the strength of the source is controlled by

$$\texttt{NU\_SOURCE} \to \frac{a\nu_{\mathrm{source}}}{\bar{c}_s} \; . \tag{6.21}$$

Chapter 7

Collisions

7.1 Pitch-angle Scattering Operator

The treatment of collisions in gyrokinetic simulations is not as intricate as that required in neoclassical simulations. In the former case, the dominant effect of collisions is pitch-angle scattering in the electron equation. Below we outline the implementation of this effect, and of the associated ion pitch-angle scattering operators.

Treating the collision operator $\hat{C}$ by operator splitting leaves us with the following evolution equation

$$\frac{\partial h_{a,n}}{\partial \hat{t}} = \hat{C}\left[h_{a,n} - z_a \alpha_a \hat{v}_{\|a} \mathcal{G}_a \delta A_{\|,n}\right] \ . \tag{7.1}$$

This has the alternative form

$$\frac{\partial f_{a,n}}{\partial \hat{t}} + z_a \alpha_a \hat{v}_{\|a} \mathcal{G}_a \delta \dot{A}_{\|,n} = \hat{C}\left[f_{a,n}\right] \ , \tag{7.2}$$

where

$$f_{a,n} = h_{a,n} - z_a \alpha_a \hat{v}_{\|a} \mathcal{G}_a \delta A_{\|,n} \ . \tag{7.3}$$

We must take care to avoid the Ampère cancellation problem when solving this equation. Furthermore, due to the viscous Courant limit on the timestep imposed by the operator $\hat{C}$ near the trapped-passing boundary, we use an implicit technique. For typical time steps and 8-point pitch-angle grids, it appears that we are probably very close to the explicit stability limit at $\nu_{ei} \sim c_s/a$. Multiplying Eq. (7.1) by $z_a \hat{v}_{\|a}$, summing over species and integrating gives

$$-\frac{2\bar{\rho}^2_{s,\mathrm{unit}}}{\bar{\beta}_{e,\mathrm{unit}}} \nabla^2_\perp \delta \dot{A}_{\|,n} + \sum_a \alpha_a z_a^2 \, V[\hat{v}^2_{\|a} \mathcal{G}^2_a \delta \dot{A}_{\|,n}] = \sum_a z_a V\left[\hat{v}_{\|a} \hat{C}\left[\mathcal{G}_a f_{a,n}\right]\right] \ . \tag{7.4}$$

It is sufficiently accurate to take $\hat{C}$ to be the pitch-angle scattering operator

$$\hat{C} = \hat{\nu}_a \frac{\partial}{\partial \xi}(1-\xi^2)\frac{\partial}{\partial \xi} \ , \tag{7.5}$$

with the corresponding identity

$$V\left[\xi \hat{C} f\right] = -2\hat{\nu}_a \, V\left[\xi f\right] \ . \tag{7.6}$$

For ions, it is convenient, and probably more realistic physically, to assume that $\hat{C}$ also conserves momentum, so that

$$V[\xi \hat{C} f] = 0 \; . \tag{7.7}$$

We can write the following equation for $\delta \dot{A}_\parallel = \partial \delta A_\parallel / \partial t$:

$$\mathcal{L}_A \delta \dot{A}_{\parallel,n} = V \left[2 \hat{v}_{\parallel,e} \hat{\nu}_{\mathbf{e}} f_{\mathbf{e},n} \right] \; . \tag{7.8}$$

Then, we solve Eq. (7.2) with a semi-implicit advance

$$\left(1 - \hat{C} \Delta t\right) \bar{f}_{a,n} \; = f_{a,n} - z_a \alpha_a \hat{v}_{\parallel a} \mathcal{G}_a \delta \dot{A}_{\parallel,n} \Delta t \; , \tag{7.9}$$

$$= h_{a,n} - z_a \alpha_a \hat{v}_{\parallel a} \mathcal{G}_a (\delta A_{\parallel,n} + \delta \dot{A}_{\parallel,n} \Delta t) \; . \tag{7.10}$$

Currently, in GYRO, we set $\mathcal{G}_a = 1$ in the final equation, since the ion collisional effects are weak and already rather approximate.

7.1.1 The Radial Basis Function (RBF) Method

We are interested in developing a method of function approximation suitable for evaluating differential and integral operators on an irregular mesh in the (θ, ξ) plane. The mesh itself is determined by features of the collisionless dynamics and cannot be altered to suit the evaluation of the collision operator. We will formulate the problem such that the θ-dependence is periodic on the interval $-\pi \leq \theta < \pi$. In the ξ domain, there are no boundary conditions (only regularity of the solution) on the interval $-1 \leq \xi \leq 1$.

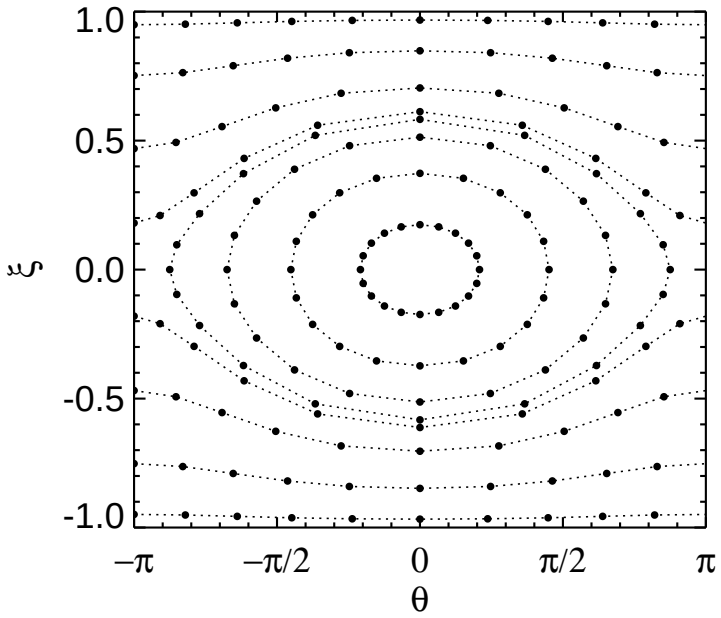

Figure 7.1: Irregular mesh in the (θ, ξ)-plane.

In reality the functions to be approximated is not in general a periodic function of θ, but rather satisfied a phase condition of the type $f(\theta + 2\pi) = f(\theta)e^{2\pi i\alpha}$. Since it is highly desireable to approximate a periodic function to eliminate boundary-related headaches, one can instead consider the associated function $g(\theta) = f(\theta)e^{-i\alpha\theta}$, which is periodic.

7.1.2 Basic RBF expansion

We start by briefly describing the basic RBF approximation. Given a function $\phi(r)$, $r \geq 0$, *centers* $\mathbf{x}_1, \ldots, \mathbf{x}_N$, and data $f_i = f(\mathbf{x}_i)$, the basic form of the RBF approximation is

$$F(\mathbf{x}) = \sum_{i=1}^{N} c_i \phi(|\mathbf{x} - \mathbf{x}_i|) \ , \tag{7.11}$$

where $|\cdot|$ is a positive-definite norm on the vector space of interest. The c_i are then chosen so that $F(\mathbf{x}_i) = f_i$. Typical RBF choices are

Table 7.1: Typical basis functions

$\phi(r)$	name	smoothness
r^3	cubic RBF	piecewise smooth
r^5	quintic RBF	piecewise smooth
$r^2 \log r$	thin-plate spline	piecewise smooth
$\sqrt{1 + (\epsilon r)^2}$	multiquadric	infinitely smooth
$e^{-(\epsilon r)^2}$	Gaussian	infinitely smooth

In practice, the infinitely smooth RBFs are difficult to use because the associated coefficient matrices $A_{ij} = \phi(|\mathbf{x}_j - \mathbf{x}_i|)$ are notoriously ill-conditioned in the limit $\epsilon \to 0$, although theoretically they are capable of spectral convergence and thus remarkably accurate approximation in this limit. Testing, nevertheless indicates that the cubic and quintic RBFs are much more robust and therefore appropriate for the mesh sizes of interest in the collision problem. In one dimension, there is a simple relationship between cubic and quntic RBFs and cubic and quintic B-splines. Thus, the remedy for boundary inaccuracy is one that is already known from the theory of spline interpolation.

7.1.3 Influence of boundaries

It is well-known that near boundaries, the accuracy of RBF approximation – like all function approximation near boundaries – can suffer a significant loss of accuracy, and can lead to stability problems when used for operator discretization in time-dependent problems. We have indeed verified that accuracy loss at the boundary is a serious issue in the ξ direction.

Curing the boundary instability problem first requires generalizing somewhat the RBF expansion in Eq. (7.11). We need to allow the locations of the centers to deviate in some cases from the locations of the fixed mesh points – even allowing them to move outside the simulation domain $-1 \leq \xi \leq 1$. So, we write

$$F(\mathbf{x}) = \sum_{i=1}^{N} c_i \phi(|\mathbf{x} - \hat{\mathbf{x}}_i|) \ , \tag{7.12}$$

where as before the c_i are chosen so that $F(\mathbf{x}_i) = f_i$. Mesh points $\mathbf{x}_i$ near the boundaries at $\xi = \pm 1$ are moved outside the boundary in an analog of the Super Not-a-Knot (SNaK) approach.

7.1.4 The method in detail

The domain of interest is topologically equivalent to the surface of a cylinder, so there is a natural the distance function

$$r_i = |\mathbf{x} - \hat{\mathbf{x}}_i| = \sqrt{2 - 2\cos(\theta - \theta_i) + (\xi - \hat{\xi}_i)^2} \tag{7.13}$$

For $s = 3, 5, \ldots$, we write

$$\phi(r_i) = r_i^s \doteq R_0(\theta - \theta_i, \xi - \hat{\xi}_i; s) \tag{7.14}$$

$$\frac{\partial}{\partial \xi}\phi(r_i) = s r_i^{s-2}(\xi - \hat{\xi}_i) \doteq R_1(\xi - \hat{\xi}_i, \theta - \theta_i; s) \tag{7.15}$$

$$\frac{\partial^2}{\partial \xi^2}\phi(r_i) = r_i^{s-4}\left[s(s-2)(\xi - \hat{\xi}_i)^2 + s r_i^2\right] \doteq R_2(\xi - \hat{\xi}_i, \theta - \theta_i; s) \tag{7.16}$$

$$\mathcal{L}f = \frac{\partial}{\partial \xi}(1 - \xi^2)\frac{\partial}{\partial \xi} f(\theta, \xi) \tag{7.17}$$

$$= (1 - \xi^2)\sum_i c_i R_1(\xi - \hat{\xi}_i, \theta - \theta_i; s) - 2\xi \sum_i c_i R_2(\xi - \hat{\xi}_i, \theta - \theta_i; s) \tag{7.18}$$

$$\doteq \sum_i c_i L(\theta, \xi, \theta_i, \hat{\xi}_i) \tag{7.19}$$

Thus, in matrix notation, we can write

$$(\mathcal{L}f)_i = L_{ij} c_j = L_{ij}(R_0^{-1})_{jk} f_k \doteq D_{ik} f_k \tag{7.20}$$

The matrices are

$$L_{ij} = L(\theta_i, \xi_i, \theta_j, \hat{\xi}_j) \tag{7.21}$$

$$(R_0)_{ij} = R_0(\theta_i - \theta_j, \xi_i - \hat{\xi}_j; s) \tag{7.22}$$

Implementation of the Crank-Nicholson scheme for the equation

$$\frac{\partial f}{\partial t} = \nu \mathcal{L} f \tag{7.23}$$

is then written as

$$f_i(t + \Delta t) = \left(1 - \frac{\nu \Delta t}{2} D\right)^{-1}_{ij} \left(1 + \frac{\nu \Delta t}{2} D\right)_{jk} f_k(t) \tag{7.24}$$

$$\doteq M_{ik} f_k(t) \tag{7.25}$$

In GYRO, we compute and store the matrix M at start-up, reducing the collision step to a matrix-vector multiply. The drawback of course is the storage, which is significant for a matrix of this type.

7.1.5 Additional comments

For a fixed number of meshpoints, the condition number of the matrix $(R_0)_{ij}$ grows rapidly. So, although the method is mathematically correct for $s = 3, 5, 7, \ldots$, in practice the scheme is probably limited to $s = 3$ and 5.

7.2 Conservative Krook Operator

The operator is an annhiliation term $-\nu f$ plus a restoring term δC.

$$Cf = -\nu f + \delta C \tag{7.26}$$

NUMBER: $$\mathcal{FV}\left[F_m^*(\theta)\delta C\right] = \mathcal{FV}\left[F_m^*(\theta)\nu f\right] \doteq S_m^{(1)} \tag{7.27}$$

MOMENTUM: $$\mathcal{FV}\left[F_m^*(\theta)v_\parallel \delta C\right] = \mathcal{FV}\left[F_m^*(\theta)v_\parallel \nu f\right] \doteq S_m^{(2)} \tag{7.28}$$

ENERGY: $$\mathcal{FV}\left[F_m^*(\theta)\varepsilon\delta C\right] = \mathcal{FV}\left[F_m^*(\theta)\varepsilon\nu f\right] \doteq S_m^{(3)} \tag{7.29}$$

To determine the restoring term, expand

$$\delta C = \sum_m c_m^1 F_m(\theta) + v_\parallel(\theta)\sum_m c_m^2 F_m(\theta) + \varepsilon\sum_m c_m^3 F_m(\theta) \tag{7.30}$$

Now we must determine each c_m as a function of the S_m.

$$A_{mm'}^{11}c_{m'}^1 + A_{mm'}^{13}c_{m'}^3 = S_m^{(1)} \tag{7.31}$$

$$A_{mm'}^{22}c_{m'}^2 = S_m^{(2)} \tag{7.32}$$

$$A_{mm'}^{31}c_{m'}^1 + A_{mm'}^{33}c_{m'}^3 = S_m^{(3)} \tag{7.33}$$

where

$$A_{mm'}^{11} = \mathcal{FV}\left[F_m^* F_{m'}\right] \tag{7.34}$$

$$A_{mm'}^{13} = \mathcal{FV}\left[F_m^* \varepsilon F_{m'}\right] \tag{7.35}$$

$$A_{mm'}^{31} = \mathcal{FV}\left[F_m^* \varepsilon F_{m'}\right] = A_{mm'}^{13} \tag{7.36}$$

$$A_{mm'}^{33} = \mathcal{FV}\left[F_m^* \varepsilon^2 F_{m'}\right] \tag{7.37}$$

$$A_{mm'}^{22} = \mathcal{FV}\left[F_m^* v_\parallel^2 F_{m'}\right] \tag{7.38}$$

Bibliography

[AL80] T. Antonsen and B. Lane. Kinetic equations for low frequency instabilities in inhomogeneous plasmas. *Phys. Fluids*, 23:1205, 1980.

[Ara66] A. Arakawa. Computational design for long term numerical integration of the equations of fluid motion: Two-dimensional incompressible flow. *J. Comput. Phys.*, 1:119, 1966.

[ARS97] U.M. Ascher, S.J. Ruuth, and R.J. Spiteri. Implicit-explicit runge-kutta methods for time-dependent partial differential equations. *Applied Numerical Mathematics*, 25:151–167, 1997.

[ARW95] U.M. Ascher, S.J. Ruuth, and B.T. Wetton. Implicit-explicit methods for time-dependent pdes. *SIAM J. Numer. Anal.*, 32:797–823, 1995.

[BC08] E.A. Belli and J. Candy. Kinetic calculation of neoclassical transport including self-consistent electron and impurity dynamics. *Plasma Phys. Control. Fusion*, 50:095010, 2008.

[Bel08] E.A. Belli. *Bull. Am. Phys. Soc.*, 53:242, 2008.

[BF85] R.L. Burden and J.D. Faires. *Numerical Analysis*. Prindle, Weber and Schmidt, Boston, 1985.

[BKC+84] C.M. Bishop, P. Kirby, J.W. Connor, R.J. Hastie, and J.B. Taylor. Ideal MHD ballooning stability in the vicinity of a separatrix. *NF*, 24:1579, 1984.

[Bur97] K.H. Burrell. Effects of $E \times B$ velocity shear and magnetic shear on turbulence and transport in magnetic confinement devices. *Phys. Plasmas*, 4:1499, 1997.

[CHT78] J.W. Connor, R.J. Hastie, and J.B. Taylor. Shear, periodicity and plasma balloning modes. *Phys. Rev. Lett.*, 40:396, 1978.

[CPC+03] Y. Chen, S.E. Parker, B.I. Cohen, A.M. Dimits, W.M. Nevins, D. Schumaker, V.K. Decyk, and J.N. Leboeuf. Simulations of turbulent transport with kinetic electrons and electromagnetic effects. *Nucl. Fusion*, 43:1121, 2003.

[CTB81] P.J. Catto, W.M. Tang, and D.E. Baldwin. Ion transport in toroidally rotating tokamak plasmas. *Plasma Phys.*, 23:639, 1981.

[CW03] J. Candy and R.E. Waltz. An Eulerian gyrokinetic-Maxwell solver. *J. Comput. Phys.*, 186:545, 2003.

[DHCS91] W.D. D'haeseleer, W.N.G. Hitchon, J.D. Callen, and J.L. Shohet. *Flux coordinates and magnetic field structure*. Springer-Verlag, Berlin, 1991.

[DJKR00] W. Dorland, F. Jenko, M. Kotschenreuther, and B.N. Rogers. Electron temperature gradient turbulence. *Phys. Rev. Lett.*, 85:5579, 2000.

[Dur99] D.R. Durran. *Numerical methods for wave equations in geophysical fluid dynamics*. Springer-Verlag, New York, 1999.

[FC82] E.A. Frieman and L. Chen. Nonlinear gyrokinetic equations for low-frequency electromagnetic waves in general plasma equilibria. *Phys. Fluids*, 25:502, 1982.

[GC81] J.M. Greene and M.S. Chance. *Nucl. Fusion*, 21:453, 1981.

[GST] S. Gottlieb, C.-W. Shu, and E. Tadmor. Strong stability preserving high order time discretization methods. *SIAM Review*, 43:97.

[Gug77] H.W. Guggenheimer. *Differential Geometry*. Dover, New York, 1977.

[HW85] F.L. Hinton and S.K. Wong. *Phys. Fluids*, 28:3082, 1985.

[HW06] F.L. Hinton and R.E. Waltz. *Phys. Plasmas*, 13:102301, 2006.

[KC03] C.A. Kennedy and M.H. Carpenter. Additive rungekutta schemes for convectiondiffusionreaction equations. *Applied Num. Math*, 44:139, 2003.

[KK58] M.D. Kruskal and R.M. Kulsrud. Equilibrium of a magnetically confined plasma in a toroid. *Phys. Fluids*, 1:265, 1958.

[KWC07] J.E. Kinsey, R.E. Waltz, and J. Candy. The effect of plasma shaping on turbulent transport and E×B shear quenching in nonlinear gyrokinetic simulations. *Phys. Plasmas*, 14:102306, 2007.

[LLHL01] W.W. Lee, J.L.V. Lewandowski, T.S. Hahm, and Z. Lin. Shear Alfvén waves in gyrokinetic plasmas. *Phys. Plasmas*, 8:4435, 2001.

[MCG+98] R.L. Miller, M.S. Chu, J.M. Greene, Y.R. Lin-liu, and R.E. Waltz. Noncircular, finite aspect ratio, local equilibrium model. *Phys. Plasmas*, 5:973, 1998.

[ML74] C. Mercier and N. Luc. Technical report, Commission of the European Communities, Report No. EUR-5127e 140, Brussels, 1974.

[PR00] L. Pareschi and G. Russo. Implicit-explicit runge-kutta schemes for stiff systems of differential equations. In L. Brugnano and D. Trigante, editors, *Recent Trends in Numerical Analysis*, pages 269–289. Nova Science, 2000.

[PR02] L. Pareschi and G. Russo. High order asymptotically strong-stability-preserving methods for hyperbolic systems with relaxation. In *Hyperbolic problems: Theory, Numerics, Applications*. Springer, 2002.

[SH97] H. Sugama and W. Horton. Neoclassical electron and ion transport in toroidally rotating plasmas. *Phys. Plasmas*, 4:2215, 1997.

[SH98] H. Sugama and W. Horton. Nonlinear electromagnetic gyrokinetic equation for plasmas with large mean flows. *Phys. Plasmas*, 5:2560, 1998.

[TLLM+99] A.D. Turnbull, Y.R. Lin-Liu, R.L. Miller, T.S. Taylor, and T.N. Todd. Improved magnetohydrodynamic stability through optimization of higher order moments in cross-section shape of tokamaks. *Phys. Plasmas*, 6:1113, 1999.

[WM99] R.E. Waltz and R.L. Miller. Ion temperature gradient turbulence simulations and plasma flux surface shape. *Phys. Plasmas*, 6:4265, 1999.

[WSCH07] R.E. Waltz, G.M. Staebler, J. Candy, and F.L. Hinton. Gyrokinetic theory and simulation of angular momentum transport. *Phys. Plasmas*, 14:122507, 2007.

[XMJ+08] P. Xanthopoulos, D. Mikkelsen, F. Jenko, W. Dorland, and O. Kalentev. Verification and application of numerically generated magnetic coordinate systems in gyrokinetics. *Phys. Plasmas*, 15:122108, 2008.